Vorticity, Kinetic Energy and Momentum Analysis of the Collision Zone Between a Plane Wall Jet and a Crossflow

Master Degree Thesis in Aeronautics Engineering

Pedro José da Costa Teixeira Santos

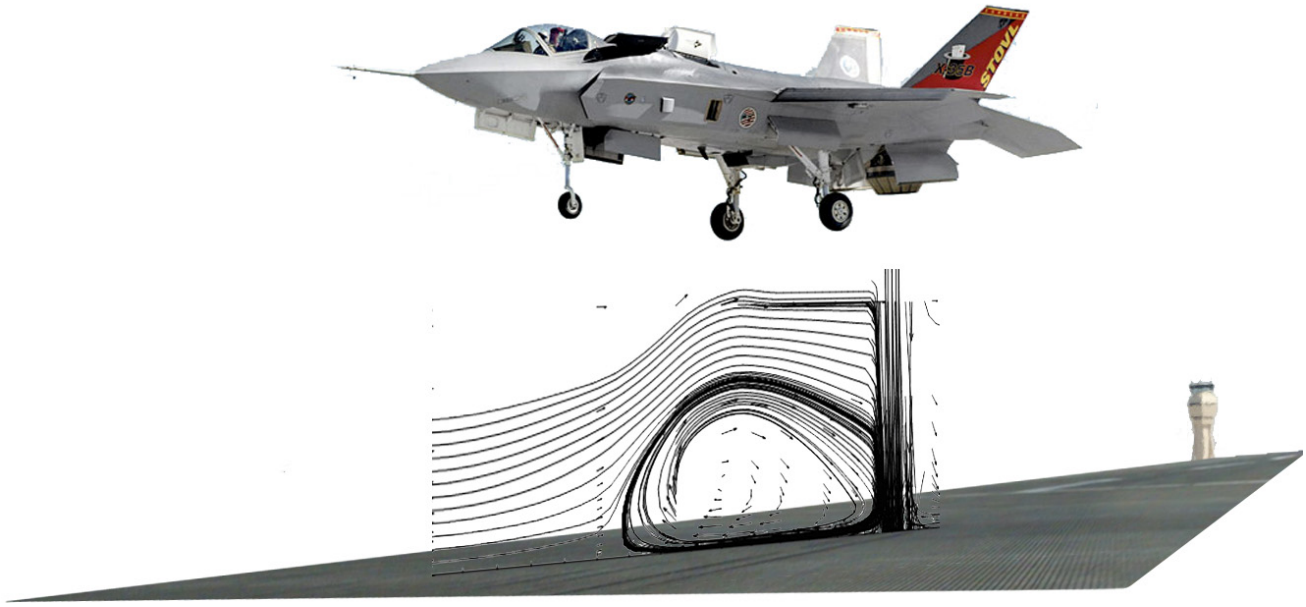

University of Beira Interior

Aerospace Sciences Department

Master Degree Thesis in Aeronautics Engineering

Vorticity, Kinetic Energy and Momentum Analysis of the Collision Zone between a Plane Wall Jet and a Crossflow

Thesis supervised by:

Professor Dr. Jorge Manuel Martins Barata

and

Professor Dr. André Resende Rodrigues Silva

University of Beira Interior

Aerospace Sciences Department

Covilhã, June 2009

Pedro José da Costa Teixeira Santos, M1715

TO MY PARENTS AND FRIENDS

Abstract

When a Short/Vertical Take-off and Landing (V/STOL) aircraft is lifting off or landing with zero or small forward momentum, a complex flow can be found under of aircraft. The lifting jets impinging on the ground giving rise to wall jets that interact between them forming an upwash or that can collide with any crosswind due to the presence of wind or due to the movement of aircraft. These type of flows have profound influences in aircraft performance, such as: lift losses; enhanced entrainment close to the ground (suckdown); engine thrust losses and re-ingestion of the exhaust gases; and, also, possible aerodynamic instabilities caused by the fountain impingement on aircraft underside.

The impingements of a lift jet on the ground origins a wall jet that flows radially from the impinging point and along the ground surface. When this wall jet meets a freestream flowing parallel to the wall in the opposite sense, the crossflow, there is the formation of a highly curved flow far upstream of the impinging jet from the perspective of the crossflow. This highly curved flow is named by ground vortex, and has profound influences on the flow development.

Measurements of these types of flows are very scarce in the literature, and are reported as a secondary flow within the impinging jet flow problem, and are, also, dispersed among many different configurations and operating conditions. The present work is included in a research program dedicated to the identification of the parameters and regimes associated with instabilities, and other secondary effects of this ground vortex flow. It is presented a detailed analysis of a ground vortex resulting from the collision between a wall jet and a boundary layer, and follows the previous study of Barata et al. (2005), which detected a small recirculation zone located upstream the separation point and not yet reported. To avoid the influence of the impinging region, created by the lift jet, a plane turbulent wall jet is produced independently using a configurations inspired in a previous study about bi-dimensional upwash flows. The wall jet collides with the boundary layer produced by a conventional wind tunnel creating the ground vortex. The experimental facility used in this work permits to study different velocity ratios between the boundary layer and the wall jet. Laser Doppler measurements are presented for a velocity ratio between boundary layer and wall jet of *0.5*, and include mean and turbulent velocity characteristics along the two normal directions in the plane of symmetry of the flow.

Vorticity, turbulent kinetic energy balances and momentum balances were determined to understand the complex flow in the collision zone near the ground wall, which is characterized by the turbulent structures that change their size and shape with time. The results revealed that the modeling of turbulence of this flow may require an adequate treatment of production of turbulent kinetic energy by normal stresses, which are predominant in the collision zone.

This work aims to improve the understanding of the essential dynamics of ground vortex flows with application to the V/STOL aircrafts.

Resumo

Quando uma aeronave de descolagem e aterragem vertical (*Short/Verical Take-off and Landing Aircraft – V/STOL*) descola ou aterra com um momento na direcção longitudinal nulo ou pequeno, forma-se um escoamento complexo na parte inferior da aeronave. Os jactos de sustentação da aeronave colidem com o solo dando origem a jactos de parede (*wall jets)* que interagem entre si formando um escoamento ascendente (*upwash*) ou que podem colidir com um escoamento cruzado (*crosswind* ou *crossflow*) devido à presença de vento ou devido ao movimento da própria aeronave. Estes tipos de escoamentos têm profundas consequências na performance das aeronaves, tais como: perdas de sustentação; sucção do avião em direcção ao solo; perdas de tracção dos motores e reingestão de gases queimados; bem como, instabilidades aerodinâmicas na parte inferior da aeronave causadas pelo escoamento ascendente.

O impacto de um jacto de sustentação da aeronave no solo origina um jacto de parede que flui, radialmente, desde o ponto de impacto ao longo da superfície do solo. Quando este jacto de parede encontra um escoamento livre que flui paralelamente à parede no sentido oposto, escoamento cruzado (*crossflow*), há a formação de um escoamento com elevada curvatura, denominado por vórtice de parede (*ground vortex)*, a montante do jacto vertical, da perspectiva do escoamento cruzado, e que tem influências profundas no desenvolvimento do escoamento.

Estudos sobre este tipo de escoamentos são escassos na literatura e são referenciados como um escoamento secundário dentro da problemática dos jactos incidentes, ao mesmo tempo que são realizados com configurações e condições diversificadas. O presente trabalho está incluído num programa de pesquisa dedicado à identificação de parâmetros e regimes associados às instabilidades e outros efeitos secundários destes escoamentos vórtices de parede. É apresentada uma análise detalhada do vórtice de parede resultante da colisão entre um jacto de parede e uma camada limite, e segue um estudo prévio já realizado por Barata et al. (2005), que detectaram uma pequena zona de recirculação a montante do ponto de separação e ainda não reportada até ao momento. Para evitar a influência da zona de impacto criada pelo jacto de sustentação ou jacto incidente, um jacto de parede plano e turbulento é produzido, independentemente, de acordo com uma configuração já utilizada para o estudo de escoamento bidimensionais do tipo *upwash*. O jacto de parede colide com a camada limite (*boundary layer*), produzida por um túnel de vento convencional, criando um vórtice de parede e o qual pode ser estudado para diferentes razões de velocidade entre a camada limite e o jacto de parede. São apresentadas medições efectuadas através de um Laser Doppler para uma razão de velocidades entre camada limite e jacto de parede de *0.5*, e incluem as características médias e turbulentas da velocidade ao longo de duas direcções normais (vertical e horizontal) no plano de simetria do escoamento.

Foram determinadas a vorticidade, os balanços de energia cinética turbulenta e balanços de quantidade de movimento para perceber a região bastante complexa ma zona de colisão próxima da parede, que contém estruturas turbulentas cujo tamanho e forma variam ao longo do tempo. Os resultados obtidos indicam que a modelação da turbulência deste escoamento poderá exigir um tratamento adequado da produção de energia cinética turbulenta por tensões normais, as quais são predominantes na zona de colisão.

Pretende-se com este trabalho melhorar conhecimento da dinâmica dos escoamentos vórtice de parede com aplicação prática às aeronaves *V/STOL*.

Acknowledgments

I would like to express my thanks and appreciations to my supervisors, Professor Doctor Jorge Manuel Martins Barata and Professor André Resende Rodrigues Silva, for their support, guidance and encouragement during these years of study at the University of Beira Interior, and the opportunity to participate and to collaborate in the activities of AeroG – Aeronautics and Astronautics Research Center.

I would like to thank to my colleague Samuel Ribeiro for the support and discussions along the experimental work that helped me to improve it.

I want to express my thanks to the Aerospace Sciences Department of University of Beira Interior, especially to laboratory technician Jorge Oliveira for his help and contribution in the modifications of the experimental facility.

I am very grateful by the support and encouragement of my all family, especially, of my parents and uncles, because along these five years they always had present to help and to encourage in the good and in the not so good moments.

A last acknowledgment is dedicated to my friends by their interest and encouragement during the last years.

Index

Figure Index

Table Index

Nomenclature

D = diameter of the jet at the nozzle exit

f = frequency of oscillation of the ground vortex

h = height of the rectangular jet nozzle slit

H = distance from the nozzle exit to the ground plane

h_V = ground vortex height

k = turbulent kinetic energy

u = instantaneous horizontal velocity component, $u = U + u'$

U = mean horizontal velocity component

u' = turbulent horizontal velocity component

U_0 = boundary layer or crossflow velocity

U_j = wall jet velocity

u'_{rms} = *rms* of the horizontal fluctuating velocity component, $\sqrt{\overline{u'^2}}$, (square root of the horizontal Reynolds stress)

$\overline{u'v'}$ = Reynolds shear stress

v = instantaneous vertical velocity component, $v = V + v'$

V = mean vertical velocity component

v' = turbulent vertical velocity component

V_j = velocity of the jet at the nozzle exit

vort = vorticity

V_R = boundary layer to wall jet (or crossflow to jet) velocity ratio, $V_j = \frac{U_0}{U_j}$

v'_{rms} = *rms* of the vertical fluctuating velocity component, $\sqrt{\overline{v'^2}}$, (square root of the vertical Reynolds stress)

X = horizontal cartesian coordinate (parallel to the wall, pointing in the sense of the jet)

Y = vertical cartesian coordinate (normal to the wall pointing upwards

Greek Symbols

δ = boundary layer thickness

Chapter I: Introduction

1. Motivation

In the last century diversified concepts of V/STOL (Vertical/Short Takeoff and Landing) aircraft were designed and tested (Figure I-1). This type of aircraft depends of a jet or a fan thrust to provide lift for takeoff and landing or, both, lift and thrust, in very low speed flights. These forces are produced by lifting jets and control jets. When a V/STOL aircraft is lifting off or landing with zero or a small forward momentum a complex flow can be found on the underside of aircraft. The lifting jets impinging on the ground giving rise to wall jets that can interact between them and to form an upwash flow or that can collide and interact with crosswind. These type of flows have profound influences in performance of aircraft, such as: lift losses; enhanced entrainment close to the ground (suckdown); engine thrust losses and re-ingestion of the exhaust gases; and, also, possible aerodynamic instabilities caused by the fountain impingement on the aircraft underside.

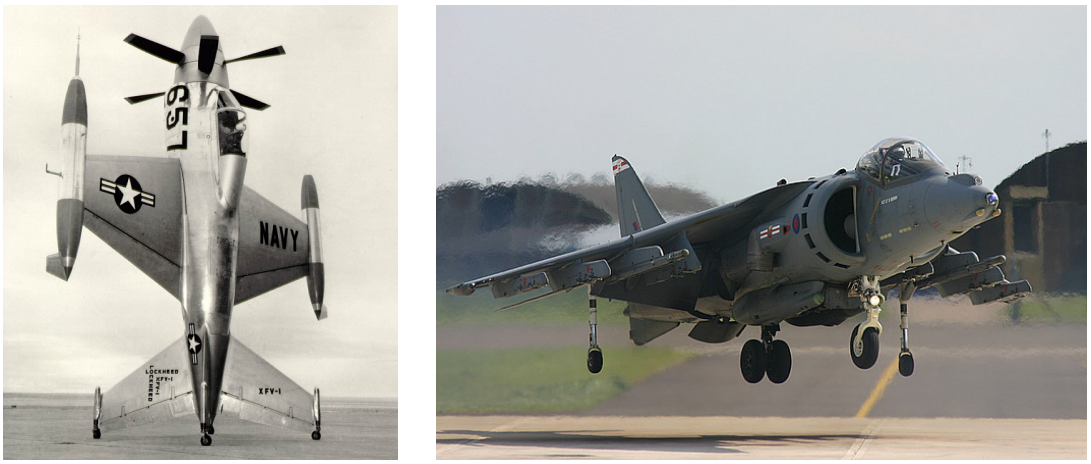

Figure I-1: Historical V/STOL aircrafts. Left side: Lockheed Martin XVF-1, first generation of V/STOL aircraft. Right side: British Aerospace Harrier, the most knowledge V/STOL aircraft.

The impingement of the lift jet on the ground creates a wall jet that flows radially from the impinging point along the ground surface. When this wall jet meets a freestream, flowing parallel to the wall in the opposite sense, such as wind, there is the formation of a highly curved flow, a ground vortex, far upstream of the impinging jet from the perspective of the boundary layer. This ground vortex has profound influences on the flow development (Figure I-2). Studies and measurements of these types of flows are very scarce in the literature and those that been reported are focused on the study of a secondary flow within the impinging jet flow problem, and are dispersed among many different configurations and operating conditions.

Figure I-2: Representation of the ground vortex flow phenomena on the underside of V/STOL aircraft (Joint Strike Fighter F-35 Variant B).

The present work is included in a research program dedicated to the identification of the parameters and regimes associated with instabilities, and other secondary effects, of this particular ground vortex flow. This study deals with vorticity, energy balances and momentum analysis of the counter-flow interaction zone resulting from the interaction between a plane turbulent wall jet and a crossflow. This work aims at improving the understanding of the essential dynamics of ground vortex flows with application to the V/STOL aircrafts.

2. Flow Configuration of V/STOL Aircrafts

In this section it is presented a detailed explanation about the flow configuration under and around a jet of a V/STOL aircraft (Figure I-2).

When the aircraft is in transition flight, the freestream or crossflow deflects the jet and, reciprocally, the jet modifies the crossflow with profound effects on the lift and moments experienced by the aircraft (Figure I-3).

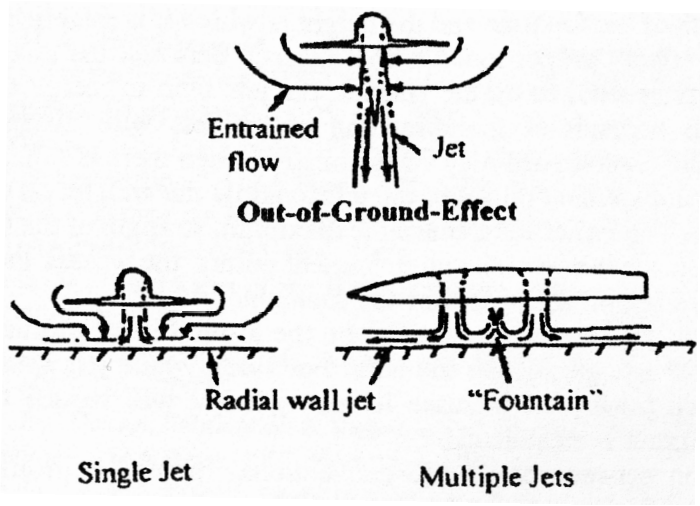

Figure I-3: Flowfield during the transition flight, Kuhn et al. (2006).

Outside of ground effect, the aircraft jet or the fan streams entrain air, which induces suction pressures on the lower surface of aircraft causing a small download or lift loss. This download can be considerably larger in the vicinity of the ground. In the case of a single jet configuration, configuration presented on this work, the impinging jet that sustains the aircraft flows radially outward form the impingement point, and the entrainment area is greatly increased, causing an increment in download, which varies inversely with the height of the aircraft above the ground. In the case of multiple jets configuration, a fountain flow is created as a result of the interaction between the wall jets that flowing outward from the impingement points of adjacent jets. This fountain produces a lifting force on the lower surface of the aircraft that balances, partially, the download created by the entrainment action of the wall jet flow on the ground. The number and arrangements of the jets affects the strength of this lifting force.

When the aircraft is executing the transition between hover to conventional flight, the lifting jet, or fan, stream is swept rearward by the interaction with the freestream, and the jet flow is rolled up into a pair of vortices (Figure I-4).

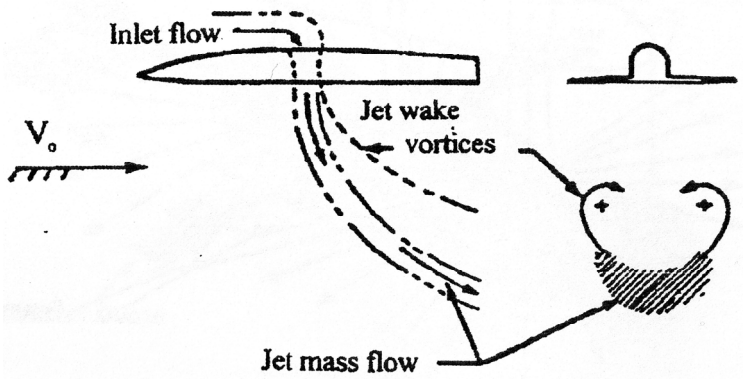

Figure I-4: Representation of flowfield during the transition between hover and conventional flight out of ground effect, Kuhn et al. (2006).

These vortices, with the entrainment action and blockage effect of the jet, induce suction pressures behind and beside the jet and positive pressures ahead of the jet that becomes lift. Generally, these induced pressures result in a loss of lift and a nose up pitching moment. If the jets or fans are located in the vicinity of the trailing edge of a lifting surface, they will induce a favorable lift through their “jet flap” action. This lift gain is accompanied, in the most cases, by a nose down pitching moment. All these phenomena, described at the moment, are present but modified by the proximity of the ground during short takeoff or landing operation (Figure I-5).

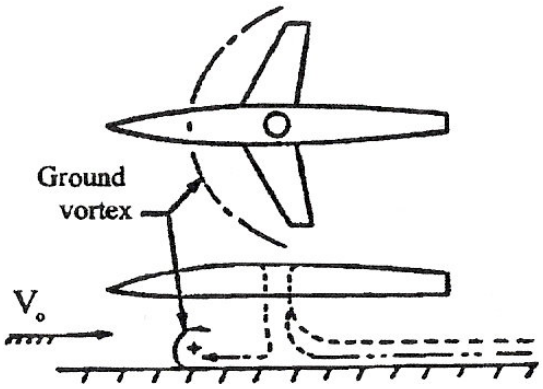

Figure I-5: Transition in ground effect. Short Takeoff/Landing Operations, Kuhn et al. (2006).

In addition the wall jet flowing forward on the ground is opposed by the freestream and rolled up into a ground vortex. This ground vortex can cause lift losses, which are balanced by a reduction of the wake vortex system caused by the truncation of the jet wake by the ground. The position and strength of the ground vortex are also factors in determining the extent of the hot gas, dust and debris, and spray problems that can be generated in short takeoff and landing operations.

3. State of the Art

In this section it is presented the state of art about the studies with relevance to the flow beneath of a V/STOL aircraft. These published studies can be divided in two areas, which are related between them. One area is about the experimental and numerical studies of one or more impinging jets in the ground with and without a crossflow. The second one is about the ground vortex phenomenon that results from the interaction between an impinging jet and the crossflow present around it. The aim of this second area is to understand and to describe the behavior of the ground vortex in the flow.

This state of art is divided in two sections. Since this work is an experimental study about vorticity, kinetic energy and momentum in the collision zone between a plane wall jet and a boundary layer, the first section presents the experimental works reported so far. The second section presents the numerical and computational works dedicated to this problem. In both sections the studies will be presented beginning by the impinging jets problem to the ground vortex problem.

3.1 Experimental Studies

The flow beneath of a V/STOL aircraft is characterized by a highly curved flow named ground vortex. This type of flow is common in nature and can be created by impermeable surfaces that deflect the flow, Castro and Bradshaw (1976). Their work was included in a research program dedicated to the complex turbulent flows. The authors studied the shear layers with complicating influences, like extra strain rates or interaction with other shear layers, using extensive one-point measurements in a mixing layer bounding of a vertical impinging jet with an irrotational core. The authors concluded that the concept of fairly thin shear layer can be useful, since in a strongly perturbed flow it is possible to define a shear layer direction. This concept also can be useful in nearly all flows with significant Reynolds stress gradients. Castro and Bradshaw (1976) described the flow as a turbulent flow with properties that have profound influences, such as, the extra strain rates and the turbulence production as result of interaction between the normal stresses and normal strains.

Flow visualization experiments were performed by Saripalli (1983). The author studied the impingement of multijet flows with fountain formation. In this study were used the configurations of two, three and four jets, and the experiments were carried out for a height of H/d=4. In the case of twin jets configuration, the author observed that the fountain located between the two nozzles moves upward and spreads spatially by entraining the surrounding fluid. Saripalli (1983) visualized the entrainment of the surrounding fluid into the wall jets, free jets, and fountain. When the distance between the two nozzles was large, the fountain presented as an independent plume of upward flow without interaction with the main jets, while with the approach of the two nozzles, there was interaction between the main jets and the fountain. Saripalli (1983) also studied the

effect of the ratio between jets momentum on the twin-jets configuration. The author observed the inclination of fountain towards the jet with lower momentum and the included angle that increased with the increment of difference in jet momentum. At a critical ratio of jet momentum, which depended on the height of the nozzle in relation to the ground, a recirculation pattern developed between the jet with lower momentum and the fountain, together with mixing of the fountain and the free jet flow. The effect on the flow of jets with different diameters was also studied, and the author observed that when the two jets presented the same momentum, the fountain flow was the vertical direction and was centered. When the mass flows of these two jets were the same, the fountain was inclined towards the larger jet and mixes with it. For the remaining configurations were observed patterns of the stagnation line in the ground.

In this context of fountain flows, Saripalli (1987) made measurements of mean velocity and turbulence on a three-dimensional fountain flow resulting from the collision of the wall jets created by the impingement of two axisymmetric jets on a ground plane. The author used three configurations with different distances between the two jet nozzles and heights in relation to the ground, giving rise to opposed wall jets with different characteristics. The measurements were performed by a two-component Laser Doppler Velocimeter in a plane connecting the nozzle centerlines at different heights above the ground, having the water as working medium. The results of mean velocity and turbulence quantities across the fountain presented some similarity in all configurations except in the fountain formation region. The author observed that the growth of the fountain had a linear behavior and he verified that the growth rates were identical in the three configurations. The fountain flow was highly turbulent, presenting turbulence intensities between *50%* and *60%*. A decay of the streamwise maximum velocity in the fountain was found, and it was inversely proportional to the height of the jets above the ground.

Although the studies previously presented have application to V/STOL aircraft problem, they were performed without the presence of a crossflow which can be responsible by the diversified phenomena on the underside of the aircraft. An experimental investigation, to model the impingement of a high velocity jet exhaust flow on the ground, was carried out by Cimbala et al. (1988). The authors used a jet with constant velocity and a crossflow with different velocities produced by a wind tunnel, getting velocity ratios between the crossflow and the impinging jet from *0.1* to *0.4*. The height *h/D* was also varied between *0.1* and *0.4*. The flow visualization experiments and the measurements were performed with a two-component Laser Doppler Velocimeter, and they revealed a highly unsteady and nonsymmetric separation bubble. The authors attributed this unsteadiness to the shear-layer vortices shed from the lip of the jet. The flow visualization results, also, indicated that these vortical structures merge into a large recirculation separation bubble, which is continuously fed by the shear layer vortices from the impinging jet and the vorticity from the oncoming boundary layer.

Cimbala et al. (1988) verified that the ground vortex decreases in size and moves downstream when the crossflow velocity is increased. The flow was extremely unsteady, but with

the increment of crossflow velocity, the unsteadiness was damped. In this work was used a large plate flush-mounted to the exit, which forced the ground vortex to move downstream and also a decrease of its size.

Cimbala et al. (1991) made an experimentally study about the ground vortex formed by a jet impinging on the ground in the presence of a crossflow. The aim of their work was to identify and to quantify the source and nature of the unsteadiness of the flow associated with the ground vortex. The measurements of frequency spectra were obtained with two hot hires mounted at various locations in the flowfield. The parameters varied in this study were the jet diameter, the height between the jet exit plane and the ground, the jet velocity and the freestream velocity. In the case of the larger jet, there were identified the vortical structures observed by Cimbala et al. (1988). The vortical structures are shed from the upstream lip of the jet and are observed to merge with each other as they travel along the edge of the jet and as they are turned upstream by the ground plane. According to the authors, these vortical structures seem to merge into the large ground vortex and lead to the turbulent appearance of the ground vortex. The authors in Cimbala et al. (1988) verified that the ground vortex is unsteady, both in size and shape, and also in location. In the present work the authors identified a large scale low frequency pulsating behavior referred as puffing of the ground vortex. The sequence of this puffing behavior was as follows. The ground vortex is very small, but growing. The shear layer vortices, which are convected with the wall jet, seem to merge into the growing ground vortex. As the ground vortex has a continuous growth, it becomes too large for the flowfield to sustain, and at this point, the entire flowfield breaks up. The large ground vortex is swept downstream, and, immediately, a new small ground vortex begins to grow upstream, and the cyclic process repeats itself. The authors, also, identified two ground vortices or separation bubbles present at the same time. They concluded that, apparently, sometimes a new small vortex forms without the completely break up of the larger one.

Cimbala et al. (1991) concluded that the ground vortex is highly unsteady and was observed to pulsate by expanding or contracting. This pulsating or puffing action occurred in a very low broadband frequency range and resulted in a significant variation in the size of the ground vortex. The low frequency oscillations were attributed to the gross features of the ground vortex flowfield. The jet fluid appears to accumulate in the ground vortex, which grows to unstable state that interacts with the crossflow. In other words, the ground vortex grows until the flowfield can not sustain itself. Then, due to the crossflow, portions of the ground vortex break away, a new ground vortex forms, and the process repeats itself. So, the low frequency puffing does not correlate with the shear layer vortices and with flowfield oscillations. The puffing frequency oscillation depends of freestream velocity, but is not influenced by the boundary layer thickness or the jet velocity. The location of the ground vortex was influenced by these parameters, but the instability not, since, according to the authors, the ground vortex forms where the momentum of the upstream flowing wall jet can no longer resist the momentum of the crossflow. On the other hand, when the

ground vortex is formed, it grows because of accumulation of jet fluid. The rate at which jet fluid enters to the ground vortex is expected to be independent of its location. So, only freestream velocity can be influence on the frequency of the puffing instability. The unsteadiness of the ground vortex gives rise to severe fluctuations in the height of vortex, mainly, when the values of velocity ratio between the crossflow and the impinging jet are low.

To reduce the mean size and the fluctuation in size of ground vortex, Harman et al. (1994), used one and two fine wire mesh screens (ground fences), bent in a horseshoe shape, located on the ground in front of the impingement point. The ground fences permitted to decrease the momentum of the upstream wall jet, giving rise an higher freestream to jet velocity ratio, and therefore, a smaller ground vortex in size and unsteadiness. For a velocity ratio of *0.15*, the addition of a single ground fence resulted in a *70%* reduction in the mean size of the ground vortex, while with the addition of two ground fences, the mean size decreased about *85%*. For the both configurations, fluctuations in size decreased nearly in proportion to the mean size. The authors concluded that the addition of theses devices on the ground can reduce the size and unsteadiness of the ground vortex without modification of the aircraft and without reduction of its thrust.

Knowles et al. (1990 and 1991) investigated, experimentally and numerically, the parameters that can influence the position of the ground vortex (cross flow to nozzle velocity ratio, nozzle height, nozzle pressure ratio, vector angle and nozzle splay) associated to the flowfields, resulting from interaction between the impingement of a single or twin jets on the ground and with a presence of crossflow. The authors, also, studied the effect of a moving ground plane in the flow. Knowles et al. (1991 and 1991) verified a relationship between the penetration distance, the separation distance and the position of vortex core. From the numerical results they conclude that CFD calculations predicted well the relationship between distances of the separation and penetration points. From the experiments Knowles et al. (1990 and 1991) also verified that the flowfield was extremely unsteady, mainly, in the presence of the twin jet fountain flow.

Barata (1989) and Barata et al. (1991a and 1993) studied the turbulent kinetic energy in the vicinity of the stagnation zone created by the impingement of a turbulent jet on a flat plate with the presence of a crossflow. The analysis carried out by the authors provide a basis for better understanding of several related but more complex practical flow fields. This analysis was based on the Laser Doppler measurements of the time resolved velocity field. The measurements have been carried out for a velocity ratio between the jet and the crossflow of *30*, a Reynolds number based on the jet exit conditions of *60 000*, and an impinging distance of *5* jet diameters. The detailed visualization studies of Barata et al. (1991b) revealed the existence of an impingement region characterized by a significant deflection of the impinging jet. The authors observed that the flow flows parallel to the ground, giving rise to a flow recirculation far upstream of the impinging jet, due to the interaction of the wall jet, produced by the impinging jet, and the crossflow. The result is a ground vortex wrapped around the impingement jet (Figure I-6), resembles the

“horseshoe” vortex structure known to be generated by the deflection of a boundary layer due to solid obstacles.

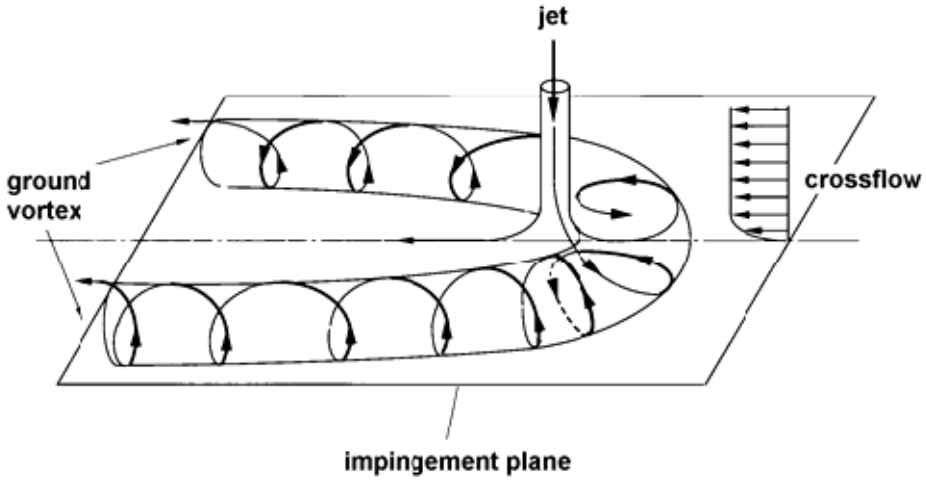

Figure I-6: Sketch of flow development for a jet impinging on a flat surface trough a low velocity crossflow. "Horseshoe ground vortex" formation, (Barata et al. 1991a and 199b).

The measurements presented by Barata (1989) and Barata et al. (1991a and 1993) were performed in the plane of the symmetry of the flow. The authors concluded that the shear layer surrounding the jets was a region of intense velocity fluctuations with maximum values located in the region of highest mean velocity gradients. In the impingement and stagnation zones associated with the formation of the ground vortex, were noted large effects of flow distortion in the turbulence structure. The analysis of the authors to the terms in the conservation equation of turbulent kinetic energy attributed this behavior of the flow to the interaction between normal stresses and normal strains. Turbulent diffusion and dissipation were important in the balance of turbulent kinetic energy, particularly, in these zones. Barata (1989) and Barata et al. (1991a and 1993) verified that along the impinging jet the production by shear stress was the largest term in the outer edge of the jet and likely to be balanced by turbulent dissipation. The distributions along the impinging jet resemble the same for a turbulent free jet, Tennekes and Lumley (1972). Along the centre of the jet, the most important term was the advection or convection term, which was related to the spread of the jet, presenting a loss of turbulent energy. With the approach to the impingement zone, the authors concluded that the turbulence production was large and higher than the largest rate of production by shear stress along the impinging jet, but was through the interaction of normal stresses with normal strains and was comparable with the advection term, which represented a gain of turbulent energy. In relation to diffusion and dissipation terms the authors expected to be large and to balance the last referred terms. This result can explain the large distortion of the mean flow in the impingement zone and the predominance of extra source term in the balance of turbulent energy due to streamline curvature. The authors verified that the budgets of turbulent kinetic energy across the radial wall jet resemble the same for a conventional

wall jet, Tennekes and Lumley (1972), with production by shear stress as the largest term and balanced by the turbulent diffusion and dissipation. The authors concluded that deceleration of the radial wall jet was associated with an increase of the advection term, representing a gain of turbulent kinetic energy, and, that, as other recirculating flows, the approach of the stagnation point associated with the ground vortex is characterized by a fast increase in the production of turbulent kinetic energy trough the interaction of normal stresses with normal strains.

Barata et al. (1987, 1989, 1991a, 1991c e 1996) made studies for a jet to cross flow velocity ratio of *30* and using a plate at the exit of the jets, to compare experimental and numerical results. The configurations used by the authors included one, two e three impinging jets. In the experimental component was used a Laser Doppler Velocimeter to do the measurements for different impinging heights above the ground plane. The experiments showed a large penetration of the impinging jets, which exhibited a similar pattern for single and twin jet configurations. The authors observed that the fountain upwash flow resulting from the collision of the radial wall jets was deflected by the crossflow. The flow in this work was confined. The grid independent numerical calculations of the single and twin jet flows, with QUICK scheme and k-ε turbulence model, represented the gross features of the flows. However, the method failed in to predict the turbulent structure of the impingement zones and fountain flow, which is not represented by the turbulent viscosity hypothesis. On other hand, the authors admitted that in the ground vortex region the numerical results can be influenced by the failure of the notion of the wall at the separation point, since the flow is no longer controlled by the wall shear stress.

In the continuation of this work Barata et al. (2004) characterized the influence of the jet to crossflow velocity ratio on the structure of the ground vortex. The flow was produced by a single round jet discharged through the upper wall of a rectangular water channel, with a large cross-section, at right angles to the channel flow. The experiments were carried out for Reynolds Numbers based on the jet exit conditions between *60.000* to *105.000*, which corresponds to jet to crossflow velocity ratios from *30* to *73*, and for an impinging height of *5* jet diameters. The visualization studies of the flow made by Barata et al. (2004) were carried out to help the choice of the measurement locations and to obtain a qualitative picture of the flow. Initial potential-core jets as well as the impingement regions were identified. The deflected jet became parallel to the ground plane and presented a behavior similar to a radial wall jet where the upstream effects of interaction caused by impingement have not influence. The wall jet interacted with crossflow and formed a vortex close to the ground plane which wraps around the impinging jet like a scarf. The results were obtained in the vertical plane of symmetry that contains the jet nozzle axis and quantifies the mean and turbulent velocity characteristics of the flow. The authors identified, clearly, the existence of the ground vortex caused by the interaction of the crossflow with the upstream wall jet resulting from the impingement of impinging jet. Two different regimes were identified. For a smaller velocity ratio the ground vortex was attached to the impinging jet while for the larger velocity ratio the ground vortex was completely detached from the impinging jet. These

characteristics of flow had influence in the flow development and are the explanation, according to the authors, for the apparent lifting on the wall jet that exists on the other side of the impinging jet. The authors attributed this result to the interference of the ground vortex in the upstream edge of the impinging get that feeds it with fluid but with low momentum. Simultaneously, the ground vortex blocks the passage of the crossflow in the vicinity of upper wall, the flow find an area reduction and suffers an increment in its acceleration, which causes the growth of the downstream wall jet at an abnormal rate near the impinging zone, and, also, an increment on the vertical velocity component. There was no separation but an abnormal deficit of momentum in downstream side of the impinging jet over the wall jet was verified. The authors observed that in the case of higher velocity ratios, since the ground vortex is detached from the jet and is also smaller in height, this effect of blockage is not so significant. Barata et al. (2004), also, identified one characteristic in each regime. High gradients of velocity fluctuations near the upstream side of the impinging jet were characteristics of the smaller velocity ratios, while for higher values of velocity ratios a more symmetric distribution and smaller gradients of turbulent quantities were obtained. The authors concluded that the shape, size and location of ground vortex were dependents of the velocity ratio, and also of the impinging distance. Associated to the different velocity ratios, two regimes were identified. One characterized by larger flow asymmetries and ground vortex dimension with a large interference in the impinging zone and downstream flow development, and, another, characterized by a symmetric impinging jet with a smaller ground vortex detached upstream with different implications on the downstream flow characteristics. Other interesting aspects observed by the authors are related with the jet exit velocity. This velocity can cause an increment in the crossflow velocity and can affect the strength of the ground vortex. A smaller height of the ground vortex in the case of higher velocity ratios is accompanied by an increment of the vortex strength. The crossflow acceleration over the ground vortex, in both regimes, together with the jet exit velocity are an indication that the influence of the upstream wall jet is not confined to the ground vortex but spreads up to the upper wall by a mechanism not yet reported.

Barata et al. (2005) presented a study about a highly curved flow resulting from the impingement of a wall jet with a boundary layer with aim to improve the understanding of the ground vortex behaviour. The experiments were carried out for a boundary layer to wall jet velocity ratio of *0.58m/s*. The authors visualized that the wall jet impinges on the boundary layer and it is strongly deflected backward at an average angle of *36deg* with the ground surface. The authors verified that in the impingement zone, the wall jet and boundary layer fluid moves in direction to the wall, giving rise to a complex flow which includes a small secondary vortex flow on the boundary layer side near the ground plane. According to the authors, seemed to exist entrainment of fluid from the lower part of the wall jet. In this work it was also concluded that flow was characterized by intense velocity fluctuations and by its anisotropy with the exception of the inclined upwash flow region. In the region where the boundary layer begins to be deflected

upward, due to the presence of the small ground vortex and near the stagnation point, the authors suggested the existence of large effects of flow distortion on the turbulence structure. The authors verified that the ground vortex development reported by Barata et al. (2004) has two different influences: one related to the collision of the wall jet and the crossflow and another associated with the enhanced flow entrainment produced by the high velocity impinging jet.

Barata et al. (2008), Silva et al. (2009a) and Barata et al. (2009) made experimental visualization studies about interaction between a plane turbulent jet and a boundary layer. The experiments were carried out using a direct digital photography and high speed movies. The author used the visualization results of the flow to provide a first insight into the nature of flow and to decide the choice of quantitative measurement locations. During this experimental study, the authors observed the collision of the wall jet wind the boundary layer, and its strong deflection backwards blocking its passage. The result was an upwash flow with an inclination angle, which was a function of velocity ratio between jet and boundary layer. They observed that the lower part of the upwash was captured by the ground vortex but an equilibrium state was achieved and no significant oscillations were detected. The fact of flow visualization have been performed in parallel longitudinal vertical planes aligned with the direction of the wall jet and boundary layer flows have also shown that possible transverse effects do not disturbed the flow.

The visualization and quantitative results reported by Barata et al. (2008) corresponds to a velocity ratio between the boundary layer of the wall jet, V_R, of *0.58* and showed a mean inclination angle of *36deg* without considerable oscillations (Figure I-7). In spite of the steady appearance of the upwash flow, they detected, near the separation point, a small and highly unstable secondary vortex flow with its shape, size and location varying almost constantly.

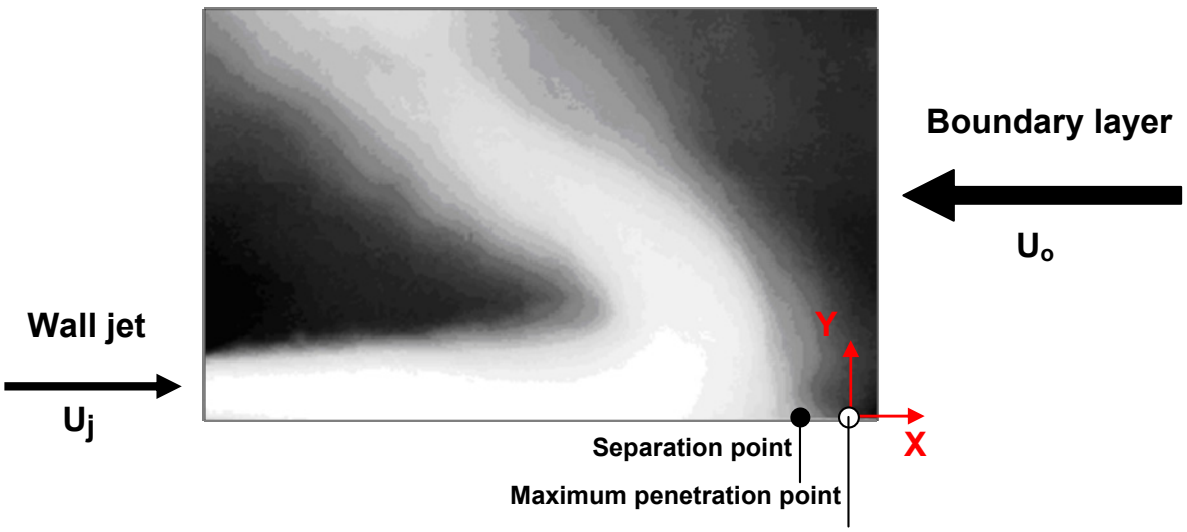

Figure I-7: Visualization of the flow in the impinging zone for V_R=*0.58* Silva et al. (2009). The authors considered the origin of coordinates near the visual maximum penetration point.

This small vortex presented a behavior similar to the “puffing” of the ground vortex as reported by Cimbala et al. (1991). First the vortex is very small and growing. The lower part of the boundary layer with anticlockwise vorticity seems to merge into the growing vortex. Since as the small vortex has a continuous growing it becomes higher than the boundary layer, and breaks up suddenly, while is convected upwards in the direction of the curved flow. Then, a new small vortex starts to grow and the cyclic process repeats itself with a mean frequency, calculated from the visualization frames about *8.33Hz* (Figure I-8).

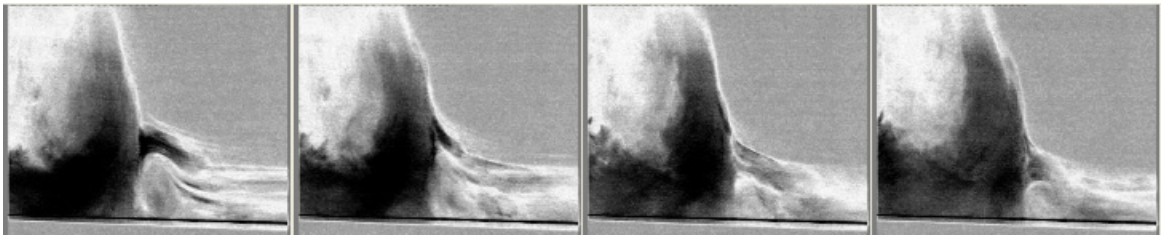

Figure I-8: Small vortex burst and new vortex growth for V_R=*0.58*, Barata et al. (2008).

Cimbala et al. (1991) justified the growth of the vortex with the shear layer vortices, which convect with the wall jet and merge into the ground vortex. The flow between the present upwash curved flow and a ground vortex resulting from an impinging jet is similar in the longitudinal vertical plane of symmetry that contains the centre of the jet exit, and where the transverse velocity component, *W*, is zero. The small secondary flow identified by Barata et al. (2008) exists, simultaneously, with the ground vortex and is located in the boundary layer side. The growth of the secondary vortex was not attributed to the wall jet shear layer vortices since the upwash flow blocks their passage. Barata et al. (2008) conclude that the nature of the secondary flow is similar to the horseshoe vortex generated by the roll up of the boundary layer by a surface mounted solid cylinder. The same authors also reported a similar conclusion in the case of higher values of velocity ratios between the wall jet and the boundary layer, the secondary vortex cannot merge into the deflected flow resulting from the counter-flow interaction of the wall jet with the boundary layer, because of strong blockage effects and inviscid associated phenomena. So, the unsteadiness reported before is, probably, associated with this kind of additional small vortex upstream of the ground vortex and due to its extreme small size could not be observed so far as in the case oh high jet to boundary layer or crossflow velocity ratios, Barata et al. (1986, 1987, 1991b, 1991c), Barata (1996) and Barata et al. (2004).

Silva et al. (2008 and 2009a) studied the separation zone of a ground vortex for a velocity ratio between boundary layer to wall jet, V_R, of 0.5, which according to Cimbala et al. (1991) would correspond to a “puffing” frequency of about *18±1Hz*. The results presented by the authors correspond to the same results of mean and turbulent velocity characteristics obtained by Barata et al. (2008). The secondary vortex identified by Barata et al. (2008) was confirmed and it was possible to verify that due to its instability it will be swept upwards by the curved flow resulting

from the collision between the wall jet and boundary layer and no “puffing” mechanism is observed.

The ordered sequence identified from preliminary visualization studies of Silva et al. (2008) and Silva et al. (2009a), for the small recirculation zone that appears near the separation point, was interpreted by the authors as an oscillation of the separation zone or of the virtual deflected flow origin, and also confirmed by the bimodal histograms of the horizontal and vertical velocity measurements obtained in the zone. For the horizontal velocity component, *U*, four different types of histograms were identified by the authors: bimodal histograms with symmetric peaks in the central region of the deflected flow; bimodal histograms with a larger positive peak in the wall jet side and a larger negative peak in the boundary layer side and near Gaussian histograms away from the collision zone. For the vertical velocity component the authors identified five different types of histograms with the bimodal pattern occurring in a slightly different region around the upwash flow. In the region of the collision zone, where the bimodal histograms were obtained, broadband humps were identified with center frequencies near of *4Hz* and *15Hz*, which is an indication of the low frequency unsteadiness. In the central zone of upwash flow, near the maximum values of mean vertical velocity component, a broadband hump with a maximum value of about *15Hz* was observed together with distinguishable high frequency peaks. The authors associated the source of the low frequency unsteadiness to a small vortex located upstream the separation point. This secondary vortex had a similar very low broadband pulsating behavior. It was conclude that the unsteadiness of the ground vortex reported before the case of impinging jets in unconfined cross-flows may also be associated with an additional small vortex upstream of separation point, but due to its extreme small size could not be observed so far as in the case of large jet-to-crossflow velocity ratios.

Recently, Saddington et al. (2009) described and quantified the turbulence characteristics of the fountain upwash flowfield resulting from the impingement of two axisymmetric jets. They had as basis the study of Saddington et al. (2005), which revealed that although the flow is generally symmetrical in the mean, the instantaneous velocity fields obtained shows a high degree of asymmetry, the presence of large-scale vortical structures and a stagnation region whose location is observed to vary randomly. The visualization of multiple jet impingement has revealed the presence of large scale coherent structures, evolving from the main jets, propagating through the wall jets and dissipating in the fountain, Cabrita et al. (2002) e Saripalli, (1983), with possible crossover of these structures from one wall jet to the opposite side of the fountain. This may be responsible, in part, for the large degree of spreading associated with fountain flows. The experiments of Saddington et al. (2009) were performed with jet exit diameters of *12.7mm* and nozzles spacing of *7* diameters, simulating the two lift-jets of V/STOL aircrafts. The experiments were performed using a PIV system and the results were obtained in the fountain upwash for a NPR (Nozzle Pressure Ratio) of *1*.05, which corresponds to a jet velocity at the nozzle exit section of *90m/s*, approximately, and a nominal non-dimensional height above the ground plane

of *2.4* nozzle diameters. The results of Saddington et al. (2009) revealed that the interaction region of the wall jet was an area of large horizontal velocity fluctuations and that contained high values of the velocity gradient $\frac{\partial V}{\partial X}$. The maximum values of vertical turbulent stress, non-dimensionalized by the jet exit velocity, occurred in a height range that corresponds, approximately, to the fountain formation region, where were observed high values of mean vertical velocity gradient $\frac{\partial U}{\partial X}$. According to the results, the authors observed that the flow is highly anisotropic in the wall jet interaction region while throughout the fountain decay region the flow presents minor levels of the anisotropy. The turbulent kinetic energy, *k*, is an important parameter to understand the physical processes in turbulent fluctuations and in turbulence modeling. The transport equation for *k* expresses the balance between convection, production, diffusion and dissipation of turbulent kinetic energy. The results of this work revealed that in the region of wall jet interaction the production of turbulent kinetic energy by normal stresses is much larger than that by shear stresses, while the shear stresses dominate the production of turbulent kinetic energy away from the centerline. In relation to the convective and diffusive plus dissipative terms, in the transport equation of *k*, they have similar magnitudes throughout the flowfields except in the interaction zone of the wall jet where diffusion and dissipation of turbulent kinetic energy revealed most negative, which balances the high production of *k* by normal stresses. The authors also presented in this study an analysis about the vorticity along the flowfield. It was observed that the vortical structures were convected in the wall jets to the base of the fountain without a relevant variation in magnitude. The low values of $\frac{\partial V}{\partial Z}$ and the high values of $\frac{\partial U}{\partial X}$, in the wall jet interaction region, have a magnifying effect on vorticity, which is transmitted to the fountain where it decays. According to the results obtained, the magnitude of the instantaneous vorticity was three times higher than the mean, and the fountain formation region is an area of vorticity production.

3.2 Computational and Numerical Studies

Van Dalsem et al. (1987) presented a numerical study using the Fortified Navier-Stokes (FNS) scheme, about an impinging jet in ground effect with the presence of a crossflow. The simulations were performed for a velocity ratio between the crossflow and the impinging jet of *0.223*, and, also, for different heights of the exit nozzle above the ground, *h/D=3*, 4, 6 and 10. The simulations of the authors permitted to identify the jet impingement and the ground vortex. However, they failed to predict, accurately, the location of the ground vortex. The authors verified that the location of ground vortex was sensitive to the level of mixing in the boundary layer produced by the fraction of the jet which moves upstream and forms the ground vortex. They concluded that the forward penetration of the ground vortex was a strong function of the turbulent

mixing in the ground vortex region, and this mixing could be modeled with modified algebraic turbulence models. In this work were also used jets with elliptic cross section and it was concluded, by the numerical simulations, that an elliptic jet with the major axes aligned with the crossflow can have advantages over a circular jet, since can permit reduce the jet deformation and the size and shape of the resulting ground vortex.

With the aim to predict the cycle of vortex formation, growth and collapse, observed experimentally by Cimbala et al (1991), Pandaya et al. (2003) studied computationally a jet impinging on the ground plane in presence of a low-speed crossflow. The numerical simulation was performed according to the results obtained by Cimbala et al. (1991). The flow was confined, and the impinging jet had a Mach number of *0.13*, while the crossflow had a Mach number of *0.013*. The computations results were obtained using the OVERFLOW code, which permitted to solve the Navier-Stokes Equations with a sufficient time step to capture the flow features associated to the small “puffing” frequencies of the ground vortex. The authors compared the results with the experiments of Cimbala et al. (1991). The results revealed that the gross features of the flowfield, the jet impingement, the puffing mechanism of ground vortex and the von Kármán vortex street, can be represented numerically with adequate turbulence model. The unsteady behavior of the ground vortex was similar to that of Cimbala et al. (1991) experiment. The size of the ground vortex and the unsteady frequencies were the same that Cimbala et al. (1991) obtained.

The ground vortex flow problem is also a subject of many numerical studies already performed. Most of them are dedicated to the study of the main fundamental configurations, single or multiple impinging jets through a crossflow Barata et al. (1989) and Barata el al (1991c and 1996). The most complex numerical study already reported included all the geometrical and flow details by simulating a complete Harrier Aircraft, Smith et al. (1991) and Chanderjian et al. (2002), but due to the inexistence of available data it was not possible to proceed to the experimental validation of the ground vortex prediction. The numerical studies that used the single impinging jet configuration have the basic configuration to study the hot gas ingestion phenomena in V/STOL Aircrafts, due to the presence of the ground vortex, Barata et al. (1989), Page et al. (1998) and Jiang et al. (2000). Most of these numerical studies use a turbulence model based on the eddy viscosity approach. The mean flowfield was predicted quite well except the impinging zone where turbulence production was found to be associated with the normal stresses, Barata et al. (1989), and the pressure term in the momentum equations is dominant Barata et al. (1991c).

LES simulations were also attempted but as far as the penetration distance is concerned no improvement over the RANS prediction was obtained. Worth and Yang (2006), used LES and concluded that all the models were still inadequate in providing more than the gross features of the mean flowfield and there is still need for further investigation to predict this flow accurately.

Silva et al. (2009b) developed a research program to identify the parameters and relevant regimes associated with instabilities and other secondary effects of ground vortex flow. This is a program with numerical and experimental components. Silva el al. (2009b), presented the computational part dedicated to the analysis of a ground vortex flow resulting from the collision of a wall jet with a boundary layer, and follows the results obtained by Barata el al. (2005), which detected a second recirculation zone upstream of the separation point and not reported at the moment for this type of flows. The computational method used to perform this work was based on the solution of the conservation laws for mass and momentum, and it is a modified version of the method that was used by Barata et al. (1986, 1987, and 1991a), and that allows good agreement with the measurements of the mean velocity field, Barata et al. (1986, 1987, and 1991a). The conditions used in the numerical simulations corresponding to the experimental conditions presented by Barata et al. (2009a and 2009b). The velocity ratio, V_R, between the boundary layer and the wall jet velocities used was *0.5*, which corresponds to a wall jet mean velocity of U_j*=13.7m/s* and a mean boundary layer of U_0*=6.9m/s*. The authors identified a cycle of *0.28s*, which is equivalent to a frequency of *3.6Hz*, for a sequence: a small vortex appearance and growing; origin of a second vortex that increases at the same time that the first is decaying; then both disappear and a new cycle begins. It was observed by the authors that during the complete sequence the location and size of the ground vortex is almost constant as well as the main flowfield in the wall jet and boundary layer. In the collision zone, near of the wall and between the separation and maximum penetration points, underneath the front of the ground vortex, were observed many alterations. Initially, the fluid of wall jet started to penetrate into the boundary layer side until a very small anti-clockwise rotating vortex to appear. Then it started to growth and seconds later it blocked the passage of the clockwise rotating fluid of the wall jet and a new small vortex appeared in the wall jet side and before the stagnation point, but now with clockwise vorticity. Whit this result the authors confirmed the observation of Pandaya et al (2003), when they performed the experimental measurements with an equivalent of a smokewire and verified that two counter-rotating vortices separated from the flow passing over the ground vortex. The second small vortex identified by Silva et al. (2009a) it was always smaller that the first one, and after it moves to the left side of separation point it is already decaying, becoming smaller until disappears, with the counterclockwise vorticity of boundary layer becoming dominant once again. The cycle presented a total period of *0.28s* and repeated itself, indefinitely, with the same characteristics. This result not permitted concluded that the mechanism is similar to the “puffing” mechanism described by Cimbala et al. (1991), although can exists some common characteristics. The authors concluded that the region near the wall, that contains the separation and maximum penetration points, was found to be of most interest to the instabilities mentioned and that a detailed set of measurements are needed to understand accurately the mechanisms involved.

4. Objective

The present work is included in a research program dedicated to the identification of the parameters and regimes associated with instabilities, and other secondary effects, of this particular ground vortex flow. It presents a detailed analysis of a ground vortex flow resulting from the collision of a wall jet with a boundary layer (Figure I-9), and follows the study made by Barata et al. (2005), which detected a small recirculating zone, located upstream the separation point and not yet reported before for this type of flows. To avoid the influence of the impinging region created by a single impinging jet, the plane wall jet is produced using a configuration inspired in a previous study of bidimensional upwash flows, Gilbert (1983).

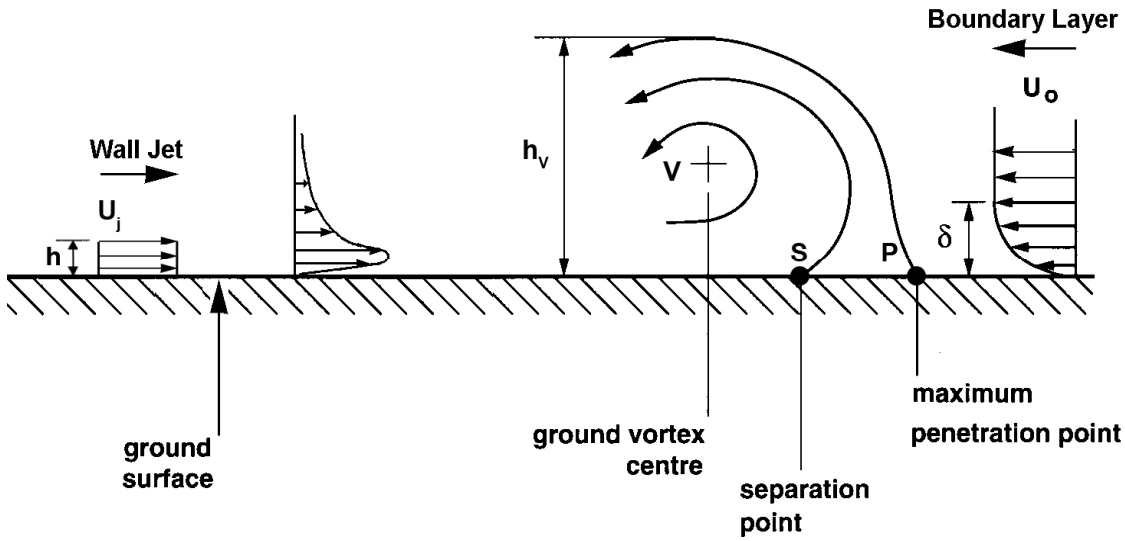

Figure I-9: Flow configuration studied in this work. The wall jet collides with the boundary layer giving rise to the ground vortex, Barata et al. (2009).

The experiments were carried out without the influence of the three-dimensional effects created by the two vortices trailing downstream from the vertical plane of symmetry, where the mean transverse velocity component, *W*, is zero (Figure I-10).

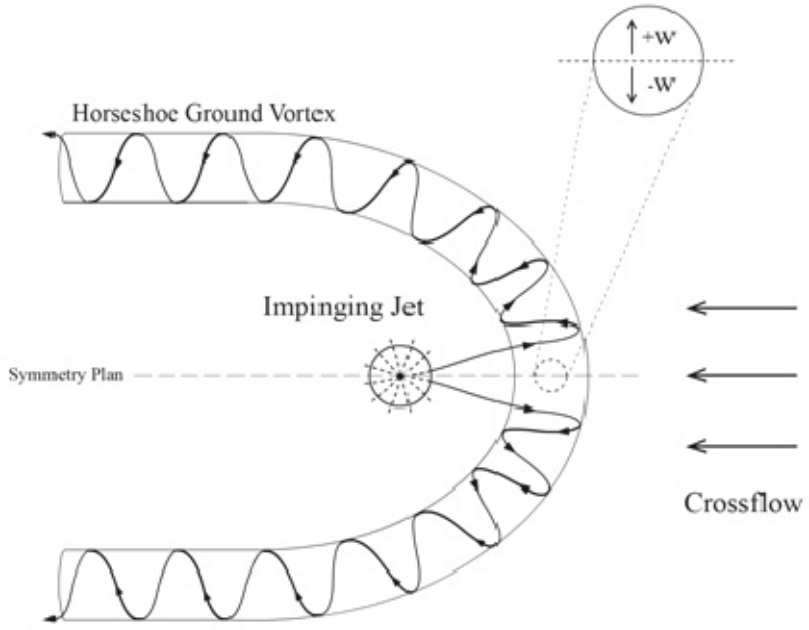

Figure I-10: Flow configuration with the indication of the plane of symmetry, where the mean transverse velocity component, *W*, is zero.

The measurements presented in this study were obtained in the plane of symmetry with the aim to evaluate the turbulent or transient effects near the separation point of the ground vortex. The flowfield was measured by a Laser Doppler Velocimeter, to determine the mean and turbulent characteristics of velocity along the flowfield.

To present a detailed analysis of the flow resultant from the interaction between the wall jet and a boundary layer, the vorticity, turbulent kinetic energy balances and momentum balances were determined, computationally, from the results obtained with the Laser Doppler Velocimeter.

Chapter II: Experimental Method

In this chapter it is described the experimental method used to perform this work. Initially, it is presented the experimental facility used to produce the wall jet and the boundary layer, and also the ground vortex that results from interaction between those two types of flows. The flowfield was characterized using a LDV (Laser Doppler Velocimeter) system and to understand how the measured results were obtained it was made a description of its functional principles and characteristics. The LDV system only permitted to measure the mean and turbulent characteristics of velocity. So, to determine the vorticity, energy balances and momentum balances it was necessary to resolve the respective equations and that are presented in Section 3 of this chapter.

1. Experimental Facility

In this study was used the same experimental facility used by Barata et al. (2005) and it is presented Figure II-1.

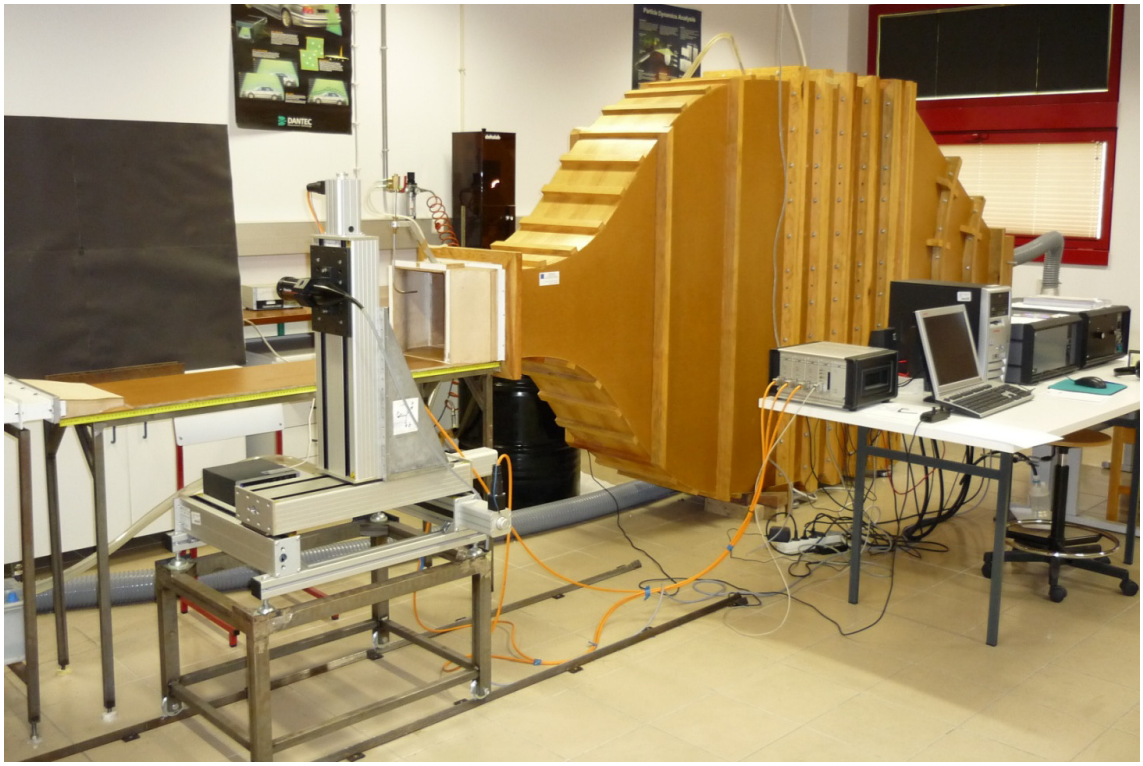

Figure II-1: Experimental facility.

The recommendations of Metha and Bradshaw (1979) for open circuit wind tunnels were followed along all the design process of facility, especially, for the boundary layer part of the flow. However, to optimize the velocity ratio, V_R, necessary for the present study, two convergent nozzles were applied in each exit as diagrammed in Figure II-2. Table II-1 summarizes the main dimensions of the convergent nozzles that were added to the experimental facility.

Table II-1: Dimensions of nozzles added to the experimental facility.

	Dimensions [mm]
Wall jet exit	11,5x280
Boundary layer exit	300x280
Distance between the wall jet and the boundary layer exits	1100

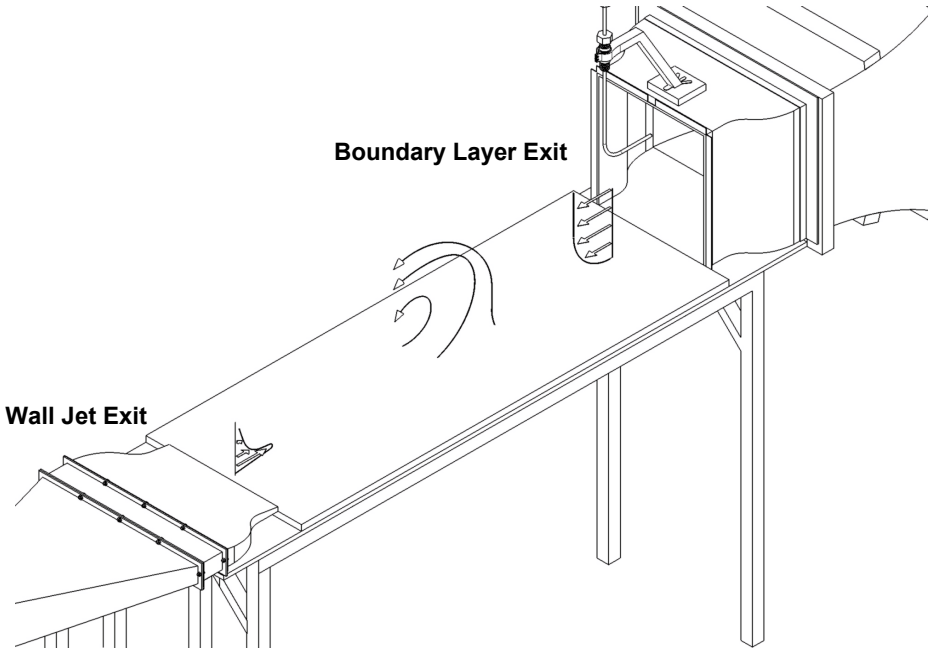

Figure II-2: Convergent nozzles added to the experimental facility.

A fan with a nominal power of *15kW* is controlled by an electronic frequency unit control and drives a maximum flow rate of *3000m^3/h* through the wall jet and the boundary layer exit sections. The flow rate in both exit sections can be controlled by two drawers which permit vary the velocity ratio between the velocity of wall jet and the velocity of boundary layer. The facility also was built to allow variable heights of the wall jet exit from *15 up to 40mm*, but in the present study was used a constant value of *16mm*.

1.1 Experimental Facility Alignment and Calibration

To obtain accurate measurements, after assembly of the new exit nozzles it was necessary to align the all experimental facility components, wall jet and boundary layer exit nozzles, seeding tracers and measurement system. The wall jet and boundary layer exit nozzles were positioned in experimental section aligned with exit sections already used by Barata et al. (2005). The measurement system and respective control system that permits to move the control volume in three directions were positioned staying parallel to the experimental section. These systems moving in parallel sense relative to test section in two railways since the system had not sufficient range to measure all test section from a single point. In relation to the seeding tracers, they were positioned inner of both exits, in a central position, in mode to obtain the best seeding quantity in the plane symmetry of measurements. A guide line was traced in the test section to represent the plane of symmetry, and the alignment was confirmed moving the control volume created by the LDV system over the guide line. Both trajectories were coincident. Due to its technical specifications it was not necessary to proceed to the alignment of LDV system.

Concluded the alignment of experimental facility it was executed the calibration process. This process was performed in function of boundary layer velocity, U_0, and dynamic pressure values for a determined frequency selected on electronic frequency unit control. An interval of frequencies was defined from *25Hz* to *45Hz* with an increment of *2.5Hz* and varying the frequencies in ascending and descending sense it was possible to obtain the relationship between dynamic pressure and boundary layer velocity, measured with a multi-manometer, for the frequency established. According to the results, presented in Figure II-3, it was possible to observe that the variation of boundary layer velocity was between *4.06m/s* which corresponds a frequency of *f=25Hz*, and *7.68m/s* which corresponds to a frequency of *f=45Hz*. In relation to the dynamic pressure its variation occurs between *1.03mm*H_2O and *3.54mm*H_2O for the minimum and maximum frequencies, respectively. During the calibration process since the velocity ratio, V_R, between the boundary layer mean velocity and the wall jet mean velocity, for each frequency selected on unit control, take values near of *0.5*, the position of ground vortex in the test section was not take in account.

Figure II-3 shows the results obtained in the calibration process and it is possible to observe the accuracy of the experimental facility. The similarity of results obtained in ascending and descending variations of frequencies it is an indication that the experimental facility permits to get results with a great accuracy.

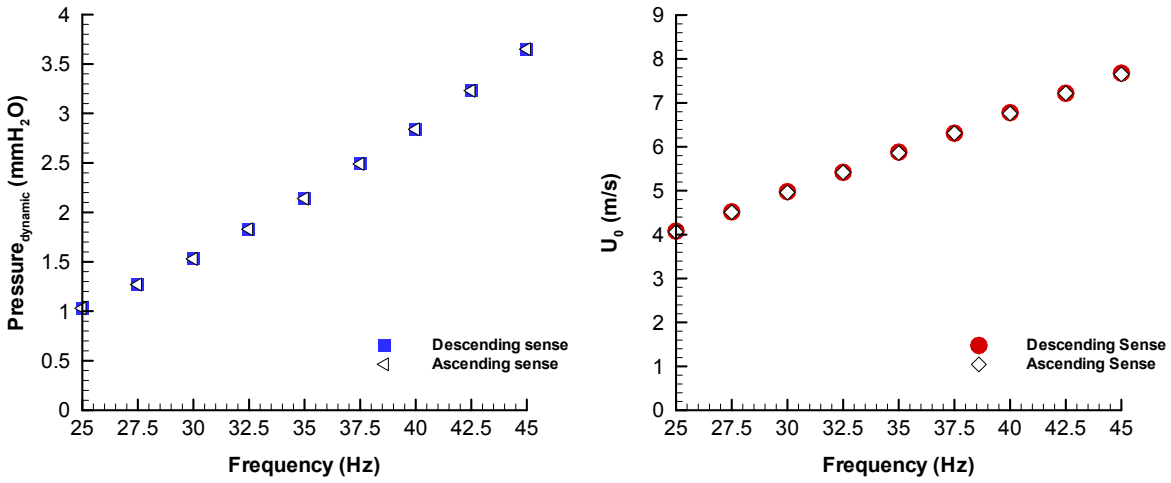

Figure II-3: Experimental facility calibration results, with the boundary layer velocity U_0 and dynamic pressure in function of frequency variation in ascending and descending senses.

1.2 Measurements

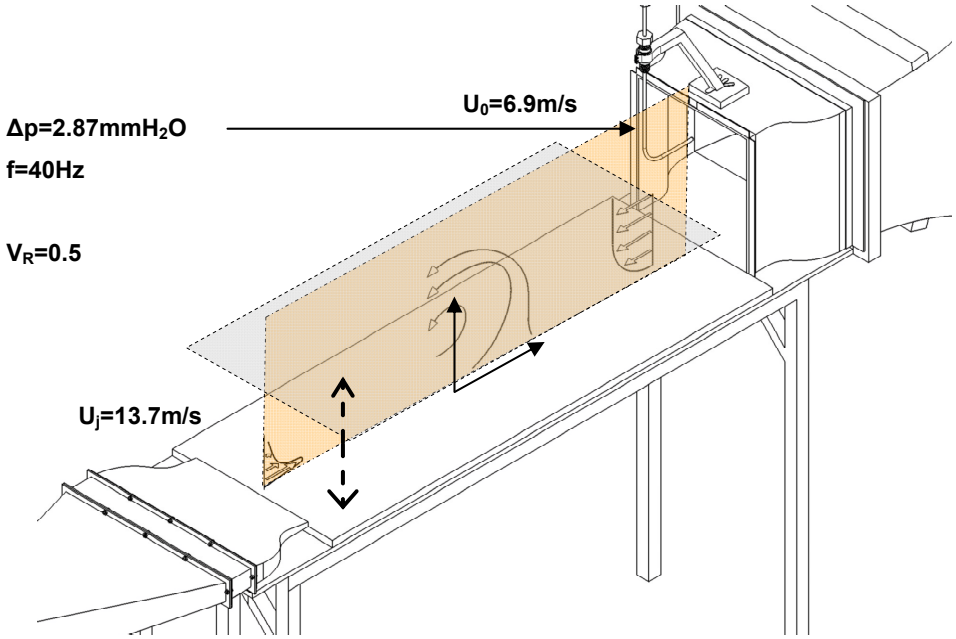

Figure II-4: Experimental facility diagram with experimental conditions of measurements.

As referenced in Chapter I, in the case of a single jet impinging on a ground surface thought a low velocity crossflow the wall jet flows radially from the stagnation point. The result of the interaction between this wall jet and the crossflow is a ground vortex wrapped around the impinging point like a horseshoe vortex. The facility used to perform this work permits to eliminate the three-dimensional effects created by two vortices trailing downstream from the vertical plane

of symmetry which makes data particularly interesting to assess the turbulent or transient effects near the separation point of the ground vortex. In this location the mean transverse velocity component, *W*, is zero. So, the measurements presented in this study were obtained at the vertical plane of symmetry as can be see in Figure II-4 in which it is represented by the yellow plan.

The origin of the horizontal, *X*, and vertical, *Y*, coordinates was taken near the visual maximum penetration point of the wall jet. The *X* coordinate is positive in the wall jet flow direction and the coordinate Y is positive upwards.

Initially, for the interval of frequencies established from *25Hz* to *40Hz*, were measured the velocity profiles of the wall jet and the boundary layer but now with a new increment of *0.5Hz*. According to the results obtained, for this study was choose, as work frequency in the unit control, a frequency near from *40Hz* which permitted to obtain a velocity ratio between the boundary layer and wall jet, V_R, of *0.5* as shows the Figure II-4. To this work frequency corresponded also a dynamic pressure of $2.87mmH_2O$. This value permitted to control the conditions of measurements in test section and was adopted as reference value for the repeatability of measurements, because the determination of dynamic pressure by the micro-manometer is not in function of temperature which permitted for each measurement similar flow characteristics.

According to the measured profiles for the dynamic pressure of $2.87mmH_2O$, Figure II-5, the wall jet had a mean velocity $U_j=13.7m/s$, while for the boundary layer the mean velocity was $U_0=6.9/ms$, which corresponds to the velocity ratio of $V_R=0.5$. These conditions are also represented in Figure II-4.

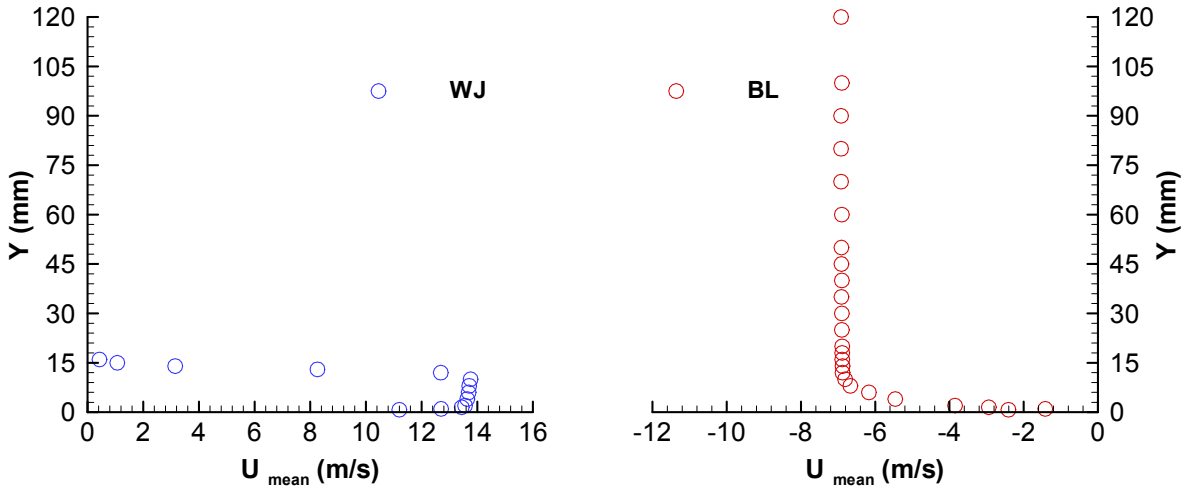

Figure II-5: Profiles of mean horizontal velocity at the convergent nozzle exit of wall jet (left side) and at the convergent nozzle of boundary layer (right side).

These profiles were measured at the exit of each convergent nozzle added to the experimental facility and are in concordance with the characteristic profiles of a wall jet or a boundary layer, respectively. The convergent nozzles permitted to obtain with accuracy the velocity profiles in each exit.

1.3 Accuracy

To keep the statistical errors sufficient low, the number of samples used in the measurements of the mean and turbulent characteristics of velocity was *10 000*. This permitted to obtain statistical errors for the mean and variance values about *1.5%* and *3%*, respectively, according to the analysis of Yanta et al. (1973).

As was mentioned the dynamic pressure was obtained by a Multi-manometer. The Multi-manometer *Furnance FCO 12* permits to measure values between $1mmH_2O$ and $20mmH_2O$, and presents an error about *±1%*.

2. Laser-Doppler Velocimeter (LDV) System

2.1 LDV Functional Principles

The laser anemometers are measurement systems that consist in non-contact optical instruments for the investigation of fluid flow structures in gases as soon as in liquids. This system has as advantage to probe the flow with focused laser beams and also can sense the velocity without disturbing the flow in the measuring volume. It is a system that requires a transparent medium with a sufficient concentration of tracer particles, also denominated seeding, and optical access to the flow.

LDV systems have as functional principle the Doppler Effect. It is a technique based on Doppler shift of the light reflected and/or refracted from a seeding particle that moves on the flow.

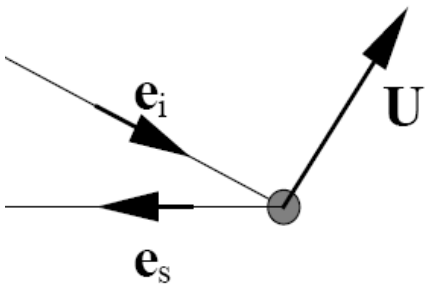

Figure II-6: Light scattering from seeding particle that moves on the flow.

The Figure II-6 shows the Doppler Effect. The seeding particle moves in the flow with a velocity represented by vector U, the unit vectors e_i and e_s describe, respectively, the direction of

incoming and scattered light. The light is scattered in all directions at once, according to the Lorenz-Mie scattering theory, but only is considered the light reflected in the receiver direction. The incoming light has a determinate velocity value *c* and a frequency f_i but since seeding particle is moving it *"sees"* a different frequency f_p, which is scattered towards the receiver. From the receivers' point of view, the seeding particle act as a moving transmitter and the movement introduce additional Doppler-shift in the frequency of the light reaching the receiver. Using Doppler-theory, the frequency of the light reaching the receiver can be calculated and, since, the seeding particle velocity *U* is much lower than the speeding of light, meaning that $\left|\frac{U}{c}\right| << 1$, with the particle velocity *U* being the only unknown parameter, in principle the particle velocity can be determined from measurements of the Doppler-shift.

2.2 LDV Characteristics

In this work the velocity field was characterized using a two-colour (two-component) Laser-Doppler Velocimeter, Dantec Flowlite 2D, which is constituted by a *10mW* He-Ne and a *25mW* diode-pumped frequency doubled Nd:YAG lasers. In both channels a Bragg-cell frequency shifting at f_0*=40MHz* is used to detect the flow reversals, Figure II-7. The half-angle between the beams is *2.8deg* and the scattered light is collected in backward scattering mode with a focal lens of *400mm*. The probe volume with calculated axis dimensions at the e^{-2} intensity locations of *135x6.54x6.53μm* and *112x5.46x5.45μm* was positioned at the required location of measurement using a traversing unit, remotely controlled by the computer software *BSA Flow* in X-Y-Z directions, with a precision of ±*0.25mm*. The Table II-2 resumes the principal characteristics of the Laser-Doppler Velocimeter.

Table II-2: Principal characteristics of the 2D Laser-Doppler Velocimeter.

	He-Ne Laser	**Diode Laser**
Wave length, λ [nm]	633	532
Focal length of focusing lens, f [nm]	400	400
Beam diameter at e-2 intensity [nm]	1.35	1.35
Beam spacing, s [nm]	38.87	39.13
Calculated half-angle of beam intersection, θ	2.78°	2.8°
Fringe spacing, δr [μm]	6.53	5.45
Velocimeter transfer constant, K [MHz/ms-1]	0.153	0.183

The horizontal, *U*, and the vertical, *V*, mean and turbulent velocities together with the shear stress, $\overline{u'v'}$, were determined by a two-channel Dantec BSA F60 processor. The two velocity

components were obtained using coincident velocity samples in both LDV channels. Therefore, the shear stress was calculated for the same seeding particle crossing the measuring control volume. The LDV system is illustrated in Figure II-7.

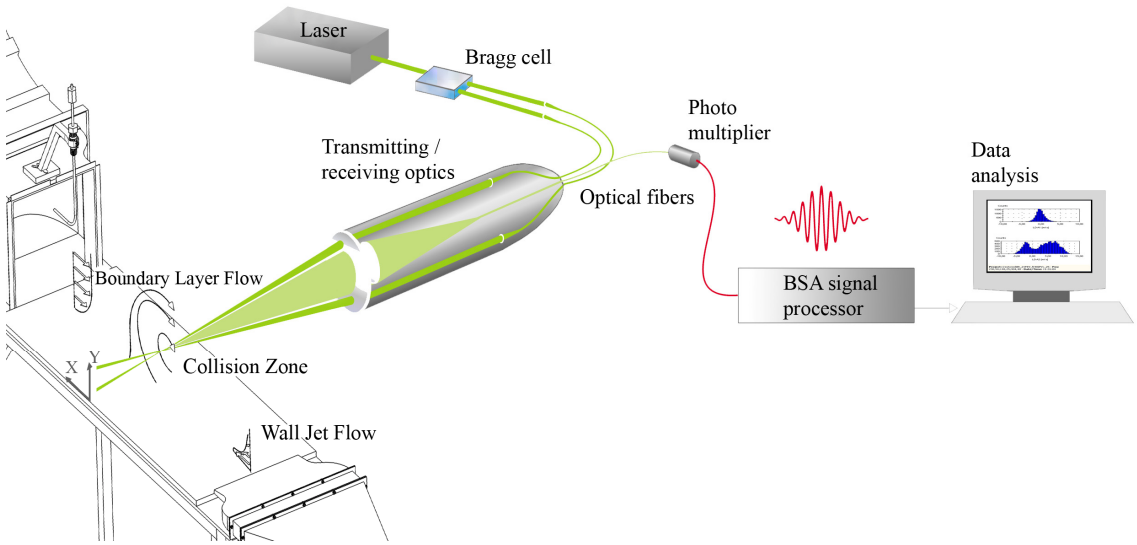

Figure II-7: LDV system diagram.

2.3 Seeding

The LDA technique not measures the velocity of the flow but the velocity of particles suspended in the flow. The seeding particles must be considered to be velocity probes, so it is important to take account some considerations about seeding.

The seeding particles must be small enough to track the flow accurately and large enough to scatter sufficient light in way to permit the photodetector to detect the Doppler frequency. The particles should also be neutrally buoyant in the fluid; in the other words they should have approximately the same density as the fluid itself. The particles should offer the minimum drag to the fluid motion, so their transport in the fluid should be made with the negligence of the body forces. These characteristics have a significant influence in the quality of the signal as well as in the data rate of the measurements. A signal with the least possible noise in the measurements and a good data rate are necessary to obtain results with a good accuracy and it is also important for the treatment of results.

The experimental facility used in this work, Figure II-1, is an open circuit wind tunnel, so the seeding particles are dispersed in the area around the experimental section. Smoke extractors were used to eliminate the seeding in excess, which permitted to improve the work conditions, as for example, to avoid the constant dirtiness of the LDV lens. The seeding used in these experiments was produced by a smoke generator *Techo-Fog Jem* and introduced in a reservoir with operation pressure of *1.5bar*, Figure II-8. After passing trough the reservoir, the seeding was

conducted to seeding tracers of the two wind tunnels. This method permitted to obtain good data rates, in order of *100Hz*, and, also, good validation rates, with values higher to *90%*.

Figure II-8: *Techo-Fog Jem* smoke generator used in the experimental work and the seeding reservoir operating at *1.5bar*.

3. Analysis of Turbulence

The turbulent flows can be described in terms of some statistically average properties, which can be useful to understand the behavior of flow at every instant of time and in average quantities as mean rates of mass, momentum, mean pressure drop or heat transfer. The statistical description was performed using the division of all randomly quantities into mean and fluctuating parts. This method was suggested by Reynolds in 1985 and the equations that govern the distribution of the mean quantities are obtained from the Navier-Stokes equations using the Reynolds averaging technique. These equations are derived assuming that the flow is incompressible, with uniform properties and applied to the bi-dimensional flow that this work aims to study using a Cartesian co-ordinate system description.

To understand the analysis of turbulence using the Reynolds method, it is only considered the horizontal velocity component as an example, but the remarks apply equally to others fluctuating variables. The Reynolds decomposition divides the instantaneous velocity *u* at any location in space into a mean velocity *U* and a fluctuation *u'* about the mean value, Equation 3.1.

$$\underbrace{\underset{\sim}{u}}_{\text{IInstantaneous Value}} = \overbrace{\bar{U}}^{\text{Mean Value}} + \underbrace{\underset{\sim}{u}'}_{\text{Fluctuation}} \quad \textbf{(3.1)}$$

The most common interpretation of the mean velocity is the average with the respect to time of the velocity at any point in the flow field, Equation 3.2, and this is usually referred to as a time-averaged velocity. The Figure II-9 represents a scheme of the method used by Reynolds and applied in this work.

$$U = \lim_{T\to\infty} \frac{1}{T} \int_{t_0}^{t_0+T} u \, dt' \quad \textbf{(3.2)}$$

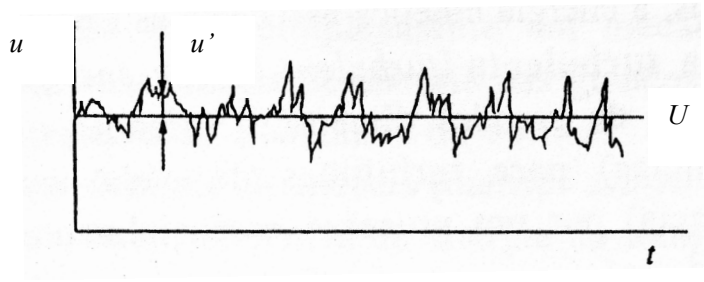

Figure II-9: Fluctuations around the mean value.

3.1 Vorticity

In the bi-dimensional flow the mean vorticity can be estimated from:

$$Vort = \frac{\partial V}{\partial X} - \frac{\partial U}{\partial Y} \quad \textbf{(3.3)}$$

3.2 Momentum Transport Equations

In the case of the bi-dimensional flow in study (*w=0m/*s) with uniform properties and without application of body forces, the momentum transport equations valid for the instantaneous motion in turbulent flow are:

$$\underbrace{\frac{\partial u}{\partial t}}_{\text{Unsteady Term}} + \underbrace{u\frac{\partial u}{\partial X} + v\frac{\partial u}{\partial Y} + w\frac{\partial u}{\partial Z}}_{\text{Convection Term}} = \underbrace{-\frac{1}{\rho}\frac{\partial p}{\partial X}}_{\text{Pressure Gradient Term}} + \underbrace{\upsilon\left(\frac{\partial^2 u}{\partial X^2} + \frac{\partial^2 u}{\partial Y^2}\right)}_{\text{Diffusion Term}} \quad \textbf{(3.4)}$$

$$\frac{\partial v}{\partial t} + u\frac{\partial v}{\partial X} + v\frac{\partial v}{\partial Y} + w\frac{\partial v}{\partial Z} = -\frac{1}{\rho}\frac{\partial p}{\partial Y} + \upsilon\left(\frac{\partial^2 v}{\partial X^2} + \frac{\partial^2 v}{\partial Y^2}\right) \quad \textbf{(3.5)}$$

Only U-momentum equation, Equation 3.4, is considered in detail. The V-momentum equation may be treated in the same way. The Reynolds-averaging technique is applied to the each term of equation.

Beginning for unsteady term:

$$\overline{\frac{\partial(U+u')}{\partial t}} = \overline{\frac{\partial U}{\partial t}} + \overline{\frac{\partial u'}{\partial t}} \quad \textbf{(3.6)}$$

The time-average of a single fluctuating quantity is zero and since in the case of this study the flow was stationary $\overline{\frac{\partial U}{\partial t}}$ is also zero. So the flow is statistically stationary flow $\overline{\frac{\partial u}{\partial t}} = 0$.

In relation to the convection term when applied the Reynolds technique the terms resumes to:

$$U\frac{\partial U}{\partial X} + V\frac{\partial U}{\partial Y} + \overline{u'\frac{\partial u'}{\partial X}} + \overline{v'\frac{\partial u'}{\partial Y}} \quad \textbf{(3.7)}$$

But the second group of terms can be re-written adding the mean of *u'* times the equation of continuity for the fluctuating motion, so:

$$\overline{u'\frac{\partial u'}{\partial X}} + \overline{v'\frac{\partial u'}{\partial Y}} = \frac{\partial \overline{u'^2}}{\partial X} + \frac{\partial \overline{u'v'}}{\partial Y} \quad \textbf{(3.8)}$$

Finally, the convection term of U-momentum equation resumes to:

$$U\frac{\partial U}{\partial X} + V\frac{\partial U}{\partial Y} + \frac{\partial \overline{u'^2}}{\partial X} + \frac{\partial \overline{u'v'}}{\partial Y} \quad \textbf{(3.9)}$$

The pressure gradient term can be re-written using the Reynolds technique in the following form:

$$-\frac{1}{\rho}\frac{\partial}{\partial X}(P+p') = -\frac{1}{\rho}\left(\frac{\partial P}{\partial X} + \frac{\partial \overline{p'}}{\partial X}\right) \quad \textbf{(3.10)}$$

However, the time-average of a single fluctuating quantity is zero, consequently, $\frac{\partial \overline{p'}}{\partial X}$ is also zero, and the pressure gradient term resumes only to $-\frac{1}{\rho}\frac{\partial P}{\partial X}$.

The last term of U-momentum Equation is the diffusion term. In this case it is only considered the first term, the others can be obtained by analogy.

$$\overline{\upsilon \frac{\partial^2 (U+u')}{\partial X^2}} = \upsilon \left(\frac{\partial^2 U}{\partial X^2} + \frac{\partial^2 \overline{u'}}{\partial X^2} \right) \quad \textbf{(3.11)}$$

Since the time-average of a single fluctuating quantity is zero, consequently, $\frac{\partial^2 \overline{u'}}{\partial X^2}$ is zero and the diffusion term resumes in equation to $\upsilon \frac{\partial^2 U}{\partial X^2}$.

Collecting all terms, the U-momentum Equation can be presented in following way:

$$U \frac{\partial U}{\partial X} + V \frac{\partial U}{\partial Y} = -\frac{1}{\rho} \frac{\partial P}{\partial X} + \upsilon \left(\frac{\partial^2 U}{\partial X^2} + \frac{\partial^2 U}{\partial Y^2} \right) - \frac{\partial \overline{u'^2}}{\partial X} - \frac{\partial \overline{u'v'}}{\partial Y} \quad \textbf{(3.12)}$$

Analogy, the V-momentum Equation is represented by:

$$U \frac{\partial V}{\partial X} + V \frac{\partial V}{\partial Y} = -\frac{1}{\rho} \frac{\partial P}{\partial Y} + \upsilon \left(\frac{\partial^2 V}{\partial X^2} + \frac{\partial^2 V}{\partial Y^2} \right) - \frac{\partial \overline{u'v'}}{\partial X} - \frac{\partial \overline{v'^2}}{\partial Y} \quad \textbf{(3.13)}$$

Taking account the equation, some interesting aspects can be verified. The convection terms non-linearity gives origin to extra terms in momentum equation. The Reynolds decomposition isolated the effects of the fluctuations on the mean flow. These extra terms in equation have as physical interpretation of extra stresses whose gradients apply forces which change the mean momentum, and they are denominated by Reynolds stresses. The components $\overline{u'^2}$ and $\overline{v'^2}$ corresponds to the Reynolds normal stresses while the cross-correlation $\overline{u'v'}$ are the shear stresses.

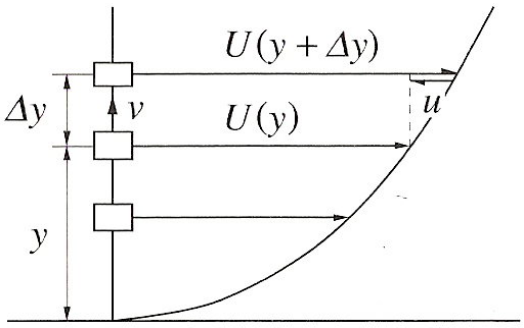

Figure II-10: Production mechanism of the correlation $\overline{u'v'}$.

Figure II-10 can help to understand how the correlations between velocity fluctuations can arise and lead to momentum transport, by other words, cause apparent stresses. Considering a turbulent flow which as the mean shear $\frac{\partial U}{\partial Y}$ as represented in the figure, positive vertical velocity fluctuations (*v'>0*) will carry fluid with low U mean momentum into an area of higher U mean momentum, it is thus likely to cause a negative u fluctuation. For negative vertical velocity fluctuations (*v'<0*), positive *u'* fluctuations will arise and hence in such a flow with $\frac{\partial U}{\partial Y}$ positive $\overline{u'v'}$ is likely to be negative and cause a flux of momentum in the negative vertical direction. So, the last term in Momentum Equation represents the momentum transference between the turbulent field and the mean field.

3.2 Turbulent Kinetic Energy Transport Equation

The Turbulent Kinetic Energy Transport Equation, *k*, obtains adding the separate equations that represent the Reynolds-stress Transport Equations $\overline{u'^2}$ and $\overline{v'^2}$. The last equations govern the distribution in space and time of Reynolds normal stresses and can be obtained from the U-momentum Equation and also using the Reynolds decomposition technique. The Equation 3.14 represents the transport of the normal stress $\overline{u'^2}$:

$$U\frac{\partial\left(\frac{1}{2}\overline{u'^2}\right)}{\partial X}+V\frac{\partial\left(\frac{1}{2}\overline{u'^2}\right)}{\partial Y}=-\left[\overline{u'^2}\frac{\partial U}{\partial X}+\overline{u'v'}\frac{\partial U}{\partial Y}\right]-\left[\frac{\partial\left(\frac{1}{2}\overline{u'^3}\right)}{\partial X}+\frac{\partial\left(\frac{1}{2}\overline{u'^2v'}\right)}{\partial Y}\right]-\frac{1}{\rho}\frac{\partial\left(\overline{p'u'}\right)}{\partial X}+\frac{1}{\rho}\overline{p'\frac{\partial u'}{\partial X}}+$$
$$+\upsilon\left[\frac{\partial^2\left(\frac{1}{2}\overline{u'^2}\right)}{\partial X^2}+\frac{\partial^2\left(\frac{1}{2}\overline{u'^2}\right)}{\partial Y^2}\right]-\upsilon\left[\overline{\left(\frac{\partial u'}{\partial X}\right)^2}+\overline{\left(\frac{\partial u'}{\partial Y}\right)^2}\right] \quad \textbf{(3.14)}$$

A similar equation can be obtained for $\overline{v'^2}$ and adding the two equations, it is obtained the transport equation of *k*, Equation 3.15:

$$\underbrace{U\frac{\partial k}{\partial X}+V\frac{\partial k}{\partial Y}}_{\text{Group 1}}=\overbrace{-\left[\overline{u'^2}\frac{\partial U}{\partial X}+\overline{v'^2}\frac{\partial V}{\partial Y}+\overline{u'v'}\left(\frac{\partial U}{\partial Y}+\frac{\partial V}{\partial X}\right)\right]}^{\text{Group 2}}\underbrace{-\left[\frac{\partial\left(\overline{k'u'}\right)}{\partial X}+\frac{\partial\left(\overline{k'v'}\right)}{\partial Y}\right]}_{\text{Group 3}}\overbrace{-\frac{1}{\rho}\left[\frac{\partial\left(\overline{p'u'}\right)}{\partial X}+\frac{\partial\left(\overline{p'v'}\right)}{\partial Y}\right]}^{\text{Group 4a}}+$$
$$\underbrace{+\upsilon\left[\frac{\partial^2 k}{\partial X^2}+\frac{\partial^2 k}{\partial Y^2}\right]}_{\text{Group 5a}}-\overbrace{\varepsilon}^{\text{Group 5b}} \quad \textbf{(3.15)}$$

Where:

$$k = \frac{1}{2}\left(\overline{u'^2} + \overline{v'^2}\right) \textbf{ (3.16)}$$

$$k' = \frac{1}{2}\left(u'^2 + v'^2\right) \textbf{ (3.17)}$$

$$\varepsilon = \upsilon\left[\overline{\left(\frac{\partial u'}{\partial X}\right)^2} + \overline{\left(\frac{\partial u'}{\partial Y}\right)^2} + \overline{\left(\frac{\partial v'}{\partial X}\right)^2} + \overline{\left(\frac{\partial v'}{\partial Y}\right)^2}\right] \textbf{ (3.18)}$$

The terms in the transport equation may be divided into five groups. The Group 1 represents the special transport of *k* by the mean motion and is denominated by convection. The second group, Group 2, represents turbulence kinetic energy *k*. They represent the rate at which the mean flow is doing work against the Reynolds stresses. The Group 3 represents the spatial transport of *k*. The Group 4 represents pressure interactions, and the last group represents the viscous diffusion of *k* (5a) and the viscous dissipation of *k* (5b).

The Equation 3.15 can be simplified, and the transport of *k* is given by:

$$\underbrace{U\frac{\partial k}{\partial X} + V\frac{\partial k}{\partial Y}}_{\text{Convection Term}} = \underbrace{-\overline{u'^2}\frac{\partial \overline{U}}{\partial X} - \overline{v'^2}\frac{\partial \overline{V}}{\partial Y}}_{\text{Production by Normal Stresses}} \underbrace{-\overline{u'v'}\left(\frac{\partial \overline{U}}{\partial Y} + \frac{\partial \overline{V}}{\partial X}\right)}_{\text{Production by Shear Stresses}} \overbrace{-\frac{\partial}{\partial X}\left(\overline{k'u'} + \frac{\overline{p'u'}}{\rho}\right) - \frac{\partial}{\partial Y}\left(\overline{k'v'} + \frac{\overline{p'v'}}{\rho}\right)}^{\text{Diffusion Term}} - \overbrace{\varepsilon}^{\text{Dissipation Term}}$$

(**3.19)**

Chapter III: Results and Discussion

This chapter contains the analysis and discussion of results, and they will be presented trough four different sections:

1. Mean and Turbulent Velocity Characteristics;
2. Vorticity;
3. Turbulent Kinetic Energy Balances;
4. Momentum Balances.

In first section is presented an analysis about mean and turbulent characteristics of the flowfield, according to the velocity profiles obtained in the measurements with Laser Doppler Velocimeter. The second section presents the results of the mean vorticity along the flowfield. The two last sections present the turbulent kinetic energy and momentum balances, respectively. In all these sections are presented horizontal and vertical profiles with the respective contours. However, the analysis of Sections 2, 3 and 4, will be made according to a flowfield division in three different regions in horizontal, and, also, in vertical direction. This flowfield division is presented in Section 2.

1. Mean and Turbulent Velocity Characteristics

Figure III-1 shows horizontal profiles of the mean horizontal, U, and vertical, V, velocity components, which quantify the mean flow characteristics of the interaction zone resulting from collision between the wall jet and boundary layer. In zone defined by $Y=12mm$ and $Y=30mm$ and $X>0mm$, the mean vertical velocity component, V, presents negative values, but at any other location of the field it is always positive (Figure III-1b). This result indicates the presence of a secondary vortex and, also, reveals that when this secondary vortex disappears, due to the highly curved flow resultant from the collision between the wall jet and the boundary layer, it is removed upwards. From the horizontal profiles of the mean horizontal velocity component (Figure III-1a), it is possible to verify that no significant deflection occurs in the impinging zone defined by $X=0mm$ for $Y<120mm$, but for $Y=90mm$ to $120mm$ the vertical velocity component suffers a substantial increment.

The measured profiles of the mean velocity component, Figure III-1, shows that the center of deflected flow cannot be estimated from the zero values of the horizontal velocity component (Figure III-1a) or the maximum values of the vertical velocity component (Figure III-1b), since does not exit coincidence between them. At $Y=90mm$ and $X=0mm$ the horizontal velocity component is close to zero while the vertical velocity component presents the maximum value at $X=-40mm$, but for $Y=120mm$ the zero value of U occurs only at $X=-120mm$ and the maximum value of V is only displaced, relative to the case of $Y=90mm$, in the crossflow direction.

From this figure it is, also, possible to conclude that the center of the secondary vortex flow is located upstream (in the jet flow sense) the separation point, but, probably, somewhere before the so called maximum penetration point (Figure I-9). This result is an indication that the secondary vortex that was identified may also be present in the others situation, depending of the velocity ratio V_R, the relative size of the clockwise vorticity zone of the wall jet and the counterclockwise vorticity of boundary layer.

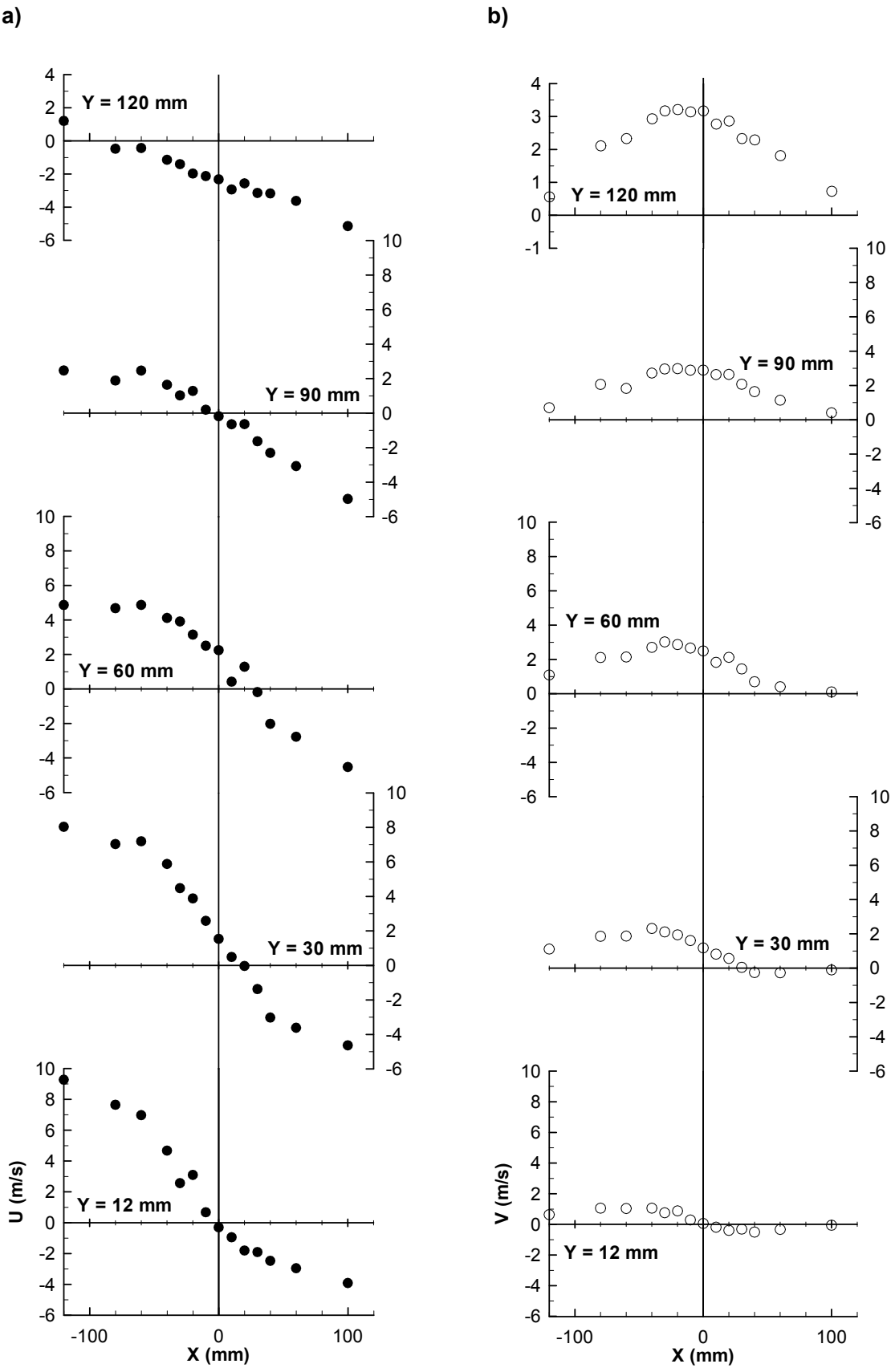

Figure III-1: Horizontal profiles of the mean velocity characteristics for V_R=*0.5*: a) horizontal component, *U*; b) vertical component, *V*.

Figure III-2 shows the horizontal profiles of $\sqrt{\overline{u'^2}}$ and $\sqrt{\overline{v'^2}}$, horizontal and vertical normal stresses, respectively, and quantify the turbulence characteristics of the collision zone between the two opposed flows and, also, of deflected wall jet flow. From this figure can observe that in the collision zone the peaks of $\sqrt{\overline{u'^2}}$ (Figure III-2a) are larger than the corresponding peaks of $\sqrt{\overline{v'^2}}$ (Figure III-2b), which gives rise to high levels of anisotropy with $\frac{\sqrt{\overline{u'^2}}}{\sqrt{\overline{v'^2}}} \approx 2.5$. The horizontal velocity fluctuations present the maximum values in the collision zone, where the mean horizontal velocity component is zero giving rise to extremely high local turbulence intensity values of $\frac{\sqrt{\overline{u'^2}}}{U}$ greater than *100%*. In the case of vertical velocity fluctuations the maximum values only coincide with the zero values of the mean vertical velocity component in the zone close to the ground plane, *Y=12mm*, and the local turbulence intensity is much smaller although can be observed high values such as *40%*, for example, at *Y=90mm* and *X=0mm*. However, these results are misleading to some extent, since, although, the LDV measurements were obtained with a sufficiently high acquisition data rate to detect the possible low frequencies characteristic of these type of instabilities, *5.2±1 Hz*, according to Cimbala et al. (1991), the total time to obtain the *10.000* measurements needed to keep the statistical errors sufficient low (*1.5%* and *3%*, respectively for the mean and variance values for a *95%* confidence interval, Yanta and al. (1973)) allow the averaging of about *20* cycles. As a consequence, instabilities might be being treated as turbulence, which means that large scale coherent and turbulent instabilities might be mixed up.

The Figure III-3 presents the horizontal profiles of shear stress, and they are generally consistent with the direction of the mean flow. Along the vertical direction of the centre of the collision zone, *X=0mm*, the shear stress is positive, which suggests that faster moving elements of the wall jet, *u'>0*, tend to move upwards with the deflected upper side of the boundary layer, *v'>0*. Similarly, the shear stress along the wall jet side of the deflected flow, *X<-40mm*, is negative because the forward movement of fluid particles corresponds to negative vertical velocity fluctuations, *v'<0*. However, far from the ground the location of the zero values of the shear stress occurs in the vicinity of *X=0mm*, for example *X=-40mm* and *Y=90mm*, but do not coincide with the central zone of the deflected flow, which is associated with the maximum of the vertical velocity component where, $\frac{\partial V}{\partial X} = 0$. In the region far from the wall, *Y>25mm*, with the approach of the separation point, *X=0mm*, $\frac{\partial U}{\partial Y}$ increases in the wall jet side (*X<0mm*) and decreases in the boundary layer side (*X>0mm*). Near the wall $\frac{\partial V}{\partial Y}$ and $\frac{\partial U}{\partial X}$ are the most important shear strains, and the magnitude of the peak of the shear stress decreases. This happens because the flow in

this region is submitted to strongly stability curvature that reduces the shear stress more than the turbulent kinetic energy.

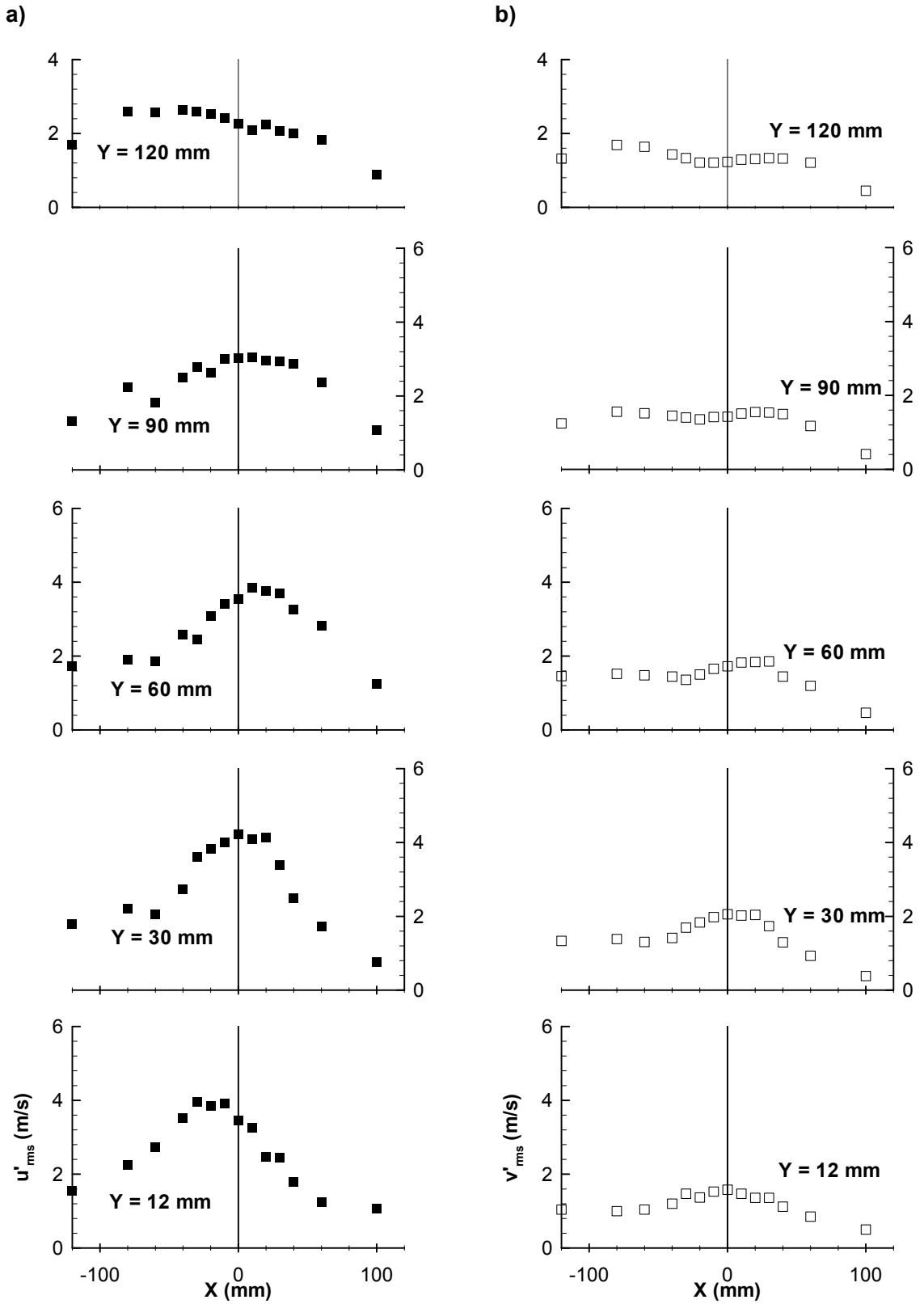

Figure III-2: Horizontal profiles of the turbulent velocity characteristics for V_R=*0.5*: a) horizontal normal stress $\sqrt{\overline{u'^2}}$; b) vertical normal stress, $\sqrt{\overline{v'^2}}$;

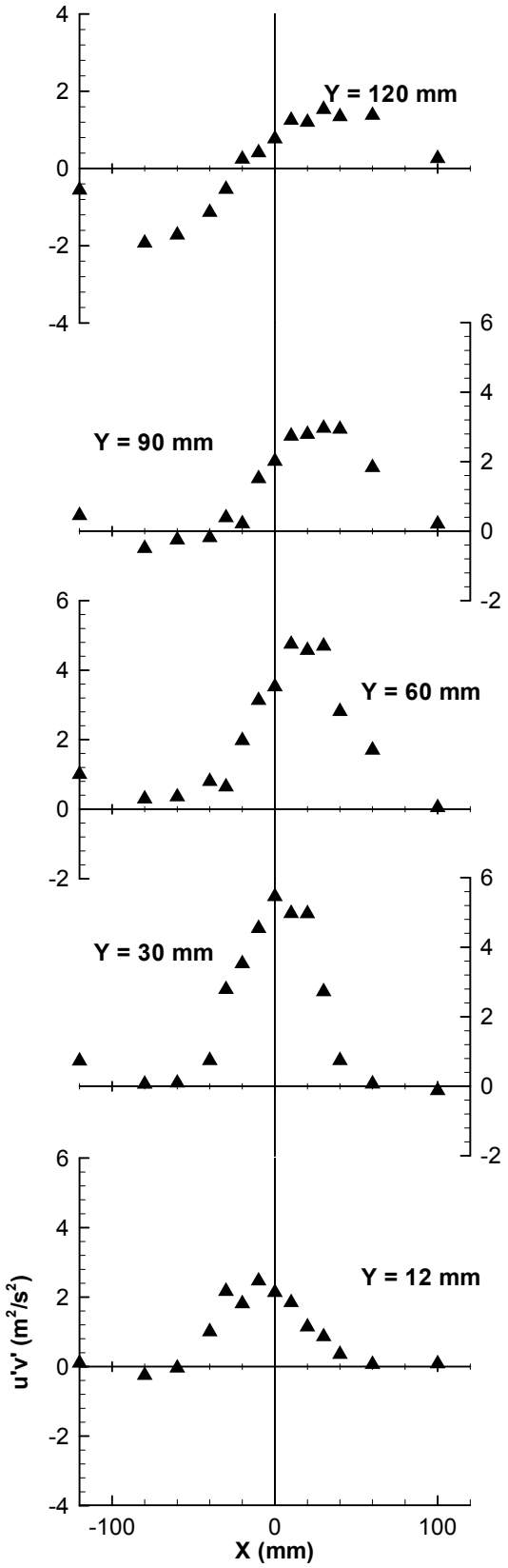

Figure III-3: Horizontal profiles of the turbulent velocity characteristics for V_R=*0.5*: Reynolds shear stress $\overline{u'v'}$.

Figure III-4 presents the vertical profiles of the mean velocity components *U* and *V*, respectively. It is possible to identify the presence of the small vortex in the boundary layer side of the separation point, *X>0mm*, in the profiles at *X=+10mm*, *+30mm* and *+60mm*. The mean vertical velocity component, *V*, (Figure III-4) changes its signs with the distance in relation to the wall, with negative values close to the wall, which reveals the existence of the counterclockwise vorticity in the collision zone. The vorticity phenomena will be presented in detail in the next section of this Chapter.

The vertical profiles of the turbulent velocity characteristics, presented in Figures III-5 and III-6, shows high turbulent intensities in the collision zone near the wall at *X=0mm.*

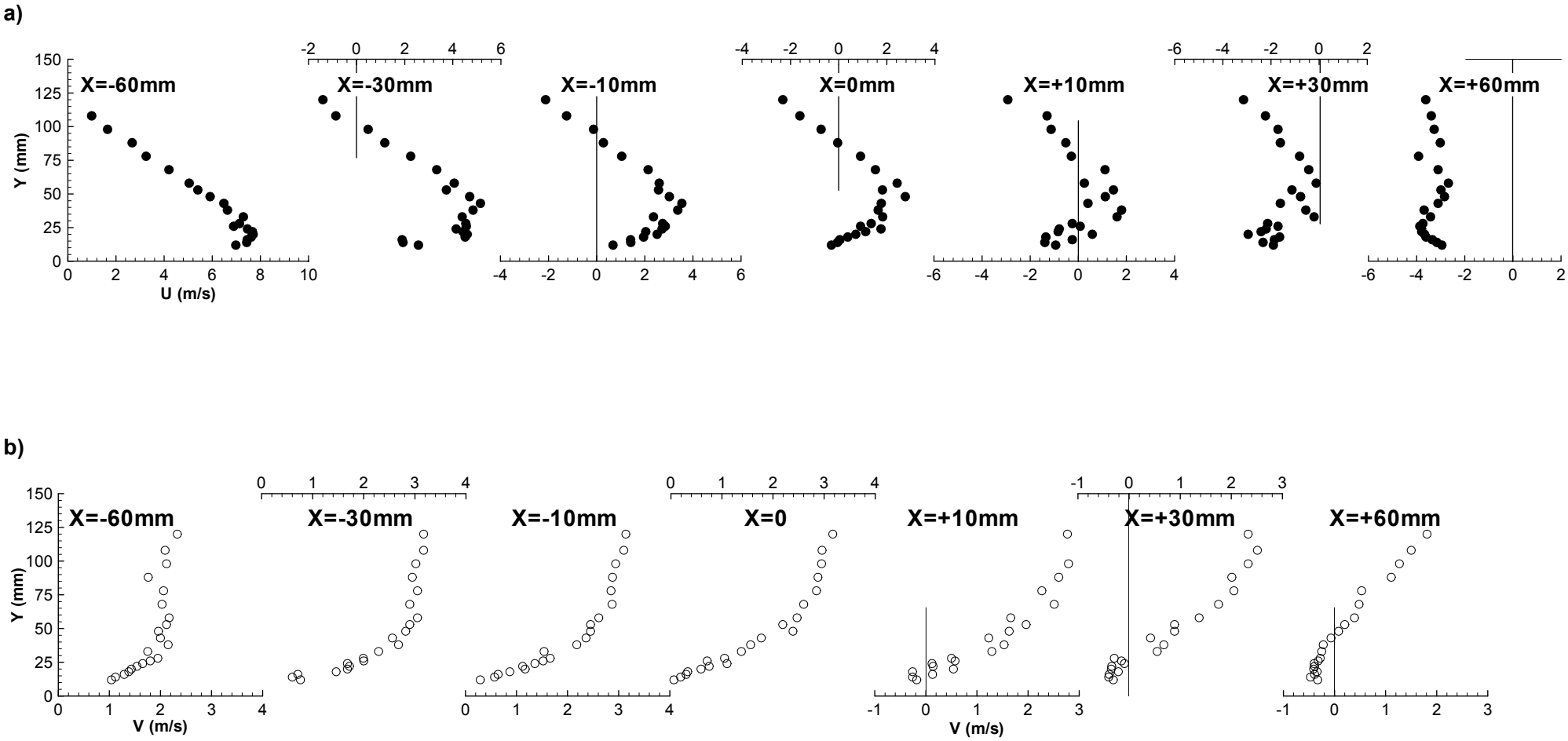

Figure III-4: Vertical profiles of the mean velocity characteristics for V_R=*0.5*: a) horizontal component, *U*; b) vertical component, *V*.

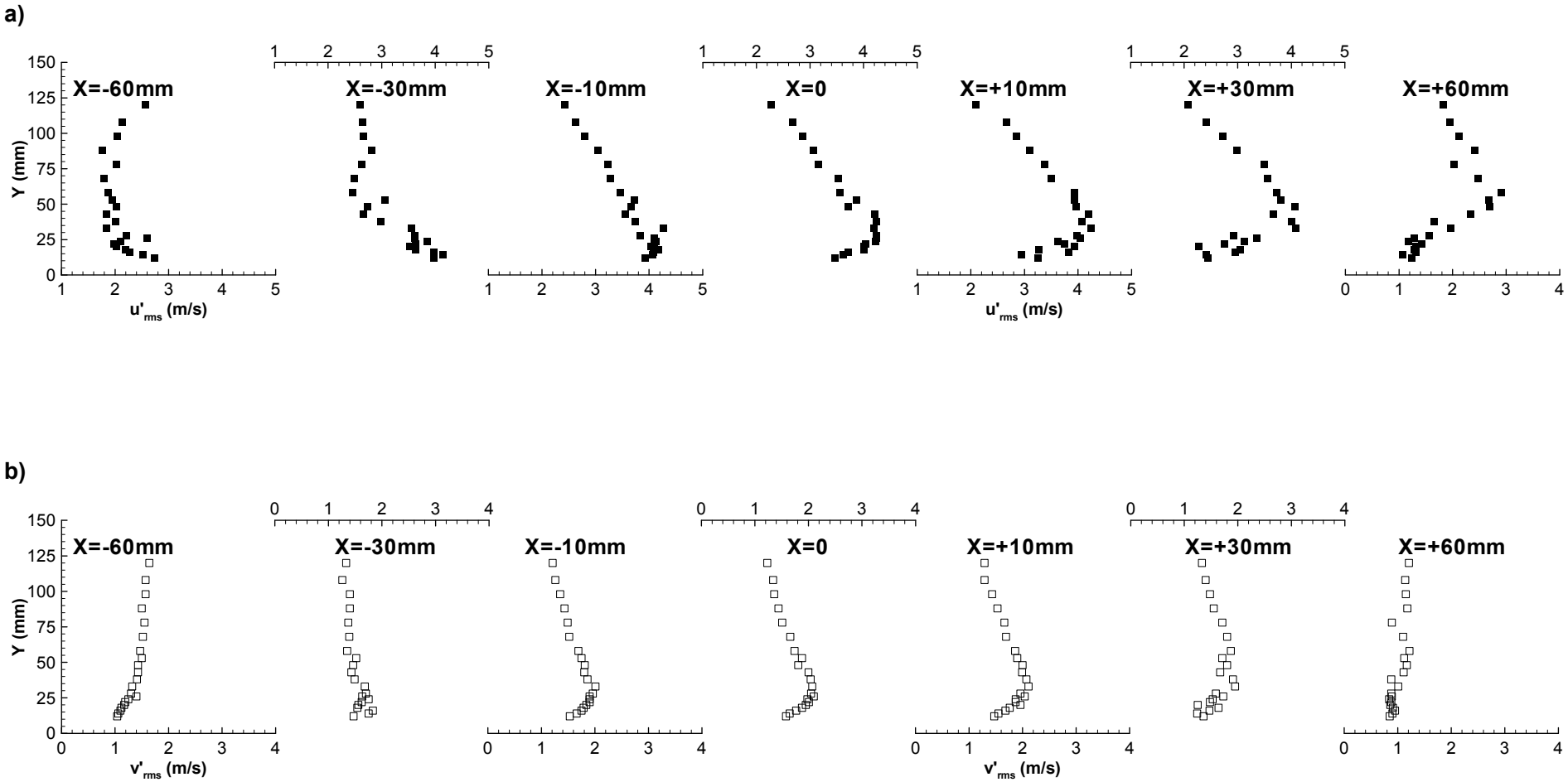

Figure III-5: Vertical profiles of the turbulent velocity characteristics for V_R=*0.5*: a) horizontal normal stress, $\sqrt{\overline{u'^2}}$; b) vertical normal stress, $\sqrt{\overline{v'^2}}$.

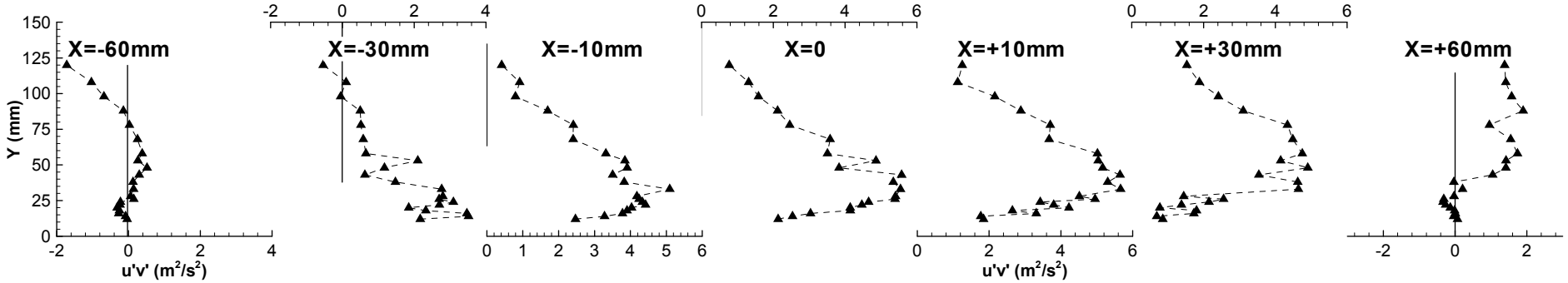

Figure III-6: Vertical profiles of the turbulent velocity characteristics for V_R=0.5: shear stress, $\overline{u'v'}$.

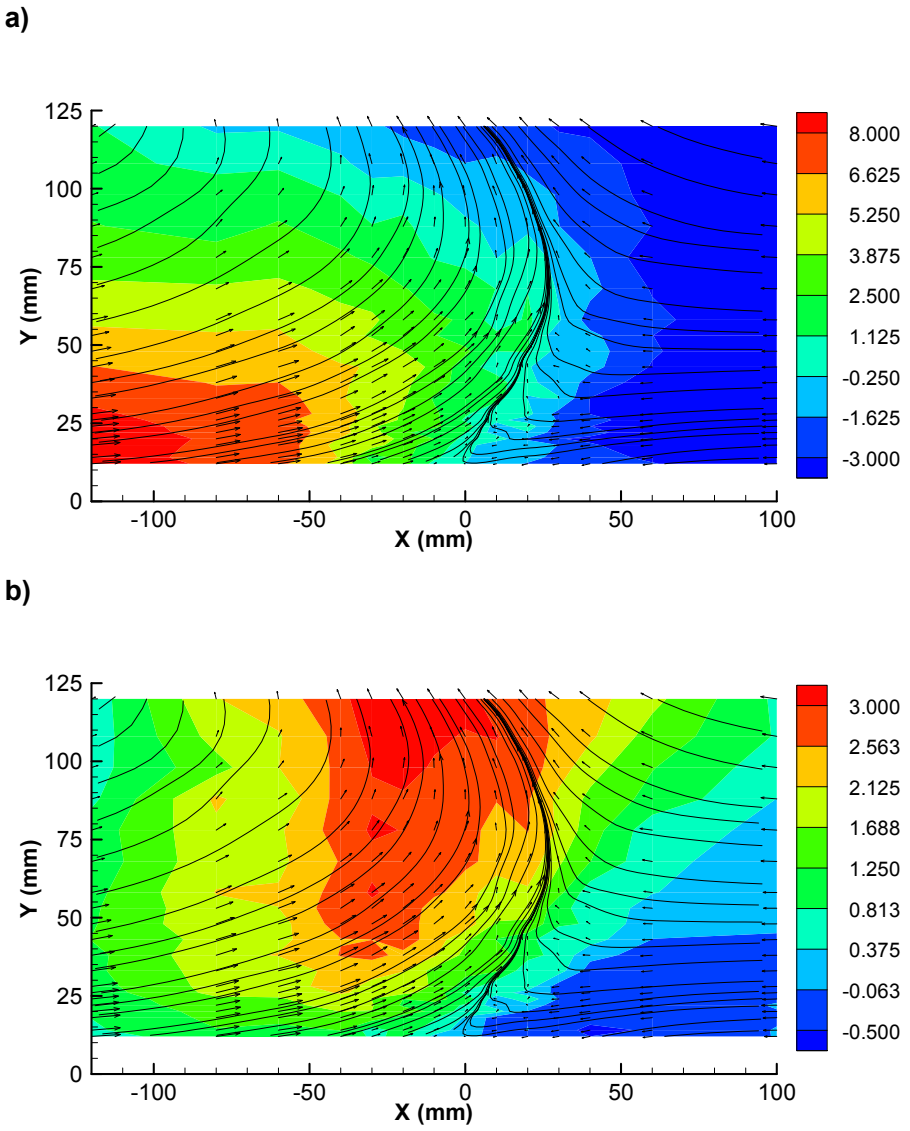

Figure III-7: Contours of the mean velocity characteristics for V_R=*0.5*: a) horizontal component, *U*; b) vertical component, *V*.

Figure III-7 presents the contours of the mean horizontal, *U*, and vertical, *V*, velocity components, which corresponds to the Figures III-7a and III-7b, respectively. The contours and the streamlines were computed from the measured vertical profiles presented from the Figure III-4 to the Figure III-6, and, also, plotted together with velocity vectors. Near the wall and in the boundary layer side, *X>40mm*, the mean vertical velocity component, *V*, is negative, while at any other point of the flowfield it presents positive values. This result confirms the presence of the secondary vortex identified in horizontal profiles of mean vertical velocity component, *V*, for *Y=12mm* and *Y=30mm* (Figure III-1b), which was, also, identified by Barata et al. (2008). According to the results, if this secondary vortex is unstable, it will be swept upwards by the curved flow that results from the collision of the wall jet with the boundary layer.

Figure III-7 b) shows the contours of mean vertical velocity component, *V*, and permits to find the center of the deflected flow that corresponds, simultaneously, to the center of the ground

vortex. It is located in the wall jet side in the zone defined by *-30mm<X<-20mm*, where the mean velocity component *V* presents the higher values. This figure indicates that the center of the secondary vortex flow is located upstream the separation point, with is centre near of *X=45mm*, but probably somewhere before the so called maximum penetration point, the point more far of the ground vortex center with velocity zero. This result indicates that this secondary vortex flow may exist in other situations, depending not only of the velocity ratio V_R, but, also, on the relative size of the clockwise vorticity of the wall jet and the counter clockwisevorticity of the boundary layer.

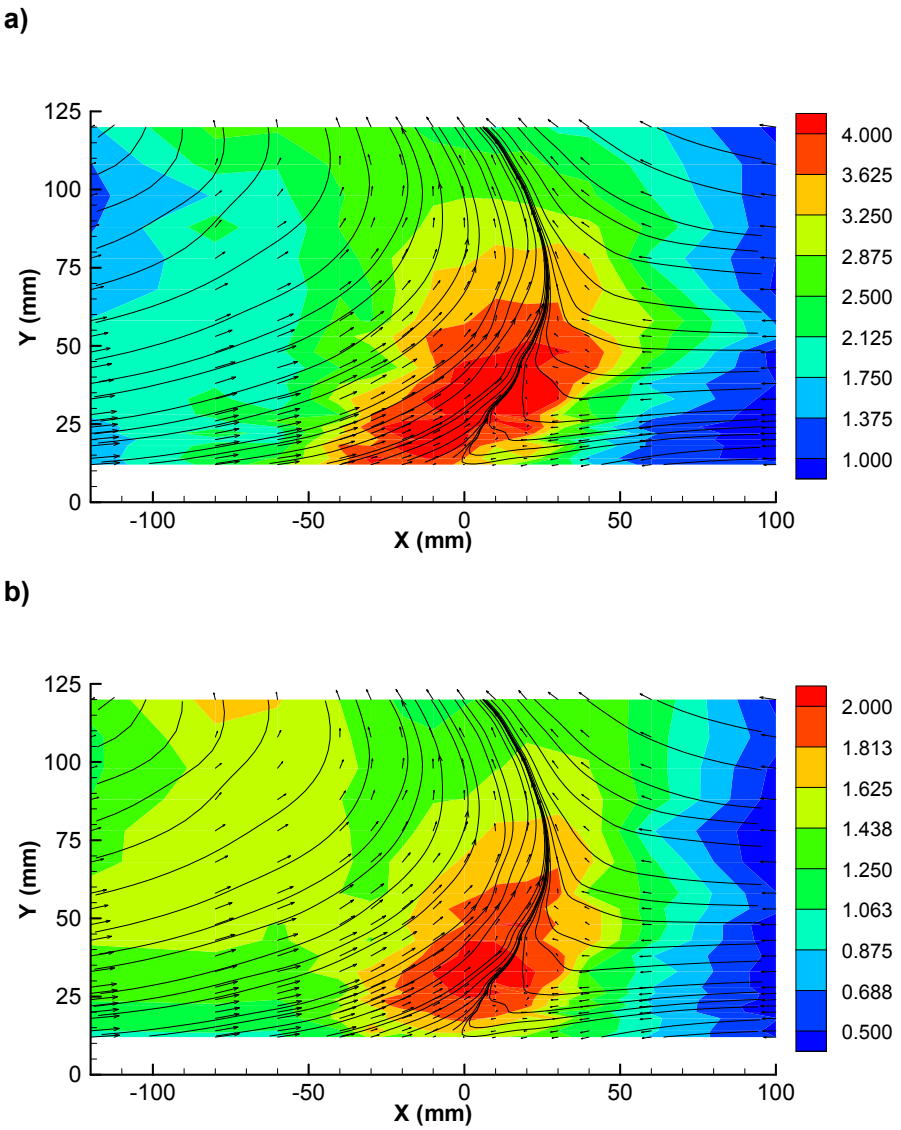

Figure III-8: Contours of the turbulent velocity characteristics for V_R=*0.5*: a) horizontal normal stress, $\sqrt{\overline{u'^2}}$; b) vertical normal stress, $\sqrt{\overline{v'^2}}$.

The contours presented in Figure III-8 shows the turbulent characteristics of velocity in the collision zone and in region of the deflected flow. As was verified in Figure III-2, in the collision

zone the horizontal normal stress peaks, $\sqrt{\overline{u'^2}}$ (Figure III-8a) are larger than the corresponding peaks of vertical normal stress, $\sqrt{\overline{v'^2}}$ (Figure III-8b), indicating the existence of high levels of anisotropy, as was mentioned. The maximum values of the horizontal velocity fluctuations can be observed in the collision zone where the mean horizontal velocity component is zero. This result indicates high local turbulence intensity values of $\frac{\sqrt{\overline{u'^2}}}{U}$ greater than *100%*. In relation to the vertical velocity fluctuations the maximum values coincide with the zero values of the mean vertical velocity component in the vicinity of the wall, so, the local turbulence intensity is much smaller. However, it should be account that the low instabilities might be being treated as turbulence.

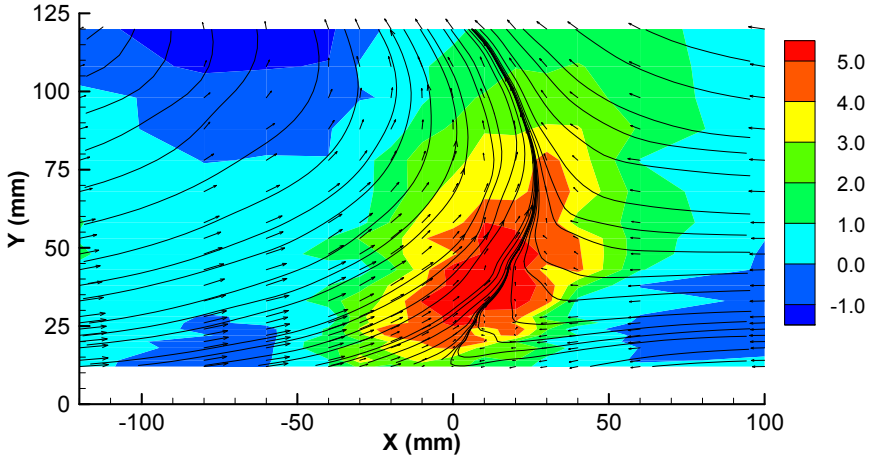

Figure III-9: Contours of the turbulent velocity characteristics for V_R=*0.5*: shear stress $\overline{u'v'}$.

Figure III-9 shows the contours of the turbulent shear stress, $\overline{u'v'}$. As the horizontal profiles presented (Figure III-3), the shear stresses are consistent with the direction of the mean flow. Along the vertical direction of the centre of the collision zone, *X=0mm*, the shear stresses are positive, indicating that the faster moving elements of the wall jet, *u'>0*, tend to move upwards with the deflected upper side of the boundary layer, *v'>0*. Similarly, the shear stress along the jet side of the deflected flow, *-110m<X<-60mm* and *12mm<Y<25mm*, is negative due to the forward movement of fluid particles that corresponds to negative vertical velocity fluctuations, *v'<0*. The figure shows that the location of the zero values of shear stress does not coincide with the central zone of the deflected flow, which is associated with the maximum of the vertical velocity component where $\frac{\partial V}{\partial X} = 0$. Near the wall $\frac{\partial V}{\partial Y}$ and $\frac{\partial U}{\partial X}$ are important shear strains, and the magnitude of the peak shear stress decrease because the flow in this region is subjected to strongly stabilizing curvature, which reduces the shear stress more than the turbulent kinetic

energy. The largest positive values of the shear stress occur near the maximum center velocity of the upwash flow, for *Y>12mm*, with surrounding values both positive in the wall jet or the boundary layer sides.

2. Vorticity

The vorticity of flowfield was calculated from the vertical profiles of mean and turbulent velocity characteristics measured with LDV System. Its analysis will be made using the horizontal and vertical profiles with the respective contours about vorticity.

The horizontal profiles will be presented following a flowfield division in three distinct horizontal regions (Figure III-10).

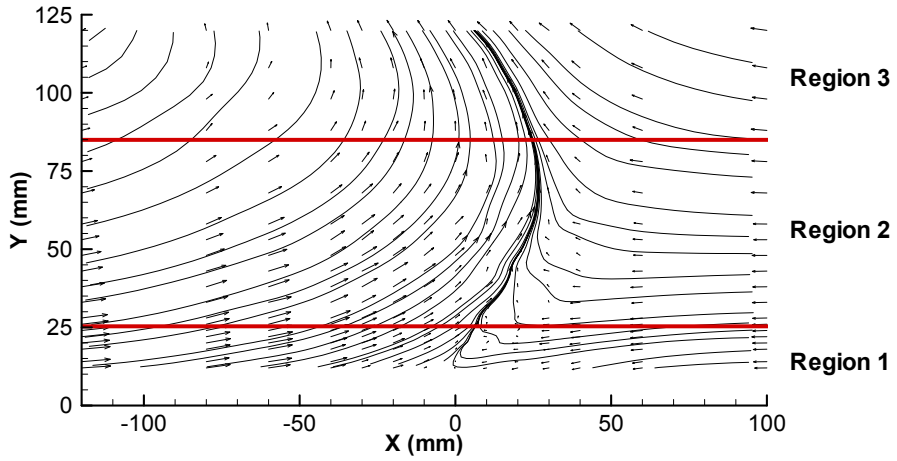

Figure III-10: Flowfield division to analyze the horizontal profiles of vorticity.
Horizontal Region 1: Vicinity of the wall, *Y=12mm* to *Y=25mm*.
Horizontal Region 2: Intermediate region, *Y=25mm* to *Y=85mm*.
Horizontal Region 3: Region far from the wall, *Y>85mm*.

The first horizontal region, Horizontal Region 1, corresponds to the vicinity of the wall and includes the interaction zone resulting from the collision between the wall jet and the boundary layer. The region is defined from the minimum height that the LDV System permitted to measure due to the beam configuration, *Y=12mm*, to the height *Y=25mm*. The second horizontal region, Horizontal Region 2, corresponds to an intermediate region that contains a larger part of the deflected flow resulting from the collision of the two opposed flows, and it is defined from *Y=25mm* to *Y=85mm*. The last region is the Horizontal Region 3 and presents the flow in the longest region from the wall.

The analysis to the vertical profiles, also, will be presented according to a flowfield division in three regions, but now in vertical direction (Figure III-11).

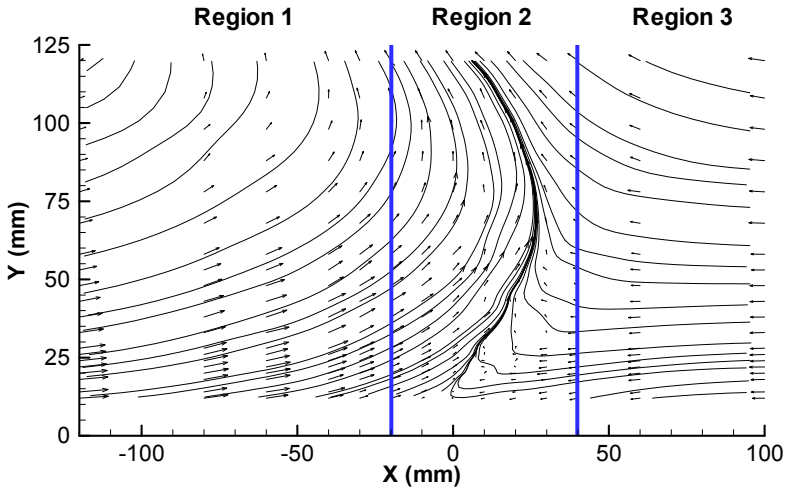

Figure III-11: Flowfield division to analyze the vertical profiles of vorticity.

Vertical Region 1: Region of the wall jet side and that contains the center of the ground vortex.

Vertical Region 2: Region of the collision zone between the wall jet and the boundary layer and that contains the deflected flow resulting from the collision.

Vertical Region 3: Region of the boundary layer side.

The first vertical region, Vertical Region 1, includes, mainly, the wall jet flow and the ground vortex center. It will be expected to understand the behavior of wall jet in the flowfield. The Vertical Region 2 is the most important region of flowfield, since contains the interaction of the wall jet with the boundary layer and, simultaneously, the secondary vortex identified by Barata et al. (2008) and in the horizontal and vertical profiles of mean velocity components *U* and *V* (Figure III-1). This, also, contains the deflected flow, which forms during the collision of the two types of flows presented. The last vertical region, Vertical Region 3, represents the boundary layer side, however, may exists some influence of it's interaction with the wall jet flow. In this region it will be expected to understand the behavior of boundary layer in the flowfield.

Figure III-12 shows the horizontal profiles of vorticity obtained in the vicinity of the wall, Horizontal Region 1 (Figure III-10). The minimum distance that was possible to measure with the LDV system was *12mm*, due to the beams of vertical component. So, under this position it was not possible to quantify the vorticity of wall jet, collision zone and boundary layer. For *Y=12mm* and *Y=14mm* the vorticity presents values near from zero in the collision zone between the wall jet and boundary layer,*-20mm<X<40mm*, and in boundary layer side, *X>40mm*, which does not permit to understand the vorticity sense in this zone. In the wall jet side the vorticity is, mainly, positive with significant positive peaks, *Y=12mm*, *Y=14mm*, *Y=18mm* and *Y=20mm*, indicating the clockwise vorticity in this zone. The horizontal profiles *Y=18mm* and *Y=20mm* present the

maximum value of vorticity, near from *0.5*, *X=-40mm*, and tends to decrease for *X=-30mm* and *X=-20mm*. This result is in concordance with Figure III-19 that shows the vorticity contours in the flowfield obtained with the vertical profiles. For *Y=20mm* and *X=-40mm* exists a zone with a peak of *0.4*, it can be an indication of a small vortex presence. In the collision zone (Figure III-12), defined by *-20mm<X<40mm*, the vorticity is always positive, two significant peaks can be observed, for *Y=18mm* and *Y=20mm*, following a decrement with to approach to the border defined by the boundary layer flow, *X=40mm*, where the flow is influenced mainly by the counterclockwise vorticity of boundary layer.

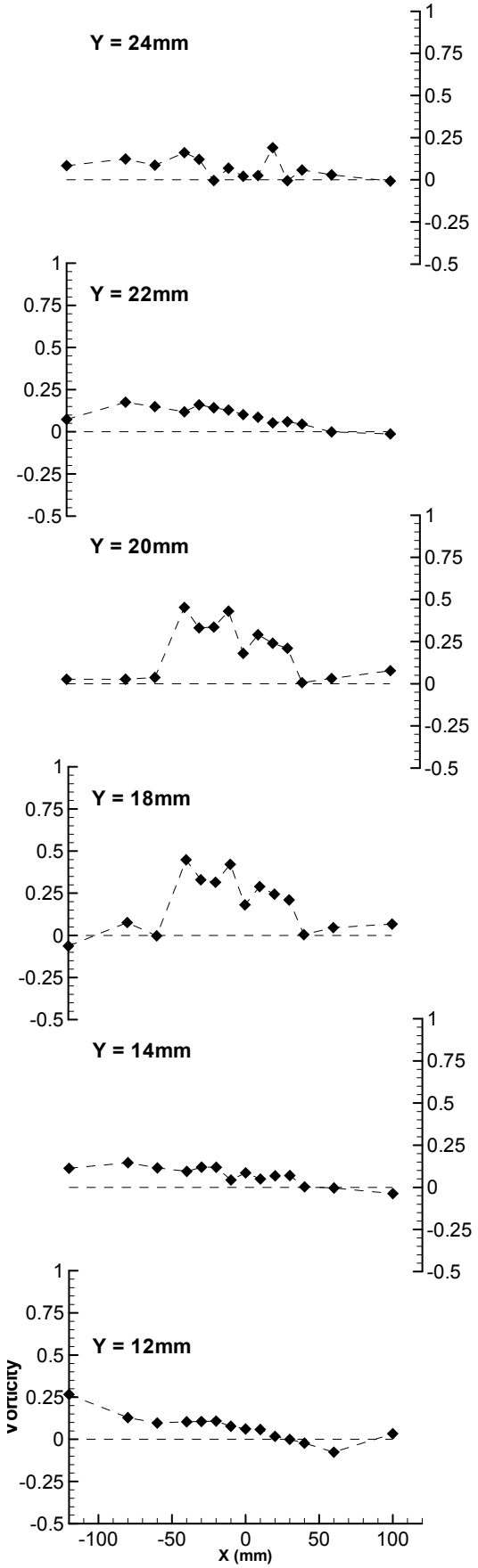

Figure III-12: Horizontal profiles of vorticity in Horizontal Region 1.

Figures III-13 and III-14 show the horizontal profiles obtained in the intermediate region of flow defined by *25mm<Y<85mm*, Horizontal Region 2. From *X=-30mm* to *X=0mm* the results revealed the existence of negative significant peaks and for *X=0mm* it is observed a positive peak, this result can be an indication of a clockwise vortex.

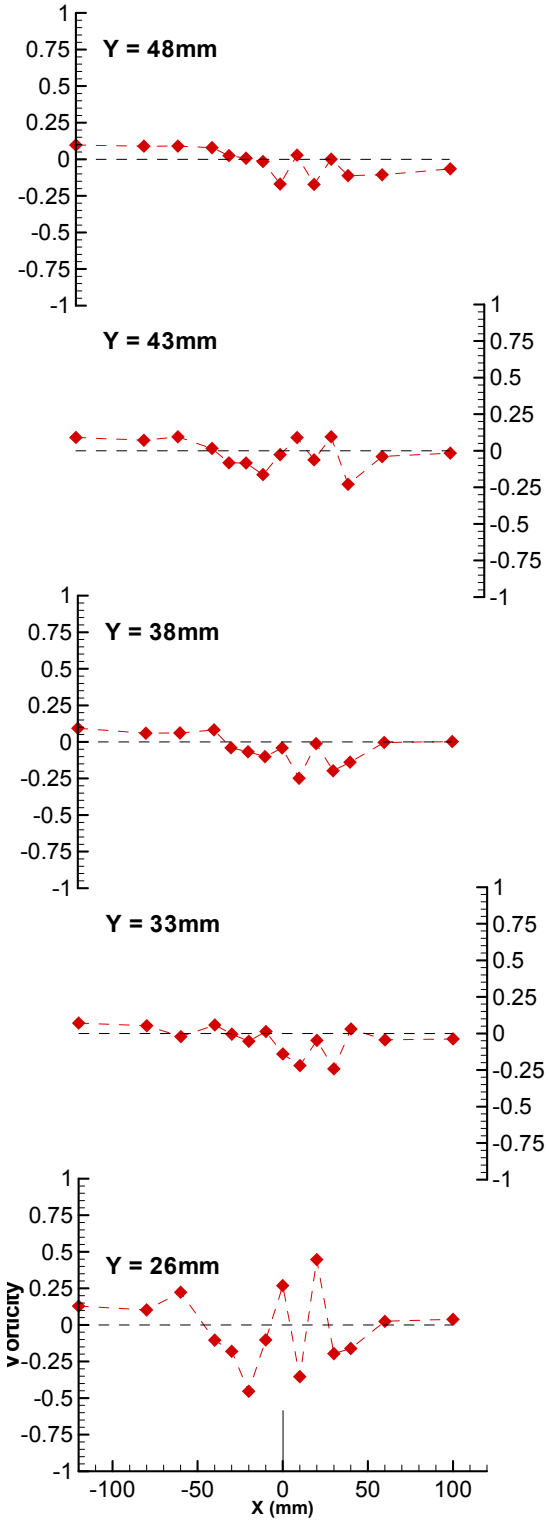

Figure III-13: Horizontal profiles of vorticity in Horizontal Region 2.

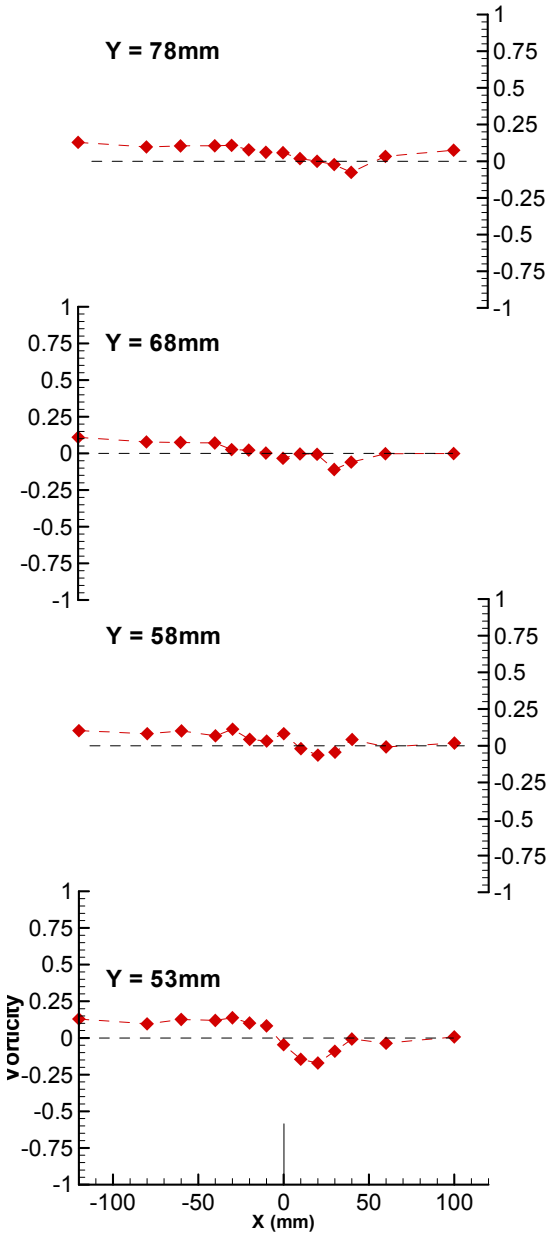

Figure III-14: Horizontal profiles of vorticity in Horizontal Region 2 (continuation).

Figure III-15 shows the horizontal profiles in the region far from the influence of the wall, Horizontal Region 3. However, only the horizontal profiles *Y=88m* and *Y=98mm* present, accurate results, since they were the last profiles measured with LDV System. The other profiles, *100mm<Y<120mm*, were obtained using the quadratic interpolation.

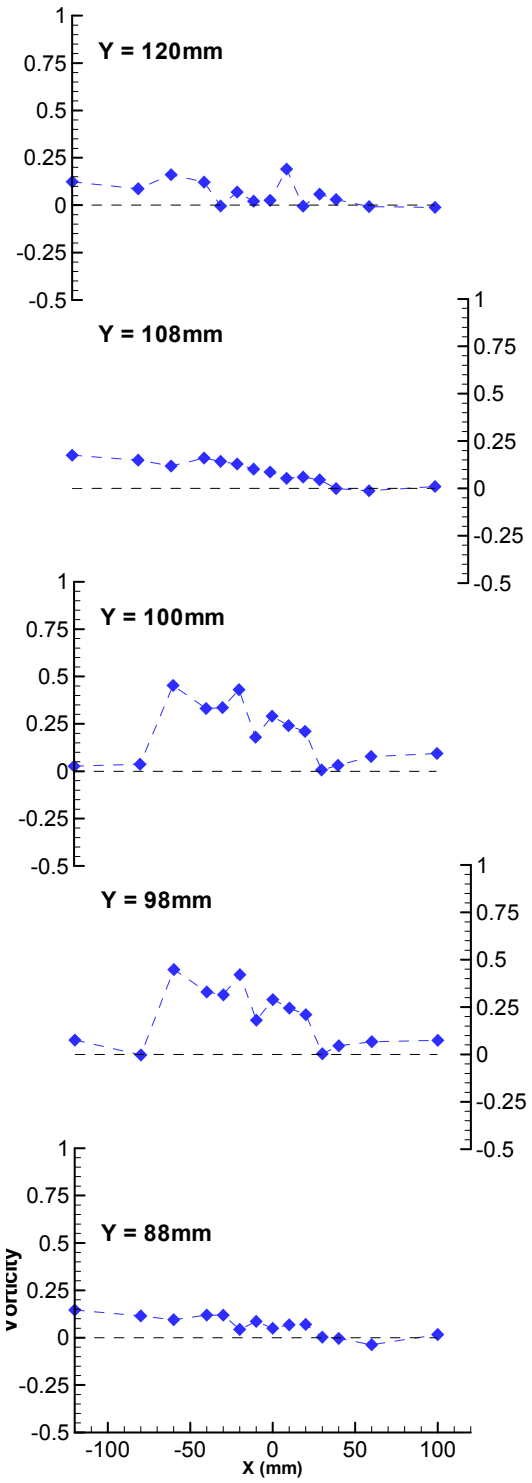

Figure III-15: Horizontal profiles of vorticity in Horizontal Region 3.

Figure III-16 shows the vertical profiles of mean vorticity in the region of the wall jet and the ground vortex. As was, already, mentioned the LDV system only permitted to measure at a minimum distance from the wall of a *12mm*. So, it was not possible to quantify the mean vorticity of wall jet with sufficient accuracy. However, according to a characteristic velocity profile of a wall jet (Figure II-5), it is possible to conclude that the lower part of profile presents vorticity in the

clockwise sense, while the higher part of profile presents vorticity in the counterclockwise sense. This result can be confirmed by the vertical profiles presented in the Figure III-16. The top of wall jet velocity profile is located near from *Y≈20mm*, as show the Figure II-5, and the vorticity, in this location, presents negative values, which corresponds to the counterclockwise sense. Beneath of this position the vorticity values are positive, indicating that this part of wall jets has clockwise vorticity.

The vertical profiles of mean vorticity in the Vertical Region 2 are presented in Figure III-17. This is the most important region of flow because contains, simultaneously, the interaction zone resulting from the collision between the wall jet and the boundary layer, the deflected flow that results from this collision, and, also, the small secondary vortex identified early and by Barata et al. (2008).

As in Vertical Region 1, it was not possible to quantify the mean vorticity immediately after the wall, due to the minimum distance that the LDV System permitted to measure. In the vicinity of wall, *Y<25mm*, the mean vorticity is always positive, with values from *0* to *0.25*, and tends to be zero with the approach to the border of boundary layer region *X=40mm*, which is characteristic of a boundary layer full developed. The vertical profiles of this figure and Figure III-16, suggest that the vortical structures were convected of the wall jet to the deflected flow without a significant variation in its magnitude. The high values of mean vorticity near the wall can be explained by the rapid decrease of the horizontal velocity component in vertical direction, due to the boundary layer presence, and, which corresponds to a high negative value of $\frac{\partial U}{\partial Y}$, while the vertical velocity component is, practically, constant in horizontal direction. So, in this zone are present high positive values of mean vorticity, indicating vorticity in clockwise direction.

According to the Figure III-17, the vorticity decays in the region of defected flow - *10mm<X<30mm*, which can be verified in the horizontal intermediate region defined by *25mm<Y<80mm*. A change in the vorticity sense is indicated by the negative peaks present in the profiles, so in the region near from the beginning of flow deflection the vorticity is, mainly, in the counterclockwise sense.

The Vertical Region 2 also contains the small secondary vortex identified by Barata et al. (2008) and, also, in this work. According the authors, this small vortex is located upstream the separation point, in the jet flow sense, near from *X=45mm* as was indicated by the horizontal profiles of Figure III-1. In this region the mean vorticity is negative, indicating that this small secondary vortex has the counterclockwise sense (Figure III-19). The vorticity sense of this small secondary vortex and the boundary layer is the same. The results are in concordance with the results of Silva et al. (2009b). However, it is important to indicate that in spite of both, the small secondary vortex and boundary layer, having the same sense, the small vortex can not be transported by the deflected flow resulting from the interaction between the wall jet and the boundary layer, since the vertical component is always positive over the vortex.

The Figures III-16 and III-17, indicates that the vortical structures are convected by the wall jet to the deflected flow. Cimbala et al. (1991) attribute the growth of the ground vortex trough the vortexes present in shear layers. These vortexes are transported by the wall jet giving origin to the growth of ground vortex.

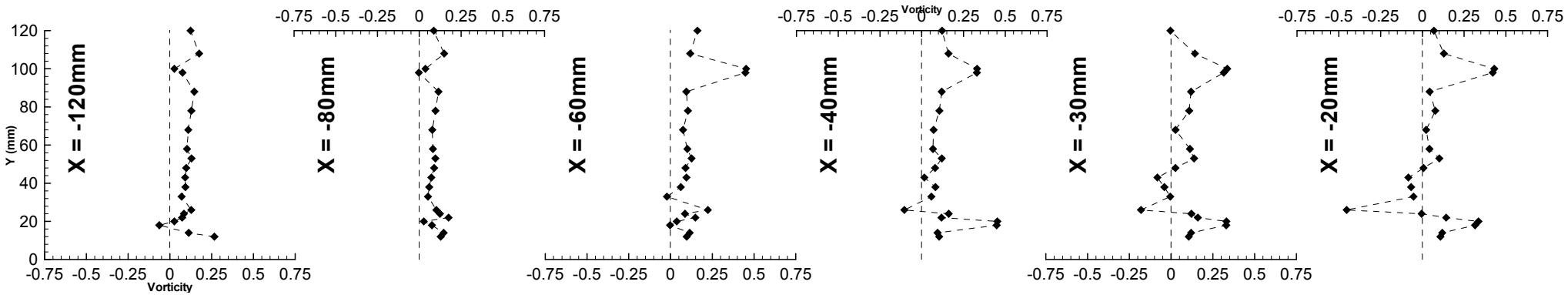

Figure III-16: Vertical profiles of mean vorticity in Vertical Region 1 (wall jet side).

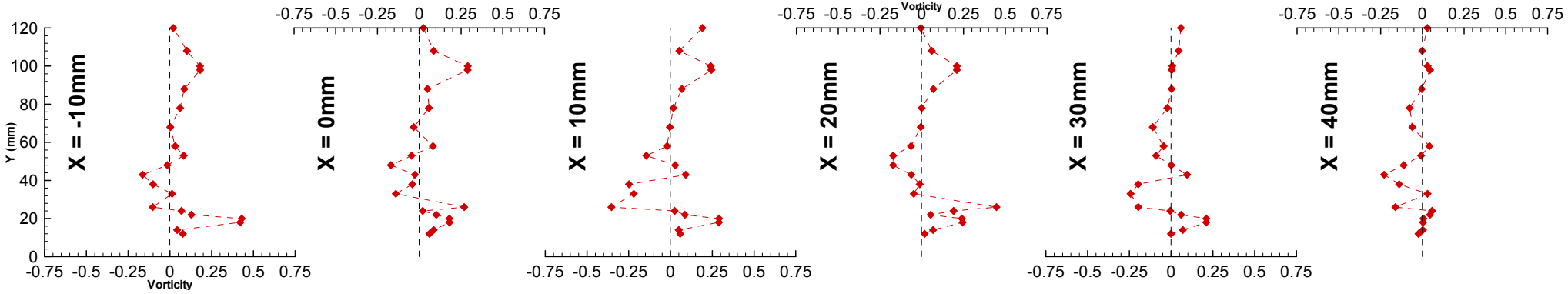

Figure III-17: Vertical profiles of mean vorticity in Vertical Region 2 (collision and deflected flow zones).

Figure III-18 shows the vertical profiles of mean vorticity obtained in Vertical Region 3. This region represents the boundary layer side, although may exist some influence of it's interaction with the wall jet flow. Due to the limitation of LDV System in to measure near the wall, *Y<12mm*, it was not possible to determine the mean vorticity, with sufficient accuracy, in the inner layer of the turbulent boundary layer. However, according to the vertical profiles presented in the figure, the boundary layer tends to present vorticity in counterclockwise sense, which can be identified from negative values for *Y<20mm*, and that can be observed in horizontal profiles of Figure III-1, *Y=12mm* and *Y=30mm*, where the two components of velocity are both negative. In relation to the outer layer of the boundary layer that corresponds to the zone where the boundary layer is totally developed, *Y>25mm*, the mean vorticity presents values near from zero. The term $\frac{\partial V}{\partial X}$ has not significant influence in the vorticity, since in a boundary layer the vertical component of mean velocity maintains, practically, constant. The same happens with term $\frac{\partial U}{\partial Y}$ in this zone of boundary layer.

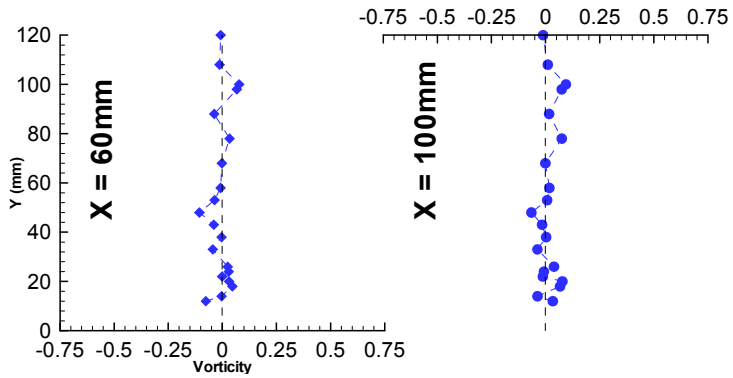

Figure III-18: Vertical profiles of mean vorticity in Vertical Region 3 (boundary layer side).

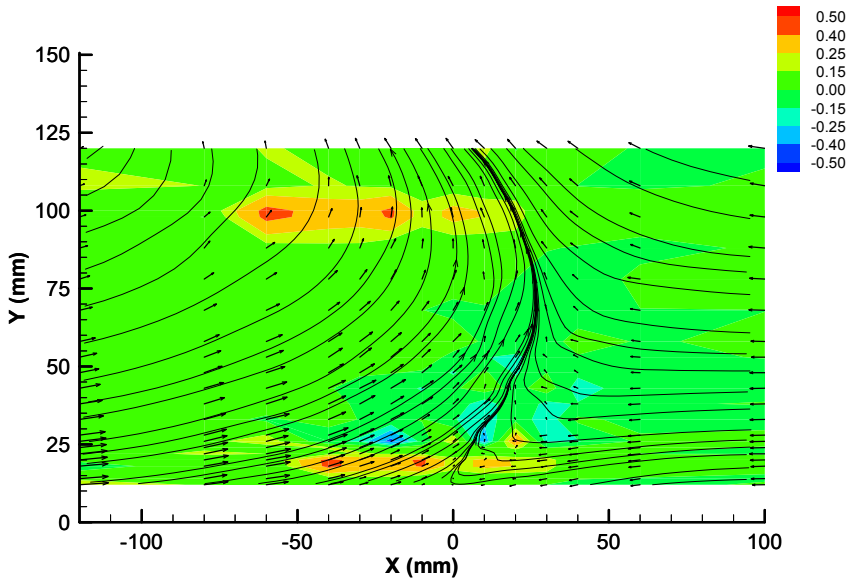

Figure III-19: Contours of mean vorticity.

3. Turbulent Kinetic Energy Balances

This section presents the turbulent kinetic energy balances obtained in vertical plane of symmetry of the flow, where the derivatives $\frac{\partial}{\partial Z}$ and the shear stress $\overline{u'w'}$ and $\overline{v'w'}$ are zero. So, the transport equation of *k*, also, presented in Section 3.2 of the Chapter 2, to determine the energy balances was the following way:

$$\underbrace{U\frac{\partial k}{\partial X}+V\frac{\partial k}{\partial Y}}_{\text{Convection Term}}=\underbrace{-\overline{u'^2}\frac{\partial \overline{U}}{\partial X}-\overline{v'^2}\frac{\partial \overline{V}}{\partial Y}}_{\text{Production by Normal Stresses}}\underbrace{-\overline{u'v'}\left(\frac{\partial \overline{U}}{\partial Y}+\frac{\partial \overline{V}}{\partial X}\right)}_{\text{Production by Shear Stresses}}\overbrace{-\frac{\partial}{\partial X}\left(\overline{k'u'}+\frac{\overline{p'u'}}{\rho}\right)-\frac{\partial}{\partial Y}\left(\overline{k'v'}+\frac{\overline{p'v'}}{\rho}\right)}^{\text{Diffusion Term}}-\underbrace{\tilde{\varepsilon}}_{\text{Dissipation Term}}$$

(3.19)

The derivatives were obtained using the quadratic interpolation from the values measured by the LDV System in the vertical plane of symmetry. The convective term was calculated by the approximation of *k* by $\frac{3}{4}\left(\overline{u'^2}+\overline{v'^2}\right)$ and the sign corresponds to the Equation 3.19, which has the signification of turbulent kinetic energy local gain when presents negative values and turbulent kinetic energy local loss when presents positive values. The production of turbulent kinetic energy by normal stresses and production by shear stresses are exact values and when they present positive values they represents kinetic energy gain. The terms of diffusion and dissipation are aggregated in the equation and will be identified in the horizontal and the vertical profiles as other terms. The diffusion and dissipation terms are obtained by difference of other equation terms,

since it was not possible to measure during the execution of the experimental work. Their sign has the same signification that in the case of the production terms. Negative values indicate kinetic energy loss.

The analysis of kinetic energy balances is made using horizontal and vertical profiles with respective contours, and following the same flowfield division used in the vorticity analysis (Figures III-10 and III-11).

Figure III-20 shows the horizontal profiles of turbulent kinetic energy in the region near of the wall, Horizontal Region 1. The convective term is always near of zero from the wall jet side to the boundary layer side with a little negative variation in the zone corresponding to the collision between wall jet and boundary layer ($X=-20mm$ to $X=40mm$). This result corresponds to a small local loss of turbulent kinetic energy in this zone that tends to decrease with the increment of distance in relation to the wall. At $Y<24mm$ the convective term tends to be zero in the collision zone defined from $X=-20mm$ to $X=40mm$. Between $Y=12mm$ and $Y=20mm$ it can be observed significant variations in remaining equation terms of turbulent kinetic energy. In the collision zone, the production by shear stresses is always higher than the production by normal stresses. This can be explained by the high values of shear stresses that occur in this zone, Figure III-1, $Y=12mm$ and $Y=30mm$. In the vicinity of wall, $Y=14mm$ and $Y=12mm$, there is, also, a significant production by normal stresses, because of high values of normal stresses resulting from horizontal velocity fluctuations, but this contribution has tendency to decrease $20mm<Y<22mm$. In the collision zone, the production of turbulent kinetic energy by shear stresses tends to be balanced by the loss of turbulent kinetic energy by diffusion and dissipation. However, the magnitude of peaks, of each these terms, tends to decrease with the increment of distance in relation to the wall. According to these profiles, in the region defined by $-20mm<X<40mm$ the production of turbulent kinetic energy is, essentially, due to normal stresses.

In the wall jet side the production of turbulent kinetic energy is nearly zero, but some variations occurs for the heights of $Y=18mm$ and $Y=22mm$. There is a small local loss by convection, and a significant loss by the other terms term of equation, that contrary to remaining flow ($X>-60mm$) is balanced by the production by the shear stresses. This region corresponds to the boundary between the wall jet and the free flow, and the interaction between them can cause such variations. In the boundary of collision zone $-60mm<X-20mm$ there are signal variations of the production by shear stresses accompanied, reciprocally, by the other terms term, in spited of the tendency of balance between them continue to occur. Theses variations of signal can be attributed to the instabilities of the flow, due to its deflection and the collision between the wall jet and the boundary layer. In relation to the boundary layer side there is a small local loss of turbulent kinetic energy by convection that tends to be zero far away from the wall.

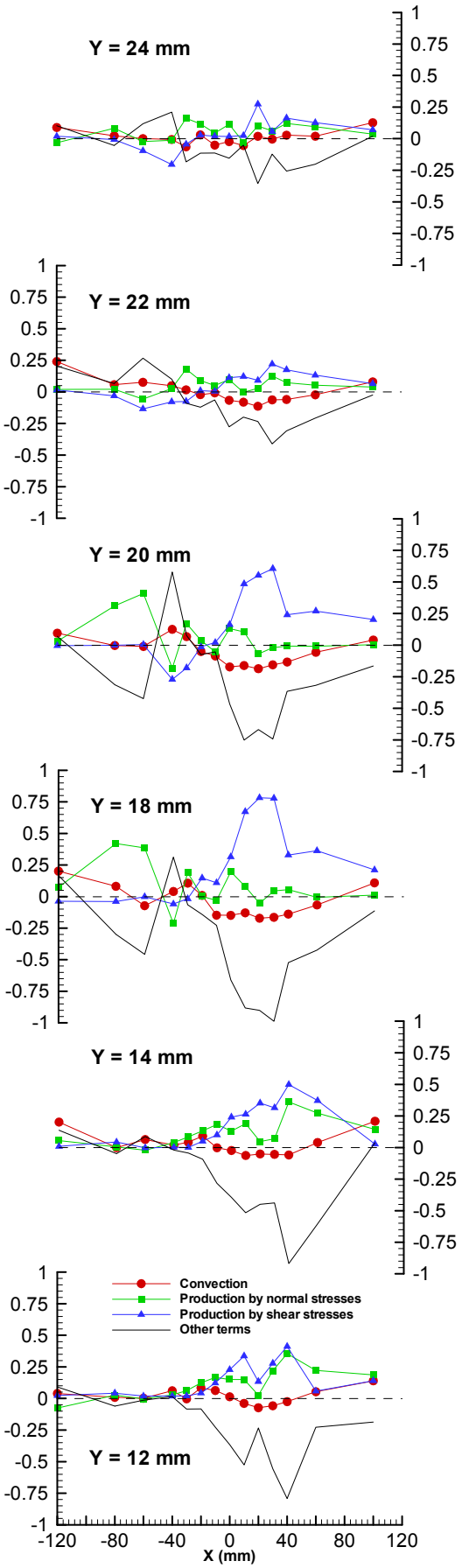

Figure III-20: Horizontal profiles of turbulent kinetic energy in Horizontal Region 1.

Figure III-21 and III-22 show horizontal profiles of turbulent kinetic energy in the intermediate region, Vertical Region 2. The production of kinetic energy by convection remains near to zero from the wall jet side to the boundary layer side. This region is located out of wall jet influence, so the turbulent kinetic energy is practically zero in the wall jet side, *-120mm<X<-80mm*. The same result is obtained in the boundary layer side. The kinetic energy associated with the boundary layer is more intense in the proximity of the wall (Figure III-20, *-12mm<Y<22mm*) and tends to be zero far from the wall (*Y>26mm*). It is in the region of deflected flow, *-20mm<X<40mm*, resulting from interaction from the wall jet with the boundary layer, that the kinetic turbulent energy suffers significant oscillations. The other terms and the production by shear stresses term suffer significant oscillations between positive and negative peaks in this region. An opposite behavior observed in the Region 1, where which term presents only negative values and positive values, respectively. These peaks have more magnitude that the peaks observed in the region near the all, however continues to exist equilibrium between them. So, the term of production by normal stresses is the dominant term and the high values of this term coincide with the high values of normal stresses presented in the horizontal profiles of the turbulent velocity characteristics in Figure III-2 for *Y=30mm* and *Y=60mm*. Figure III-8 shows the respective contours of turbulent velocity characteristics and in the region of deflected flow there are high values of normal stresses, which can be associated to the production of turbulent kinetic energy. Although, to exist high values of shear stresses in this region, the production by shear stresses is balanced by the production of the other terms.

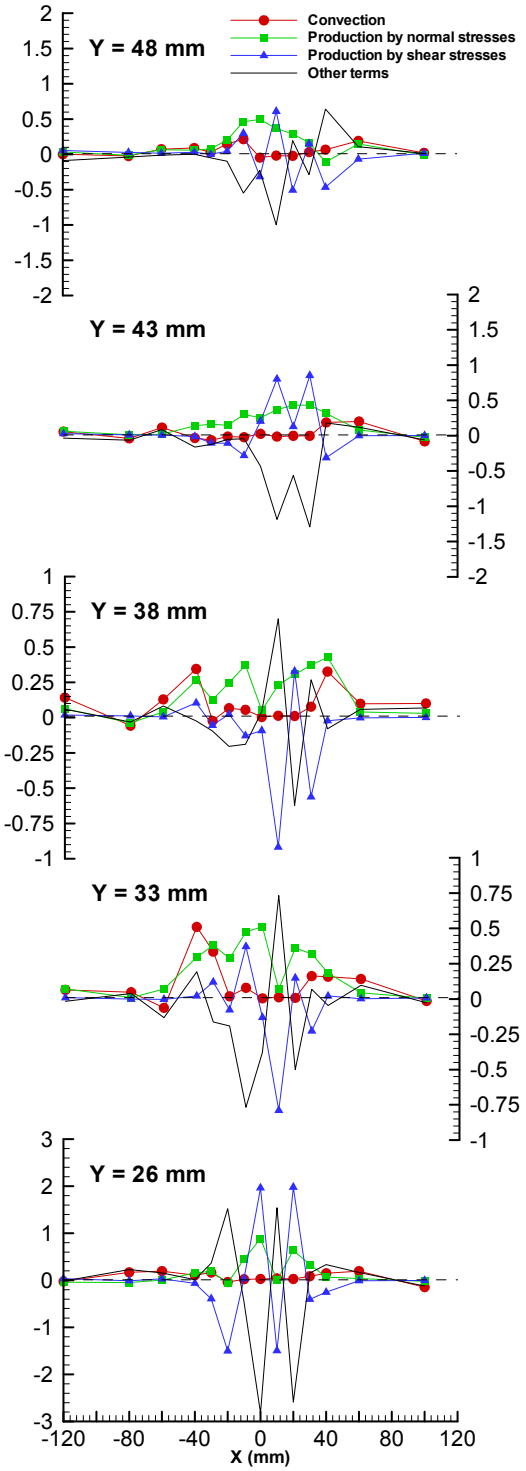

Figure III-21: Horizontal profiles of turbulent kinetic energy in Horizontal Region 2.

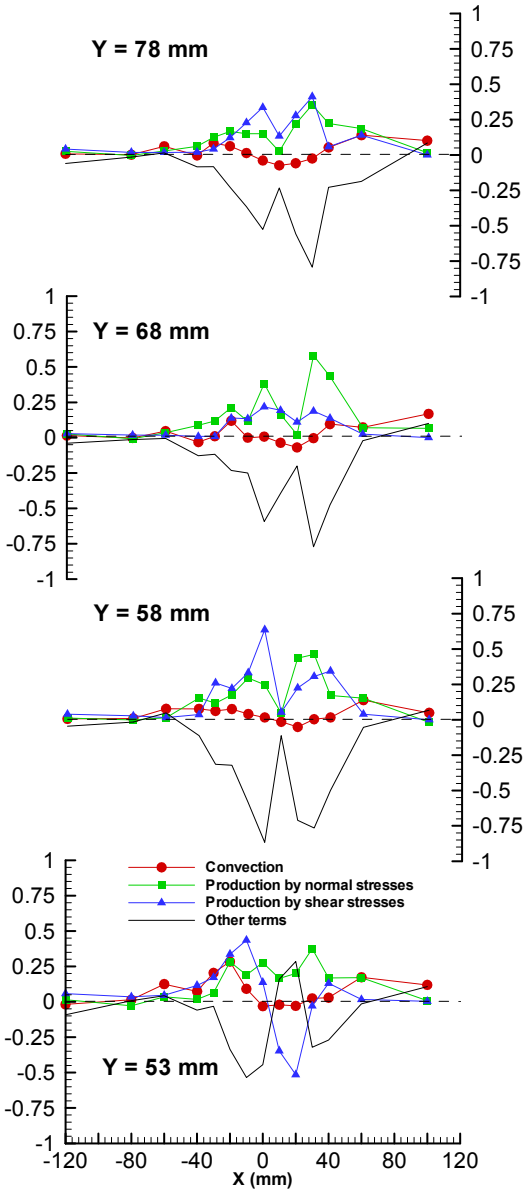

Figure III-22: Horizontal profiles of turbulent kinetic energy in Horizontal Region 2 (continuation).

Figure III-23 shows the horizontal profiles in the region far from the influence of the wall, Horizontal Region 3. The production is in general equilibrium with dissipation. The convection term is very small when compared with the remaining terms. However, only the horizontal profiles *Y=88m* and *Y=98mm* present, accurate results, since they were the last profiles measured with LDV System. The other profiles, *100mm<Y<120mm*, were obtained using the quadratic interpolation.

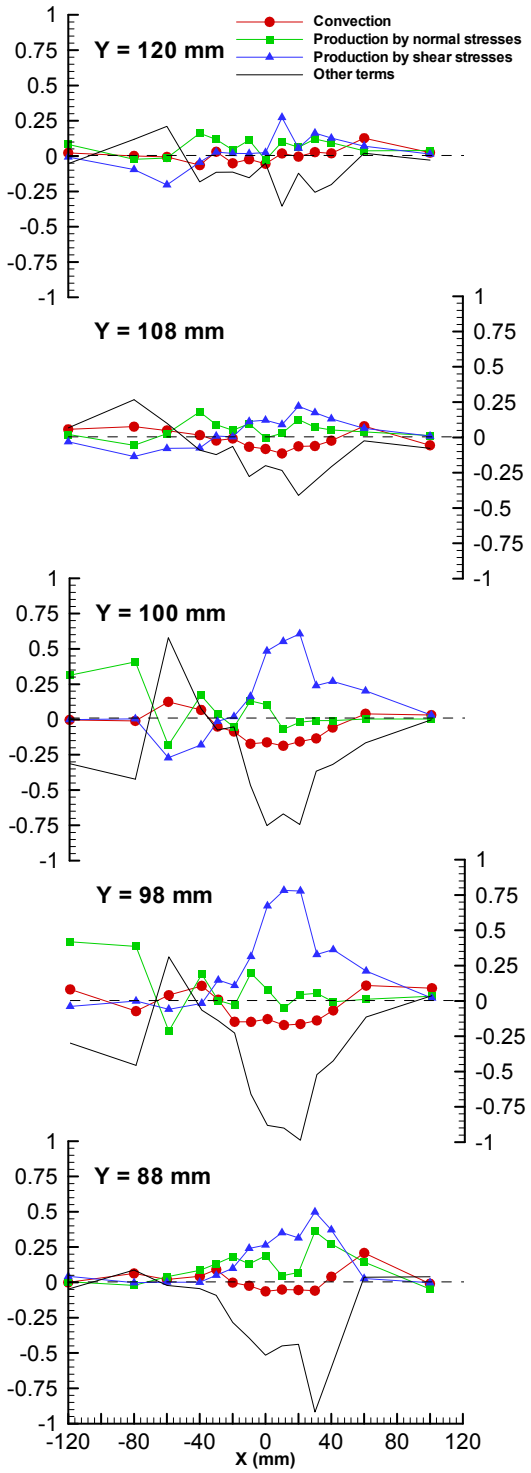

Figure III-23: Horizontal profiles of turbulent kinetic energy in Horizontal Region 3.

Figure III-24 shows vertical profiles of turbulent kinetic energy budgets in the region where the wall jet is preponderant and that contains the center of ground vortex, Vertical Region 1. Far from wall vicinity the terms of turbulent kinetic energy are practically zero, since this zone it is not affected by the development and the growth of wall jet. However, with the approach to the flow deflection and collision zones (*-40mm<X<-20mm*), defined in Vertical Region 2, are present some

oscillations in terms of turbulent kinetic energy equation. Near the wall, the terms of turbulent kinetic energy suffer significant oscillations. At the wall jet exit the production by normal stresses is balanced by the production by shear stresses. The convective term and the other terms term (diffusion and dissipation) assumes an important relevance in turbulent kinetic energy budgets, with the production by other terms not to be sufficient to balance the energy loss due to the convective term. With approach to the boundary of collision zone, the convective term tends to zero and the production of turbulent kinetic energy by normal stresses becomes preponderant, however being balanced by the diffusive and dissipative terms. The increment of production by normal stresses can be explained by the importance of shear strains $\frac{\partial U}{\partial X}$ and $\frac{\partial V}{\partial Y}$ near the wall and by the significant values of normal stresses in this zone, as show the horizontal profiles presented in Figure I-2. Near of collision zone (*-40mm<X<-20mm*) exists significant oscillations in terms of turbulent kinetic energy. These oscillations may be an influence of the instabilities that occurring in the collision zone and during flow deflection. In the vicinity of the wall, the diffusive and dissipative terms assume a great importance in production of turbulent kinetic energy. However, they have a tendency to be balanced by the loss caused by the term of production by shear stresses. This term becomes more important, since results by the high values of shear stress $\overline{u'v'}$ in this region (*-40mm<X<-20mm*), as show the horizontal profiles of shear stress presented in Figure I-3 and the respective contours presented in Figure III-9. The convective term represents a significant turbulent kinetic energy loss that tends to be smaller with approach to the collision zone. This loss is balanced by the gain resulting of production by normal stresses, since in this zone *X=-40mm*, *X=-30mm* and *X=-20mm* the values of normal stresses are significant as can be see in contours of Figures III-7 and III-8.

The vertical profiles of turbulent kinetic energy budgets in the region of interaction zone, resultant from the collision between the wall jet and the boundary layer, are presented in Figure III-25. This is the most important zone in the flowfield, since permits to understand the turbulent structure created by interaction between of the two opposed flows. Along this region the convective term not presents any significant contribution to the loss or gain of turbulent kinetic energy, since it remains zero from wall vicinity (*Y<25mm*) to the region far from the wall *(Y>85mm*). However, near of boundary layer side (*X=30mm* and *X=40mm*) for *Y<25mm* exists a small contribution of this term to the production of kinetic energy. Comparing, this zone with the zone where the wall jet is predominant, in this zone there is a local gain of turbulent kinetic energy by convection.

According to the profiles, the diffusive and dissipative term and the production by shear stresses become predominant, taking upper values, when compared with the Vertical Region 1. However, with exception to the profile *X=10mm*, the production of turbulent kinetic energy by shear stresses tends to be balanced by the loss of turbulent kinetic energy by diffusion and dissipation. This loss of energy is minor in the border of boundary layer (*X=30mm* and *X=40mm*)

accompanied by a reduction in production by shear stresses. The described behavior of these terms are verified along the all vertical direction of vertical profiles, since *Y=12mm* to *Y=120mm*. In this zone from *X=-10mm* to *X=40mm* the shear stresses $\overline{u'v'}$ take the maximum and highest values in relation to the other vertical zones, as shows Figures III-3 and III-9 that present the horizontal profiles and contours, respectively, of shear stresses. This result can explain the predominance of the term production by shear stresses in this zone. Near the wall *Y<25mm*, the production of turbulent kinetic energy is by convection, since this term presents negative values, and by normal stresses, since this term presents positive values. The contribution of convective term to the production of turbulent kinetic energy is minor than the production due to the normal stresses and shear stresses. So, the collision zone between the wall jet and the boundary layer presents a behavior similar to a wall jet. For the region far from the wall *Y>25mm*, since the convective term is practically zero, the production of turbulent kinetic energy is due to the normal stresses. Although, in the border of boundary layer and for *30mm<Y<50mm* the convective term contributes for a small loss of energy. The production of turbulent kinetic energy, essentially, by normal stresses in this region far from the wall can be explained by the maximum and highest values of normal stresses that exist in this region when compared with the other vertical regions. Figures III-2 and III-8 show that the highest values of normal stresses happen for the Vertical Region 2.

Near of position *X=10mm*, is a zone where exists important instabilities, due to the collision of the two opposed flows, the deflection of flow and, also, due to the presence of the small vortex identified in this work and by Barata et al. (2008). So, they can be the cause for the variation of diffusive and dissipative term and production by shear stresses term in turbulent kinetic energy. These terms have an opposite behavior in relation to the other profiles in the collision zone, since there is a gain of kinetic energy due to diffusion and dissipation balanced by a loss by shear stresses.

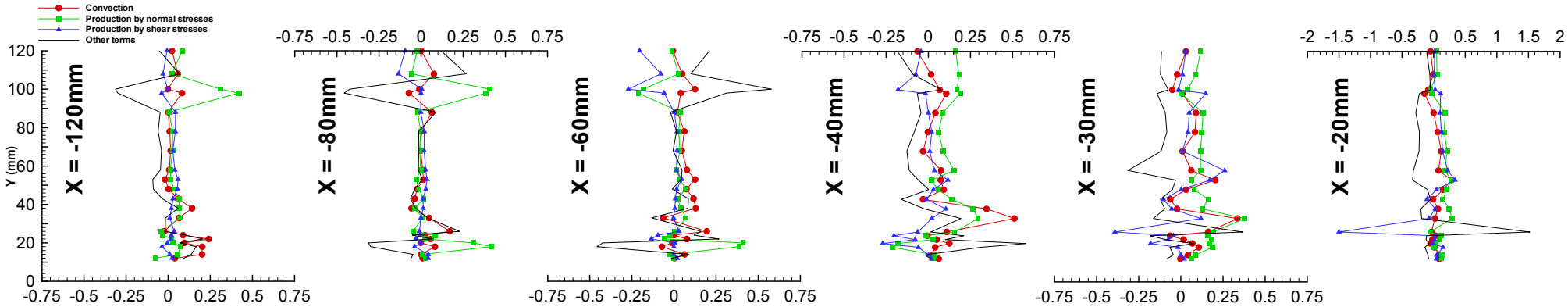

Figure III-24: Vertical profiles of turbulent kinetic energy budgets in Vertical Region 1 (wall jet side)

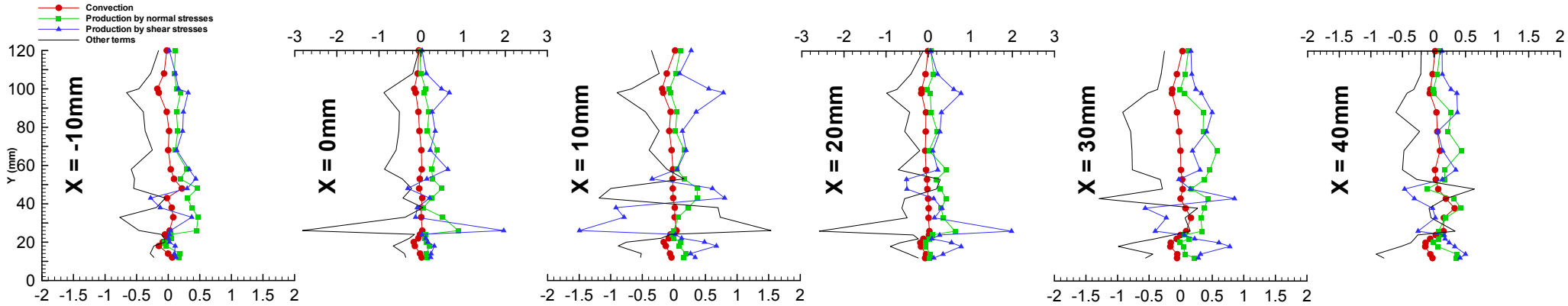

Figure III-25: Vertical profiles of turbulent kinetic energy budgets in Vertical Region 2 (collision and deflected flow zones).

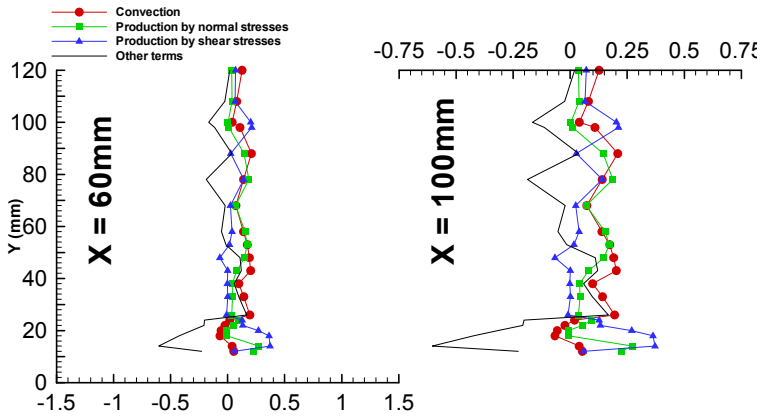

Figure III-26: Vertical profiles of turbulent kinetic energy budgets in Vertical Region 3 (boundary layer side).

Figure III-26 shows vertical profiles of turbulent kinetic energy in the region where the influence of boundary layer is dominant. In the vicinity of wall, *Y<25mm*, the production of turbulent kinetic energy by convection, normal stresses and shear stresses, is not sufficient to avoid the loss of energy by diffusion and dissipation. Out of vicinity of wall, *Y>25mm*, the diffusive and dissipative term tend to balance the production by shear stresses term, and the production of turbulent kinetic energy by normal stresses tend to be balanced by the loss of energy by convection.

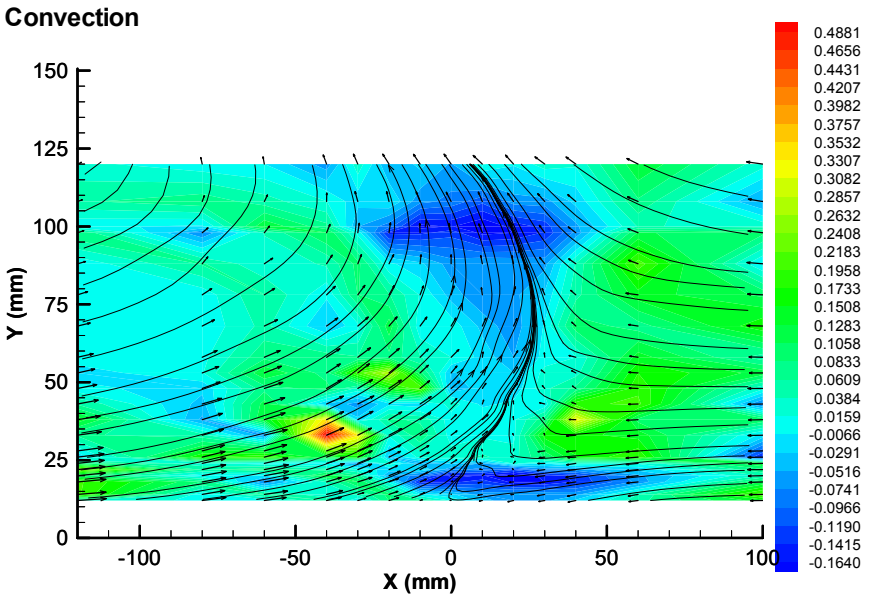

Figure III-27: Contours of the turbulent kinetic energy production, *k*, by convection.

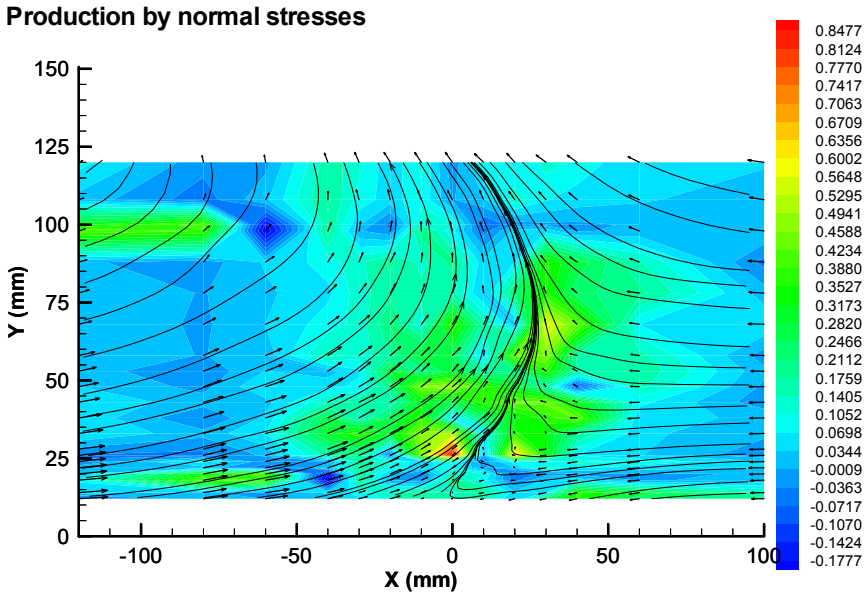

Figure III-28: Contours of turbulent kinetic energy production, *k*, by normal stresses.

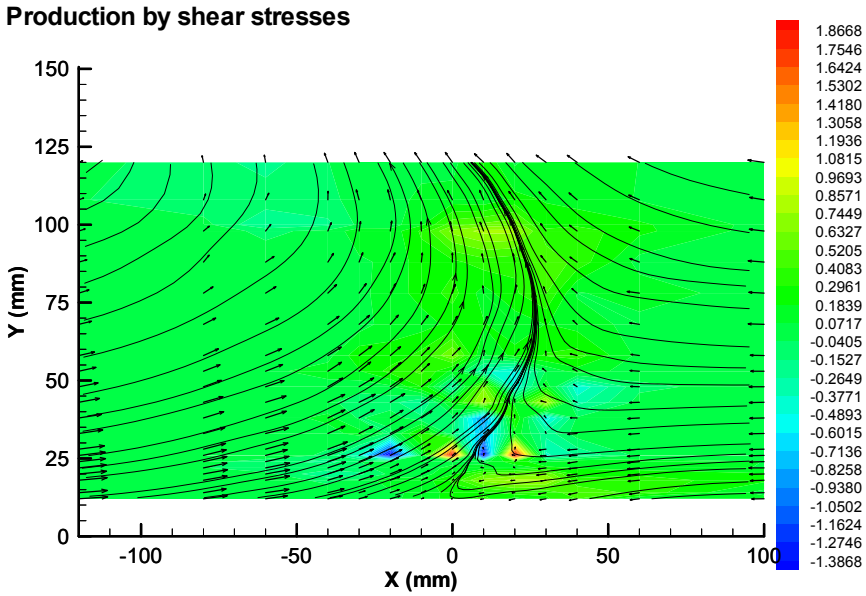

Figure III-29: Contours of turbulent kinetic energy production, *k*, by shear stresses.

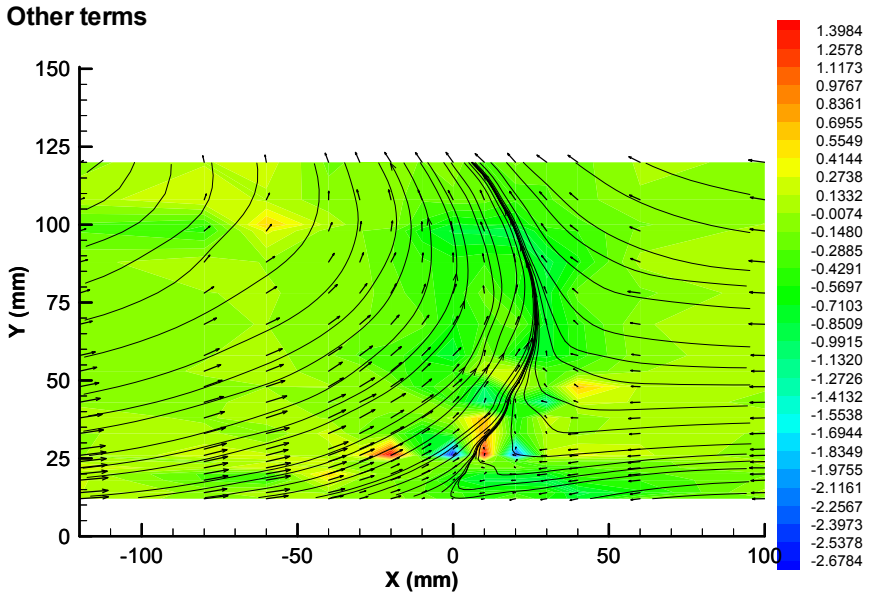

Figure III-30: Contours of turbulent kinetic energy production, *k*, by diffusive and dissipative term (other terms).

Figures from the Figure III-27 to Figure III-30 show the contours of turbulent kinetic energy balances by convection, production by normal stresses, production by shear stresses and the other terms, respectively. The contours together with the streamlines were computed from the vertical profiles presented from the Figure III-24 to the Figure III-26.

As was verified in the vertical profiles of Figure III-21, in the collision zone of the two opposed flows, there is a local gain of turbulent kinetic energy by convection (Figure III-27 - *10mm<X<40mm* and *Y<25mm*). In the region of the deflected flow the convective term not presents any significant contribution to the loss or gain of turbulent kinetic energy. From the Figure III-28 and III-30, with the approach of the boundary of the collision zone, from *X=-80mm* to *X=-40mm* the production by normal stresses of turbulent kinetic energy becomes preponderant with tendency of to be in equilibrium with the diffusive and dissipative terms. In the vertical profiles of Figure III-24, was observed significant oscillations in the terms of turbulent kinetic energy, in the zoned defined by *-40mm<X<-20mm* and *25mm<Y<30mm*. These oscillations can be an influence of the instabilities that occurring in the collision zone and during flow deflection. The diffusive and dissipative terms, Figure III-30, assume a great importance in production of turbulent kinetic energy, although exists the tendency of to be balanced by the loss caused by the shear stress production term, Figure III-29.

Figures III-29 and III-30 shows that in the collision zone, *-10mm<X<40mm*, the diffusive term together with dissipative term and the production by shear stresses become predominant, and the production of turbulent kinetic energy tends to be balanced by the loss of turbulent kinetic energy by diffusion and dissipation. In the same zone and near the wall, *Y<25mm*, the production of turbulent kinetic energy is by convection, Figure III-27, although exists, also, a contribution of production by normal stress, Figure III-29. The small contribution of convective term to the

production of turbulent kinetic energy, although less than the production due to normal stresses and shear stresses in this zone, indicates that this zone presents a behavior similar to a wall jet.

The region near of position *X=10mm*, is a region characterized by important instabilities caused by the collision of the two opposed flows, and, also, due to the existence of the small vortex identified in this work and by Barata et al. (2008). This can be an explanation for the variation of diffusive and dissipative term together with the production by the shear stresses term, Figure III-30 and Figure III-29, respectively. In this zone, there is a gain of kinetic energy due to diffusion and dissipation that is balanced by a loss by shear stresses.

4. Momentum Analysis

The momentum analysis will be presented using the same flowfield division presented in the section about vorticity and turbulent kinetic energy. However, the momentum analysis will be divided in two components, the momentum analysis of horizontal velocity component *U*, and momentum analysis of vertical velocity component *V*. It will be presented the horizontal and vertical profiles about it parameter of analysis of turbulence, and the respective contours.

4.1 Momentum Analysis of Horizontal Velocity Component *U*

The momentum transport equation of the horizontal velocity component is given by the Equation 3.12 presented in the Section 3.2 of the Chapter II.

$$U\frac{\partial U}{\partial X}+V\frac{\partial U}{\partial Y}=-\frac{1}{\rho}\frac{\partial P}{\partial X}+\upsilon\left(\frac{\partial^2 U}{\partial X^2}+\frac{\partial^2 U}{\partial Y^2}\right)-\frac{\partial\overline{u'^2}}{\partial X}-\frac{\partial\overline{u'v'}}{\partial Y} \quad \textbf{(3.12)}$$

The derivatives $\frac{\partial}{\partial Z}$ and the shear stress $\overline{u'w'}$ and $\overline{v'w'}$ are zero, since the measurements were performed in the vertical plane of symmetry of the flow. The derivatives in equation terms were calculated using the quadratic interpolation from the values measured by the LDV System.

Figure III-31 shows the horizontal profiles of horizontal velocity component momentum balances, U-momentum, in the vicinity of the wall, as defined by the Horizontal Region 1. This horizontal profiles shows that the transport of momentum by molecular diffusion can be negligible, since its value is practically zero from the wall jet to the boundary layer side. The term that represents the turbulent diffusion presents a similar behavior to the molecular diffusion term. However, in the collision zone of the wall jet with the boundary layer, *-40mm<X<10mm* and for *Y=18mm* and *Y=20mm*, there is a small contribution to the momentum of *U*. This small and positive variation can be explained by the high values of normal and shear stresses that occur in

this zone, Figure III-8 and Figure III-9, which suggest that faster moving elements of the wall jet tend to move upwards with the deflected upper side of the boundary layer. This result can indicate a small transference of momentum in horizontal velocity component by turbulent diffusion in the collision zone along the vertical direction. Far from the wall, *Y=22mm* and *Y=24mm* the turbulent diffusion term tends to be zero.

Figure III-31 also shows that along the all flowfield the convective term presents negative values with the exception to the boundary layer side *X>40mm*. However, the transport of momentum by convection is balanced by the term of pressure gradient, since this term presents positive values, except in boundary layer side, and with a similar magnitude of the values of the convective term. In the wall jet side, *-120mm<X<-60mm*, the both terms presents significant values, and with the approach to the collision zone they tend to zero, but it is in the collision where these two terms present important peaks, *-40mm<X<10mm* and *Y=18mm* and *Y=20mm*. This result can be explained by the great deceleration of the wall jet and the boundary layer as result of their collision, which implies an important variation in momentum of the horizontal velocity component. The effect of these terms in the momentum of *U*, in the collision zone, tends to be smaller far from the wall, *Y=22mm* and *Y=24mm*.

Figures III-32 and III-33 present the horizontal profiles of U-momentum in the region of the deflected flow that results from the collision between the two opposed flows. As was verified in the vicinity of the wall, Horizontal Region 1, the U-momentum transport equation term by molecular diffusion is zero, and the tendency of the convection term to be balanced by the pressure gradient term maintains. For *-10mm<X<40mm* and *26mm<Y<43mm*, the zone that represents the collision between the wall jet and the boundary layer, exists some oscillations in the values and, also, in the sign of the turbulent diffusion and pressure gradient terms. However, this oscillations tends to disappear far from the wall, *Y>43mm*. These oscillations can be caused by the instabilities that exist in the zone, the deflection of flow and the presence of the small vortex identified in this work and by Barata et al. (2008). The oscillations of the turbulent diffusion can be, also, due to the high values of normal and shear stresses that are present in the zone (Figures III-8 and III-9). Along the vertical direction the term tends to zero, tendency that is accompanied by the diminution of the normal stresses and shear stresses, Figures III-8 and III-9, *-10mm<X<40mm*.

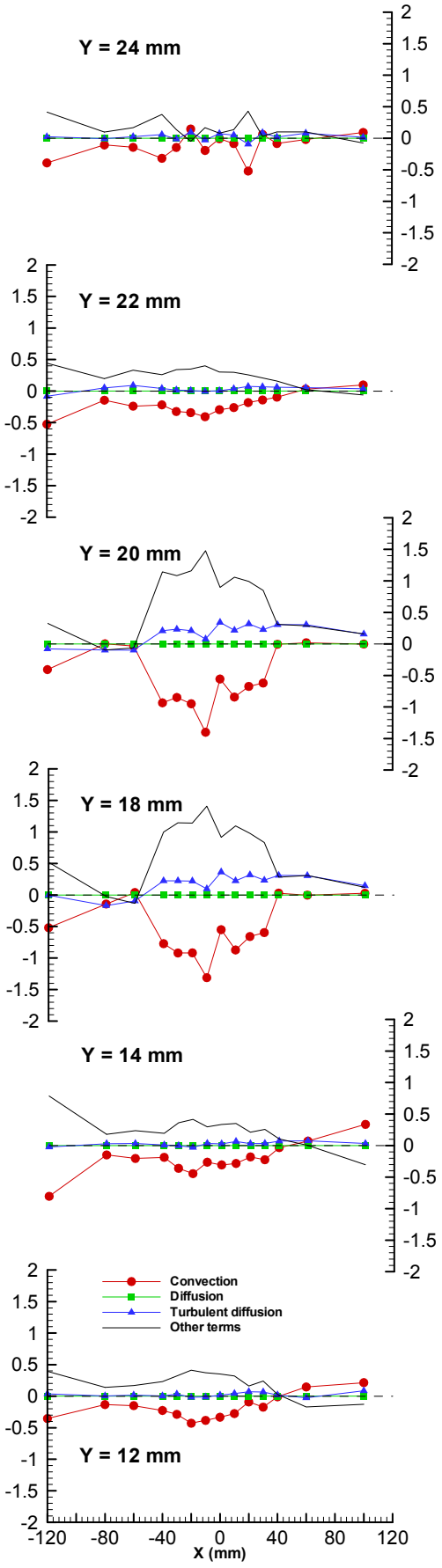

Figure III-31: Horizontal profiles of U-momentum in Horizontal Region 1.

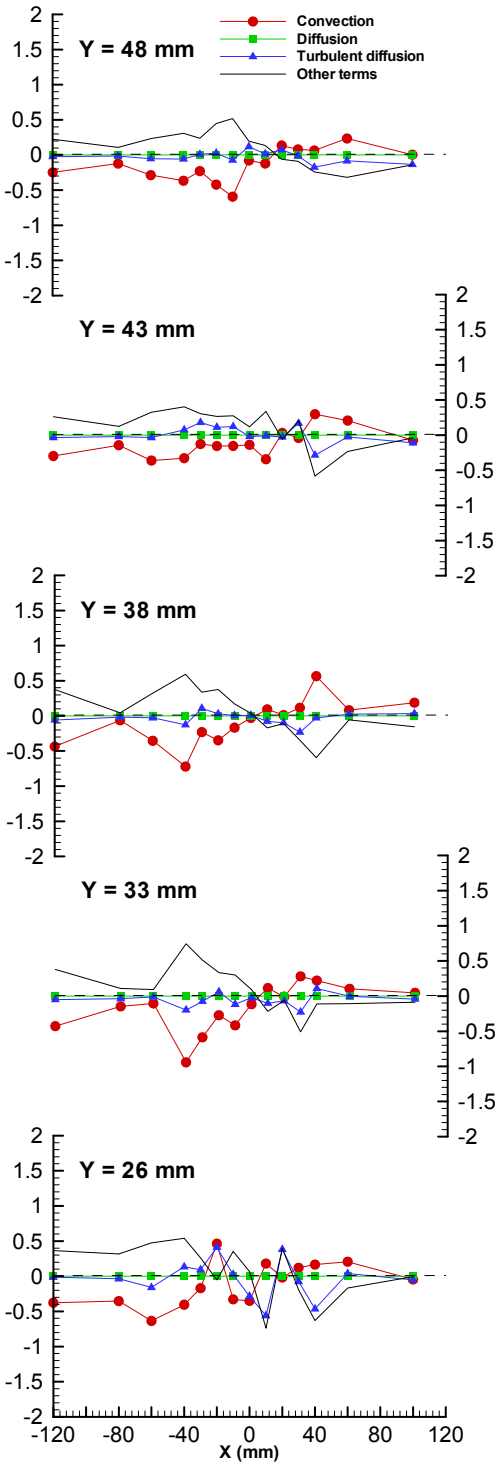

Figure III-32: Horizontal profiles of U-momentum in Horizontal Region 2.

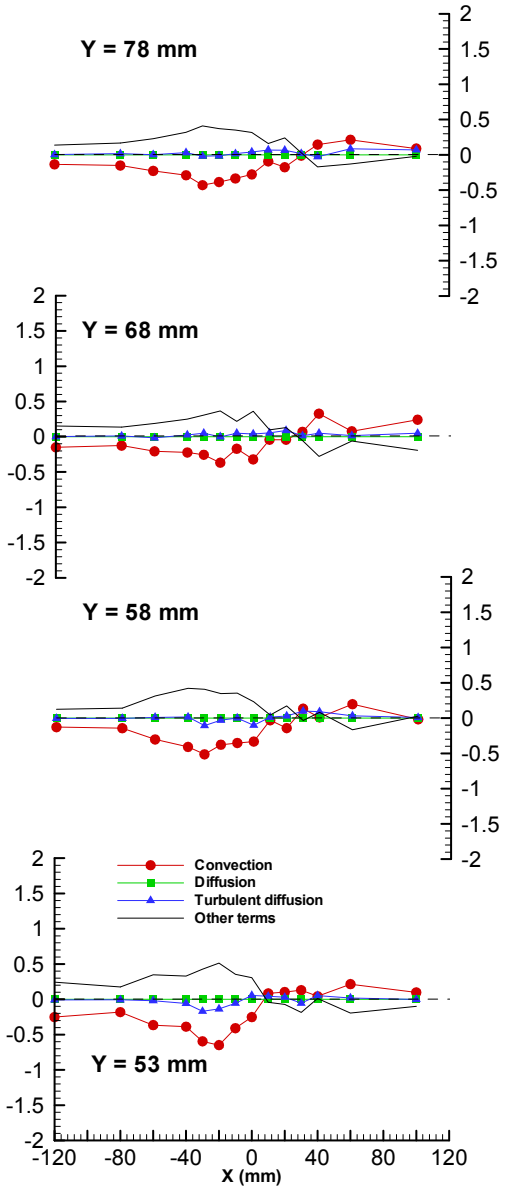

Figure III-33: Horizontal profiles of U-momentum in Horizontal Region 2 (continuation).

The horizontal profiles of U-momentum in the region far from the influence of the wall are presented in Figure III-34. The U-momentum transport equation terms have the same behavior described in the last paragraph. However, only, the horizontal profiles *Y=88mm* and *Y=98mm* present accurate results, since the remaining horizontal profiles are obtained trough quadratic interpolation.

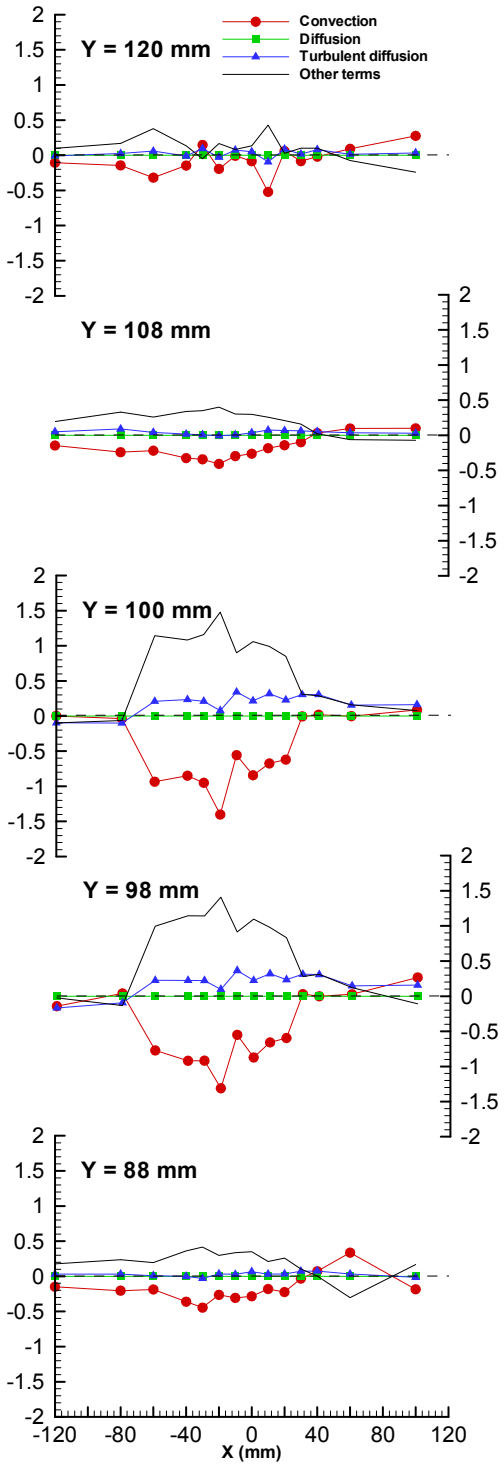

Figure III-34: Horizontal profiles of U-momentum in Horizontal Region 3.

Figure III-35 presents the vertical profiles of U-momentum transport equation obtained in the wall jet region. As was verified previously in the horizontal profiles, the molecular diffusion is negligible along the flowfield. This result can be confirmed by the vertical profiles obtained in the Vertical Regions 2 and 3, where the same term of U-momentum transport equation is, practically zero.

According to the vertical profiles, the predominant terms are the convective term and the pressure gradient term, and they becomes significant with the approach to the border of the collision and deflection zones, *X-40mm*, *X=-30mm*, and *X=-20mm*. Near the wall, *Y<25mm*, the convective term and the gradient pressure term present higher values than in the remaining region, *Y>25mm*, and they have, also, higher values in the periphery of the collision zone, *-40mm<X<-20mm*, than in the wall jet side, *X=-120mm and X=-80mm*. This result can be due to the influence of the collision zone, because a large decrement in the velocity is caused by the collision of the wall jet and the boundary layer, giving rise to a significant variation of momentum of the horizontal velocity component, *U*. However, the convective term tends to be balanced by the pressure gradient term increment. The importance of convective term, also, can be explained by the importance of the shear strains $\frac{\partial V}{\partial Y}$ and $\frac{\partial U}{\partial X}$ in the vicinity of the wall. In the region defined by *25mm<Y<80mm*, the values of the convective and gradient pressure terms are higher in the border of the collision zone than in the wall jet zone, *X=-120mm* and *X=-80mm*. This result can be explained by the deflection of the flow that results from the collision of the two opposed flows. In relation to the turbulent diffusion term, it is practically zero in the vicinity of the wall jet exit, *X=-120mm* and *X=-80mm*. However, in the border of the collision zone *-40mm<X<-20mm*, and near of the wall, *Y<25mm*, the turbulent diffusion terms becomes important because of the collision of the two opposed flows. The shear stresses tend to increase from the wall jet exit to the collision point, and, also in the vertical direction, Figure III-9. The normal stresses also present the same behavior, Figure III-8. The faster moving elements of the wall jet tend to move upwards with the deflected upper side of the boundary layer. So, the deceleration of the flow can be associated with a transfer of momentum by turbulent diffusion. For the Vertical Region 1, as was verified in the horizontal profiles, the convective term is, always, balanced by the gradient pressure term.

Figure III-36 shows the vertical profiles of U-momentum in the zone of collision between the wall jet and the boundary layer. Once again the diffusion term is practically zero along the flowfield. It is possible to conclude that the momentum of horizontal velocity component *U* in the collision zone and in the deflection zone of the flow it is not affected by the molecular diffusion. Similarly, to the last vertical region, the convective term and the pressure gradient term are the predominant terms. Near of the wall, *Y<25mm*, both terms present high values, and continues to verify the tendency of equilibrium between them. The behavior of the U-momentum equation terms, in the collision region, *-10mm<X<20mm*, is similar to the behavior described, previously, for the vertical profiles between *-40mm<X<-20mm* of Figure III-35.

Figure III-36 shows that the convective and gradient pressure terms present a significant magnitude in the region where the flow is deflected, defined by *-10mm<X<0mm* and *25mm<Y<85mm*. With the approach to the boundary layer side, *X>20mm*, the magnitude of both terms tends to be zero in the zone defined by *25mm<Y<85mm*. The deflected flow moves upwards, and the movement of the fluid elements, in this zone, is essentially in the vertical

direction. So, the horizontal mean velocity component is nearly zero, which can be associated with a low momentum of *U*. The vertical mean velocity component, *V*, is the predominant component.

In the collision zone, *-10mm<X<40mm* and *Y<25mm*, due to the equilibrium between convection and pressure gradient terms, the momentum of horizontal velocity component is affected, mainly, by the turbulent diffusion. With the approach to the boundary layer side, *X>10mm*, and for the heights between *25mm<Y<40mm*, the turbulent diffusion term presents a significant oscillation, with change of sign, a behavior only identified in this zone.

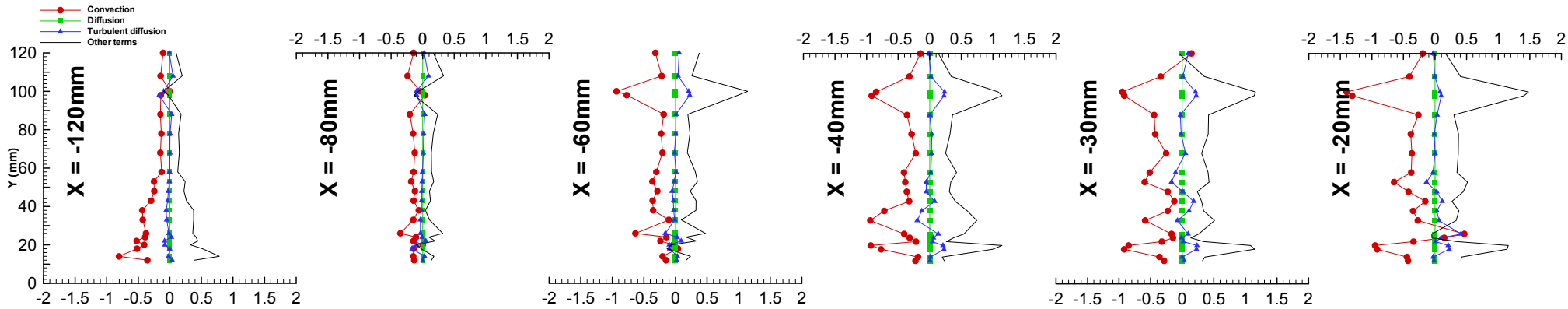

Figure III-35: Vertical profiles of U-momentum in Vertical Region 1 (wall jet side).

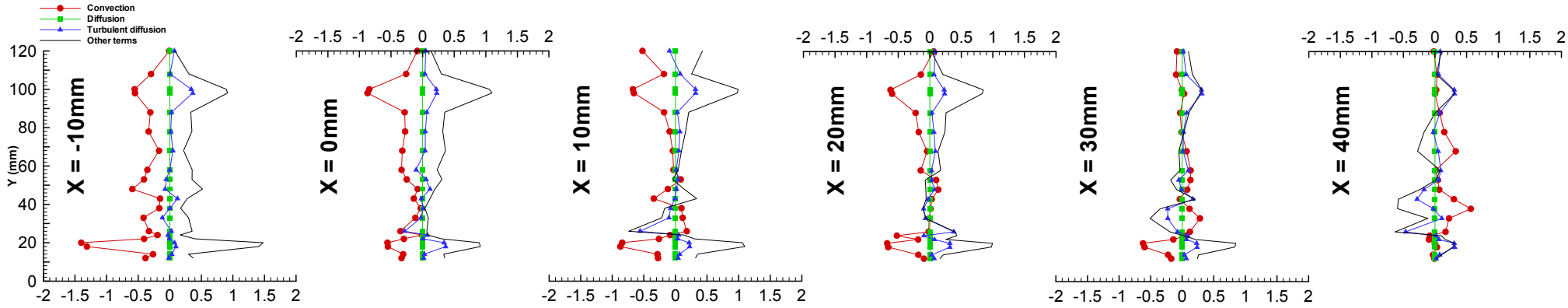

Figure III-36: Vertical profiles of U-momentum in Vertical Region 2 (collision and deflected flow zones).

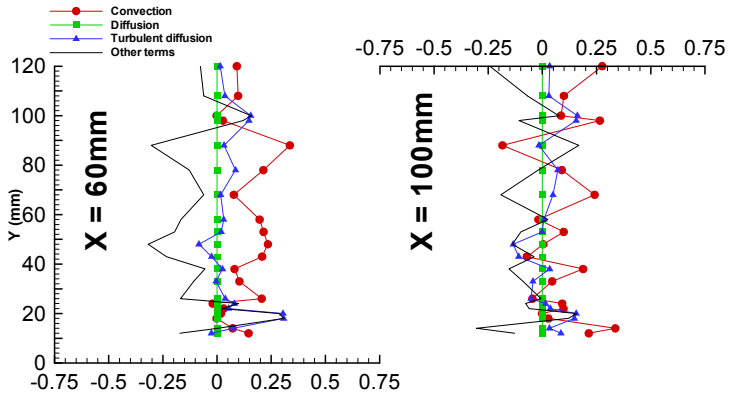

Figure III-37: Vertical profiles of U-momentum in Vertical Region 3 (boundary layer side).

Figure III-37 presents the vertical profiles of U-momentum in the boundary layer side. The behavior of the U-momentum equation terms is similar to the behavior in the other vertical zones. However, the magnitude of all terms are minor than in the other zones. The momentum of horizontal velocity component, *U*, continues to be dependent, mainly, of the turbulent diffusion term.

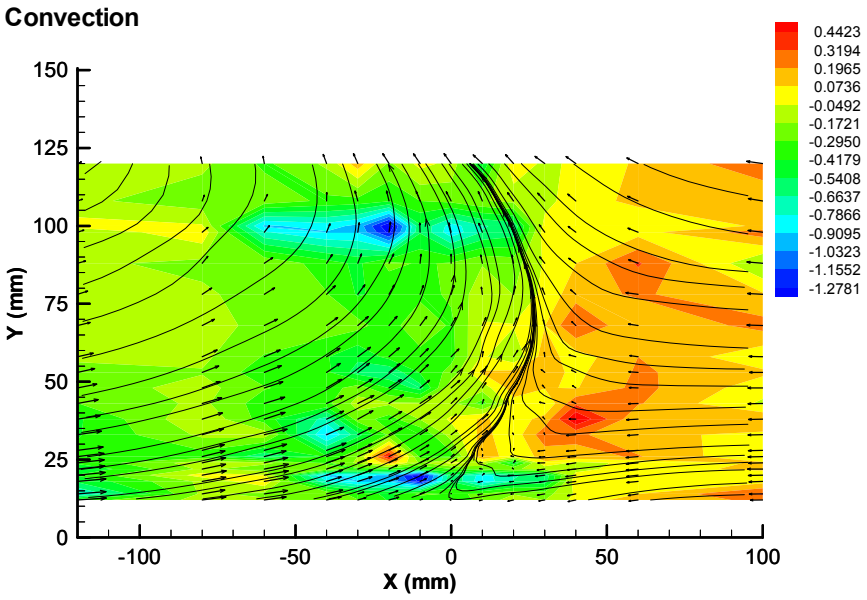

Figure III-38: Contours of U-momentum by convection.

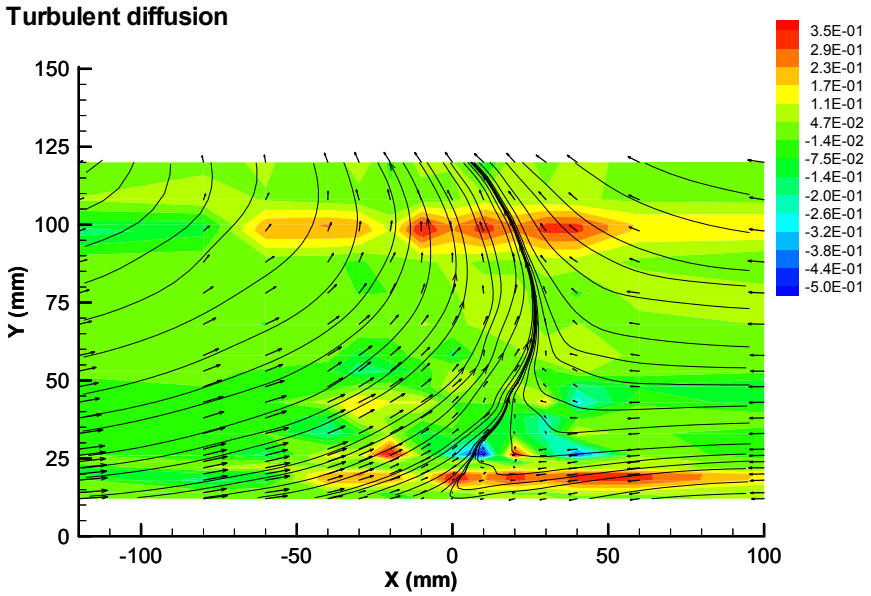

Figure III-39: Contours of U-momentum by turbulent diffusion.

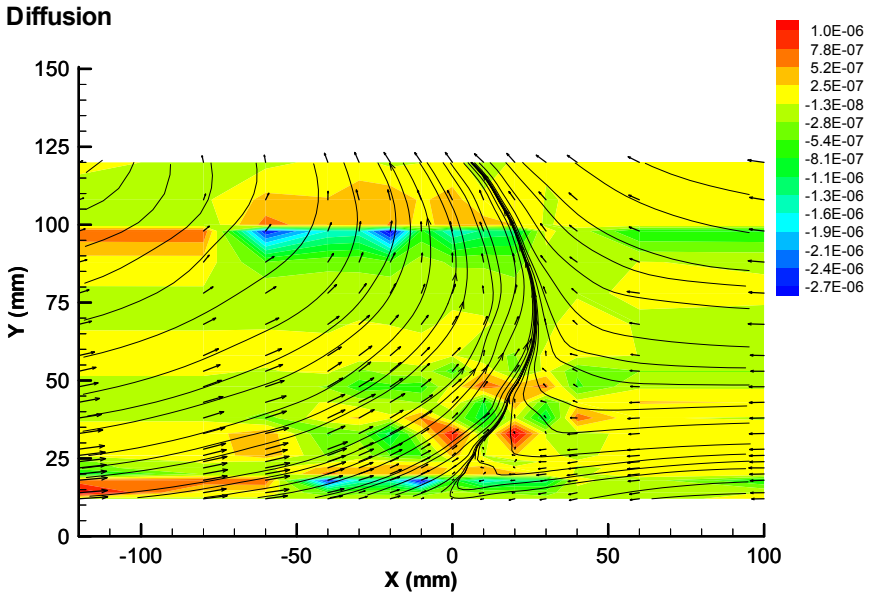

Figure III-40: Contours of U-momentum by diffusion.

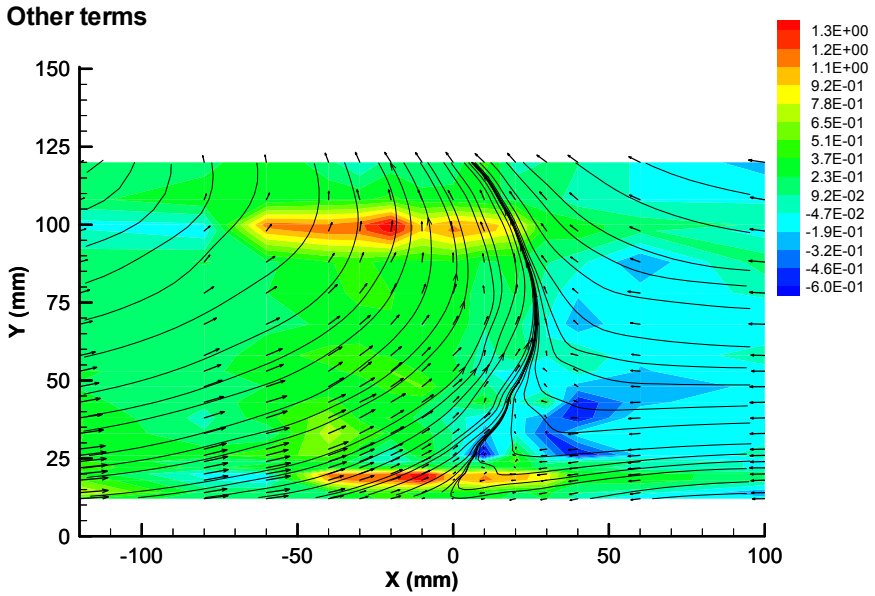

Figure III-41: Contours of U-momentum by other terms (pressure gradient term).

Figures from Figure III-38 to III-41 present the contours of U-momentum equation terms along the all flow field. These results show that the molecular diffusion is negligible in the momentum of horizontal velocity component, *U* (Figure III-40). In the collision zone defined by the *-10mm<X<40mm* and *Y<25mm* the gradient pressure term is very important in U-momentum. However, this term is balanced by the convection term as can be seen in Figure III-38. According to the contours of the convection and pressure gradient term, exists equilibrium between these two terms along the all flowfield, including the collision zone and the deflection of the flow. This result was also confirmed by the horizontal profiles and vertical profiles presented in this section.

The momentum of horizontal velocity component, *U*, is related, mainly, with the turbulent diffusion term, Figure III-39. This term has a great importance in the collision zone defined by *-10mm<X<40mm* and *Y<25mm*, and also in the boundary layer side, near of the wall *Y<25mm*. The turbulent diffusive becomes important due to the collision of the two opposed flows. The shear stresses tend to increase from the wall jet exit to the collision point, and, also in the vertical direction, Figure III-9. The normal stresses also present the same behavior, Figure III-8. The faster moving elements of the wall jet tend to move upwards with the deflected upper side of the boundary layer. So, together with the deceleration of the flow can be associated a transfer of momentum by turbulent diffusion.

4.2 Momentum Analysis of Vertical Velocity Component *V*

The momentum transport equation of the vertical velocity component is given by the Equation 3.13 presented in the section 3.2 of the Chapter III.

$$U\frac{\partial V}{\partial X}+V\frac{\partial V}{\partial Y}=-\frac{1}{\rho}\frac{\partial P}{\partial Y}+\upsilon\left(\frac{\partial^2 V}{\partial X^2}+\frac{\partial^2 V}{\partial Y^2}\right)-\frac{\partial\overline{u'v'}}{\partial X}-\frac{\partial\overline{v'^2}}{\partial Y} \quad \textbf{(3.13)}$$

The derivatives $\frac{\partial}{\partial Z}$ and the shear stress $\overline{u'w'}$ and $\overline{v'w'}$ are zero, since the measurements were performed in the vertical plane of symmetry of flow. The derivatives in equation terms were calculated using the quadratic interpolation from the values measured by the LDV System.

Figure III-42 presents the horizontal profiles of the momentum of vertical velocity component, *V*. From the wall jet side to the boundary side, the term that represents the molecular diffusion presents values near of zero. So, in the vicinity of the wall this term can be negligible. The turbulent diffusion terms also presents a similar behavior. However, in the collision zone, *-10mm<X<40mm* and near the wall *Y<82mm*, it presents small negative values and tend to be zero far away from the wall (Figures III-24, III-43 and III-44). This result can be explained by the values of normal and shear stresses that occur in such location, Figures III-8 and III-9, although the contribution of the turbulent velocity characteristics is not sufficient for the turbulent diffusion term present higher values. Similar to the behavior of the momentum of horizontal velocity component, *U*, the convective term tends to be in equilibrium by the pressure gradient term. These terms are predominant in the wall jet side, *-120mm<X<40mm*, and in the boundary layer side *40mm<X<100mm*. However, in the Vertical Region 2, and in the heights that corresponding to the collision of the wall jet with the boundary layer, *14mm<Y<22mm* the both terms presents significant oscillations. This result may be explained by the unsteady characteristic of this zone. The faster moving elements of the wall jet tend to move upwards with the deflected flow, which can be associated a transfer of momentum to the vertical mean velocity component, between the collision and the deflection of the flow. This transfer can cause the acceleration of the flow in the vertical direction. In the zone defined by *-10mm<X<40mm*, far from the wall, the values of the V-momentum equation terms tends to zero.

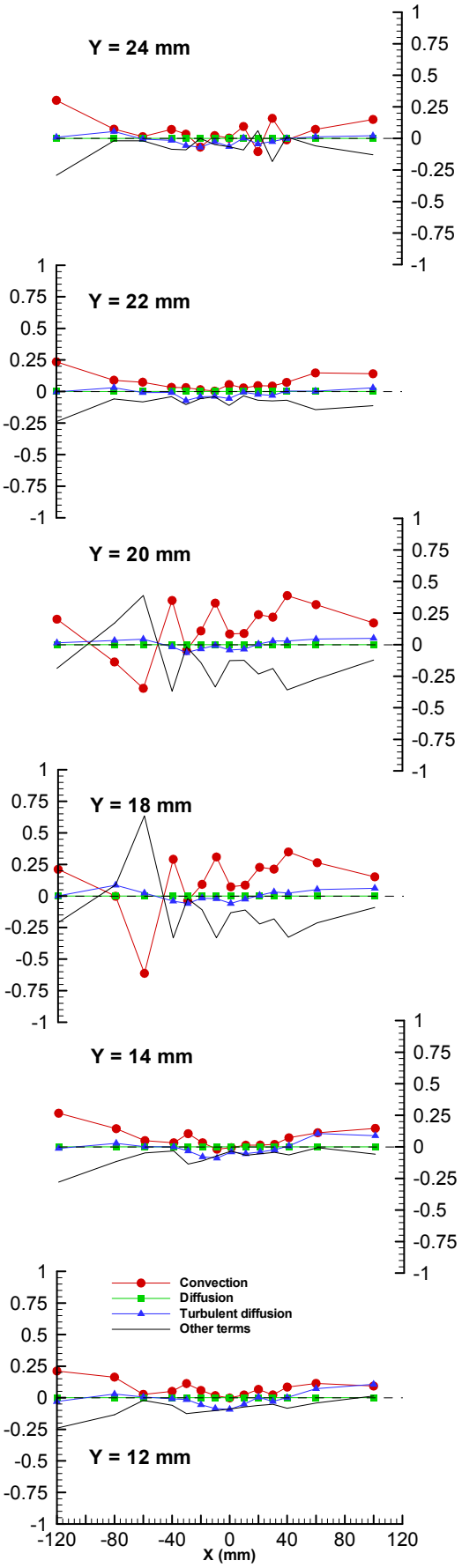

Figure III-42: Horizontal profiles of V-momentum in Horizontal Region 1.

Figure III-43 and III-44 show the horizontal profiles of V-momentum in Horizontal Region 2, the intermediate region that contains the deflection of flow resultant from the collision between the two opposed flows. According to the profiles, the molecular diffusion is, also, negligible. From the wall jet side to the boundary layer side, the convective term is always balanced by the pressure gradient term. In the vicinity of the collision between the two opposed flows, *Y=26mm* and *Y=23mm*, exists small variations in the V-momentum equation terms. This result can be due to the deflection of flow. The fluid elements tends to move upwards, after the collision of the wall jet and the boundary layer, which can be associated a transfer of momentum to the vertical mean velocity component, with the flow acceleration in the vertical direction. Far away from the wall the terms *Y>43mm* the terms of V-momentum equation tends to zero.

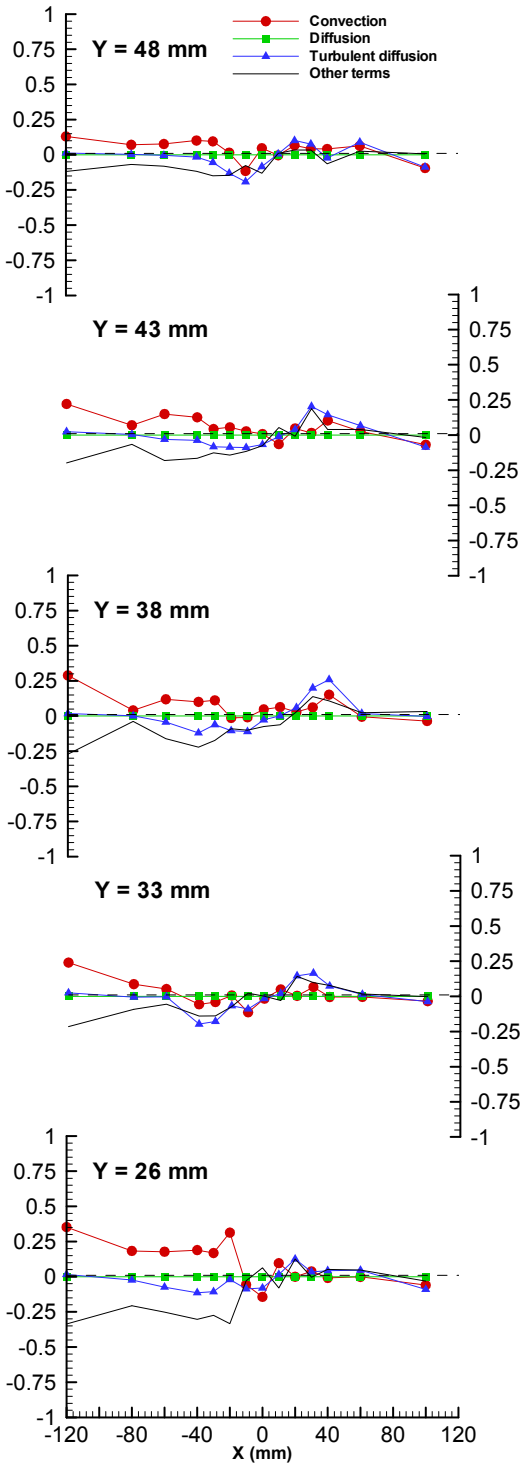

Figure III-43: Horizontal profiles of V-momentum in Horizontal Region 2.

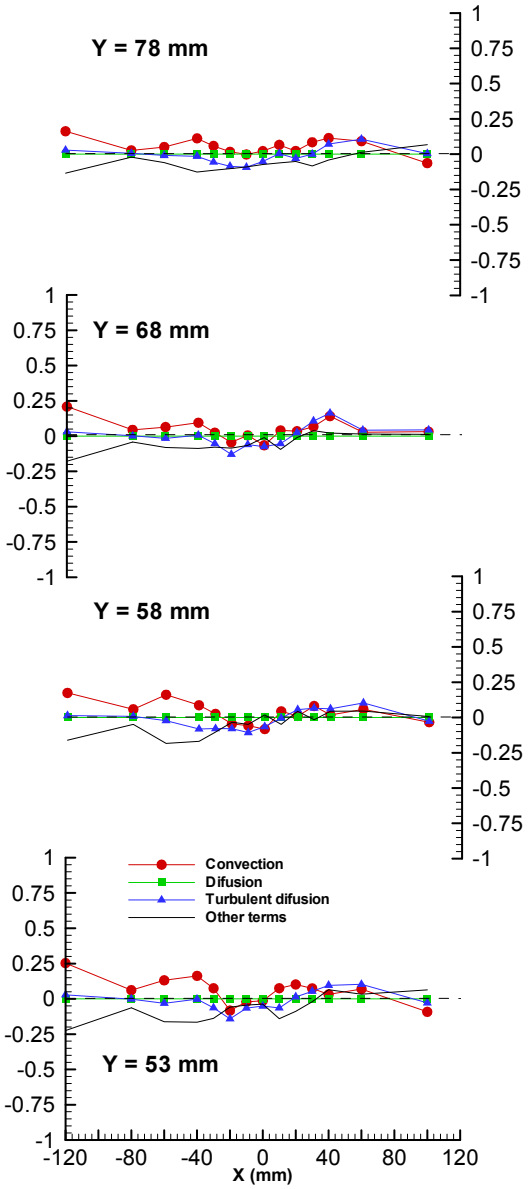

Figure III-44: Horizontal profiles of V-momentum in Horizontal Region 2 (continuation).

Figure III-45 present the horizontal profiles of V-momentum in the region far from the influence of the wall. The V-momentum transport equation terms have the same behavior described in the last paragraph. However, only, the horizontal profiles *Y=88mm* and *Y=98mm* present accurate results, since the remaining horizontal profiles are obtained trough the quadratic interpolation.

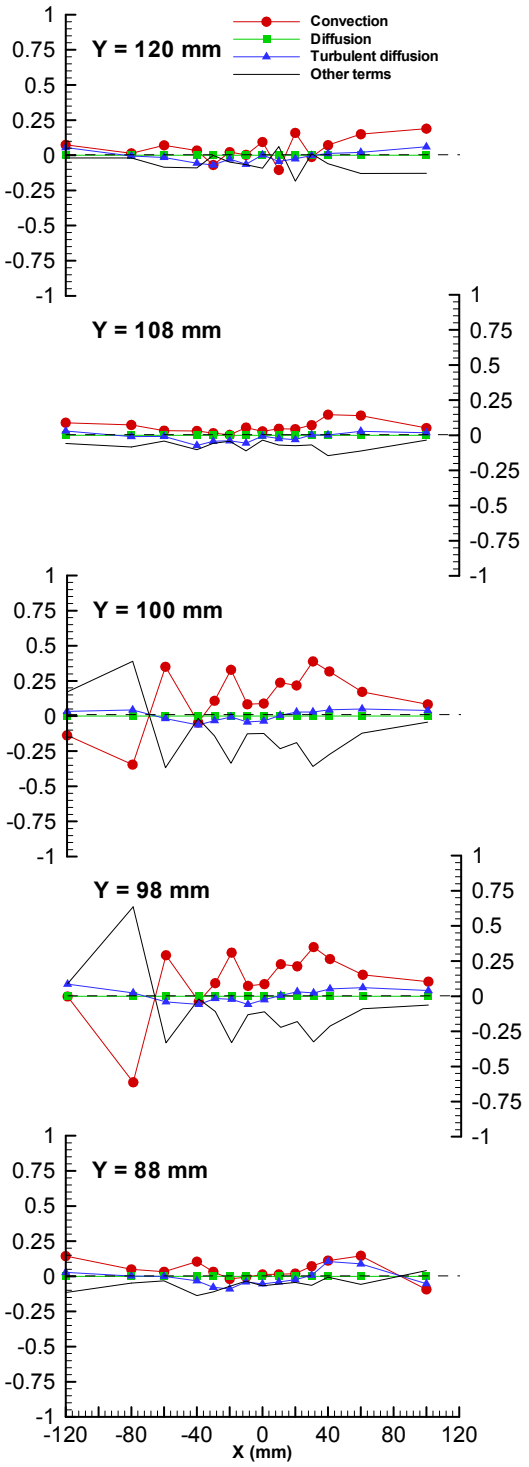

Figure III-45: Horizontal profiles of V-momentum in Horizontal Region 3.

Figures III-46 and III-47 show vertical profiles of V-momentum in Vertical Regions 1 and 2, the wall jet side and the collision and deflection zones, respectively. The Figures shows that the molecular diffusion term can be negligible along the all flowfield. A result already confirmed by the horizontal profiles. In the collision and deflection zones the V-momentum by convection is always balanced by the pressure gradient term. These terms are predominant in the collision zone between the wall jet and the boundary layer, and also, in the boundary layer side, near of the wall

(Figure III-28). The turbulent diffusive term is very small along the deflection of the flow, and, also, in the collision zone. After the deflection of the flow, $Y>25mm$ and $20mm<X<100mm$, (Figure III-47 and III-46). The momentum of V is very small, since the flow has as main direction the horizontal direction.

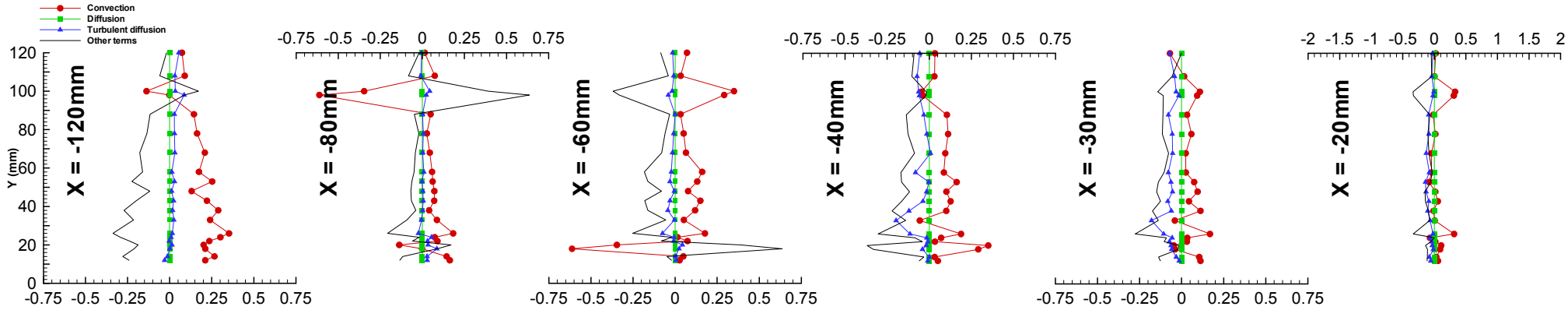

Figure III-46: Vertical profiles of V-momentum in Vertical Region 1 (wall jet side).

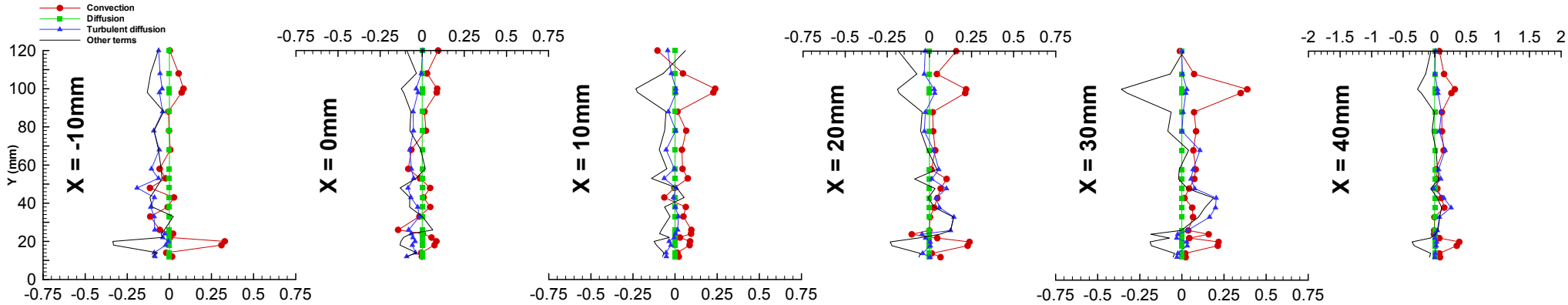

Figure III-47: Vertical profiles of V-momentum in Vertical Region 2 (collision and deflection zones).

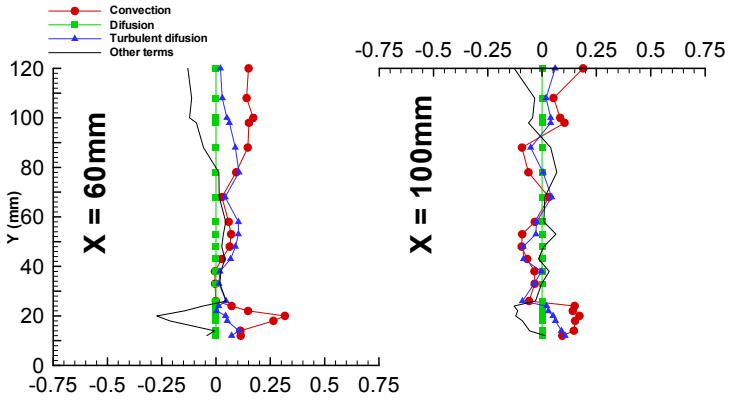

Figure III-48: Vertical profiles of V-momentum in Vertical Region 3 (boundary layer side).

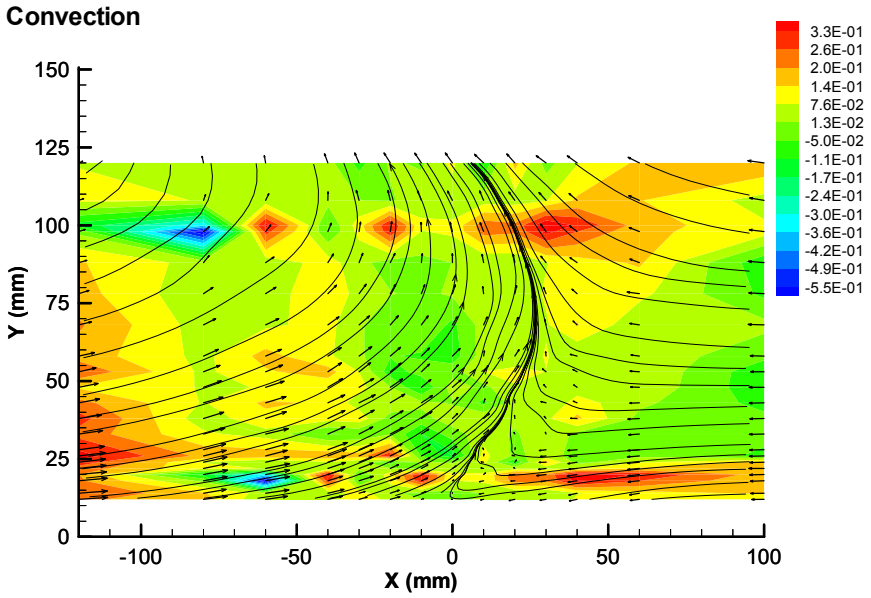

Figure III-49: Contours of V-momentum by convection.

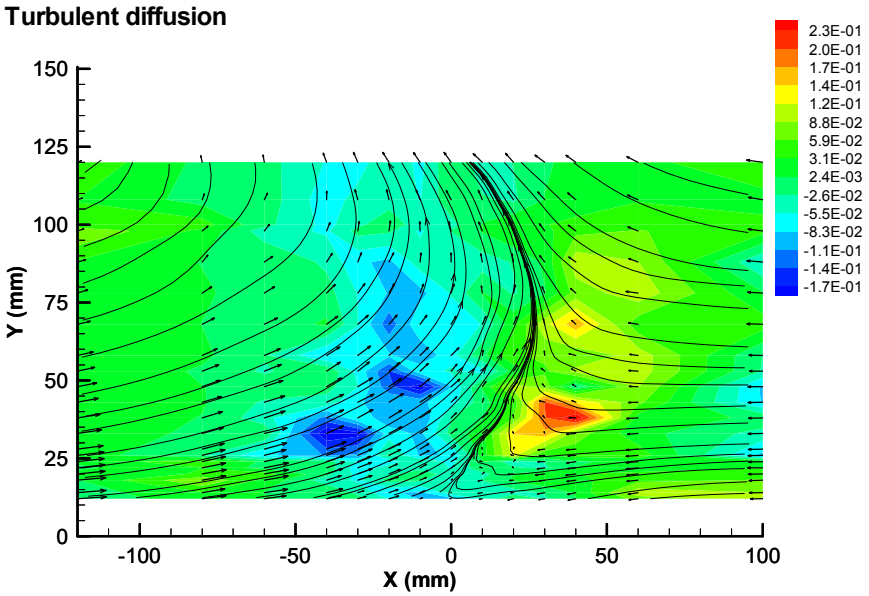

Figure III-50: Contours of V-momentum by turbulent diffusion.

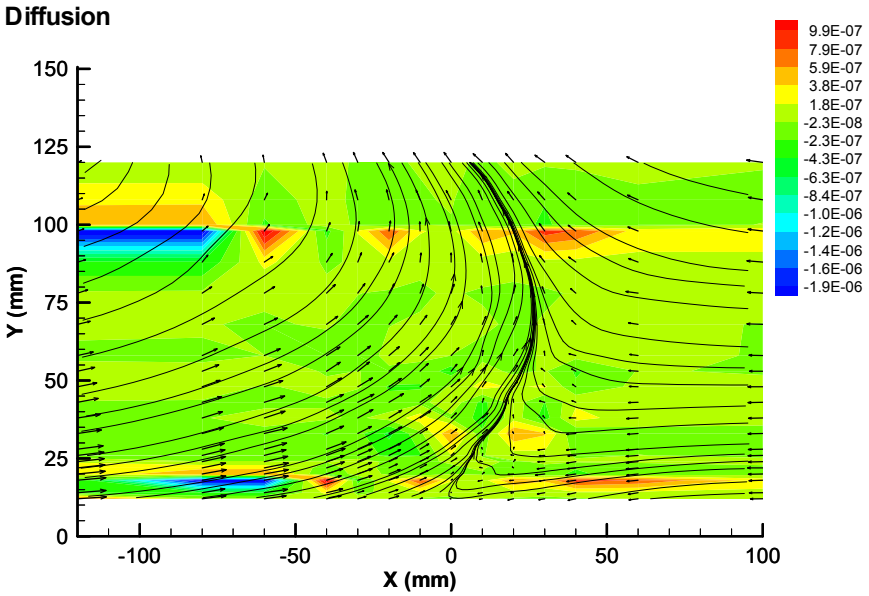

Figure III-51: Contours of V-momentum by diffusion.

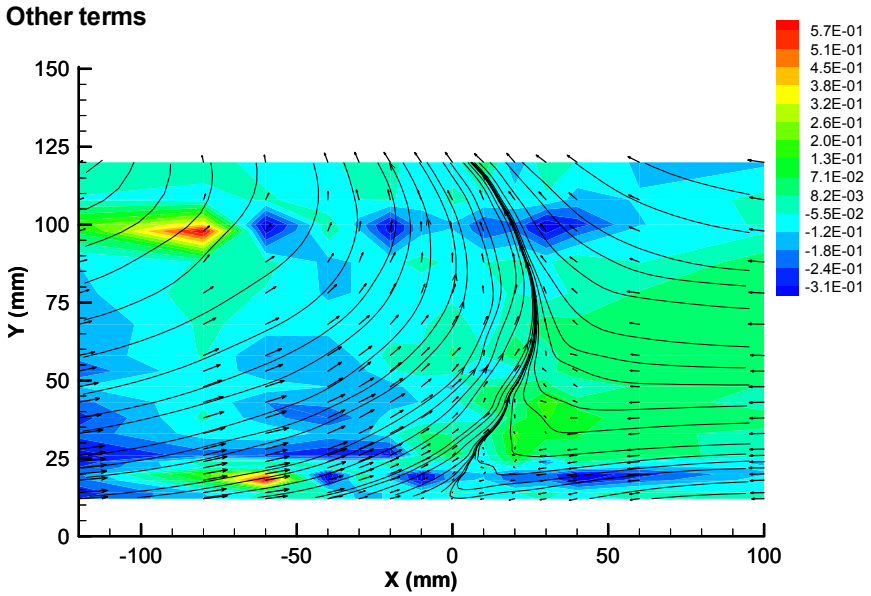

Figure III-52: Contours of V-momentum by other terms.

Figures from Figure III-49 to III-52 show the contours of V-momentum equation terms along the flowfield; convection; turbulent diffusion; molecular diffusion; and the pressure gradient, respectively. Figure III-51 shows that the momentum of vertical velocity component, by molecular diffusion can be negligible. This result can be confirmed by the horizontal profiles presented in this section. According to Figures III-49 and III-52 can be concluding that the momentum of the vertical velocity component, *V*, by convection is balanced by the pressure gradient term, along the all flowfield including the collision and the deflection of the flow zones. These terms are predominant in the collision zone between the wall jet and the boundary layer, and, also, in the boundary layer side, near of the wall. The turbulent diffusive term (Figure III-50) is very small Figure III-50 in the collision zone, *-10mm<X<40mm*, and, also, in the deflection zone flow.

The results revealed that the momentum of horizontal mean velocity component, *U*, is preponderant in relation to the momentum of vertical mean velocity component, *V*. A result that can be explained by the strong deceleration of the flow in the horizontal direction, due to the impact of the two opposed flows.

Chapter IV: Conclusions

The present work is included in a research program dedicated to the identification of the parameters and regimes associated with instabilities, and other secondary effects of the ground vortex. A detailed analysis of a ground vortex resulting from the collision between a wall jet and a boundary layer was presented. This work follows a previous study carried out by Barata et al. (2005), which detected a small recirculating zoned located upstream the separation point and not yet reported before for this type of flows.

The experiments were performed for a velocity ratio between the boundary layer and the wall jet, V_R, of *0.5*. Laser Doppler measurements of mean and turbulent velocity characteristics, in vertical plane of symmetry of the flow, were presented and discussed together with the vorticity, the turbulent kinetic energy and momentum balances.

The results revealed the existence of the small secondary vortex flow identified by Barata et al. (2008). This small vortex is located upstream, in the wall jet flow sense, the separation point. When this vortex disappears it is removed upwards by the highly curved flow resultant from the collision between the two opposed flows. The centre of the secondary vortex flow is located upstream the separation point, but, probably, somewhere before the so called maximum penetration point. The analysis of vorticity suggests that the vortical structures were convected in the wall jet to the deflected flow, resultant from the interaction between the wall jet and the boundary layer, without significant variation in its magnitude. The collision zone presents high positives values of vorticity. So, it is characterized by the clockwise vorticity. The results about vorticity indicate that the small vortex identified in this work and by Barata et al. (2008) has the counterclockwise sense.

The turbulent kinetic energy balances revealed that in the collision zone of the wall jet with the boundary layer there is a local gain of energy by convection. In the region of the deflected flow the convective term not presents any significant contribution to the loss or gain of turbulent kinetic energy. The results revealed that in the collision zone the diffusive and dissipative term and the production by shear stresses term become predominant, and that the production of turbulent kinetic energy tends to be balanced by the loss by diffusion and dissipation. In the same zone, but near the wall, the production of turbulent kinetic energy is by convection, by normal and shear stresses. The small contribution of convective term to the production of turbulent kinetic energy is less than the production due to the normal stresses and shear stresses. The collision zone between the wall jet and the boundary layer presents a behavior similar to a wall jet. In general the results indicate that the modeling of turbulence of this flow may require an adequate treatment of production by normal stresses, which is important in the collision zone.

The analysis to the momentum of the horizontal velocity component and the vertical velocity component revealed that the molecular diffusion can be negligible. In the collision zone the

pressure gradient term is very important in U-momentum. However, it is balanced by the convection term, result that is applied to the all flowfield. The turbulent diffusion term is, also, important in the collision zone, and in the boundary layer side, near of the wall.

In relation to the V-momentum, the result revealed that the convection is, also, balanced by the pressure gradient, along the all flowfield including the collision and the deflection of the flow zones. These terms are predominant in the collision zone and, also, in the boundary layer side. The turbulent diffusive term is very small in the collision zone and in the deflection zone flow.

The momentum of horizontal mean velocity component, *U*, is preponderant in relation to the momentum of vertical mean velocity component, *V*. A result that can be explained by the strong deceleration of the flow in the horizontal direction, due to the impact of the two opposed flows.

Bibliography

Kuhn, R., Margason, R. and Curtis, P., "Jet Induced Effects The Aerodynamic of Jet and Fan Powered V/STOL Aircraft in Hover and Transition", *Progress in Astronautics and Aeronautics*, *AIAA Publication*, Vol. 217, 2006.

Castro, I.P. and Bradshaw, P., "The Turbulence Structure of a Highly Curved Mixing Layer", *Journal of Fluid Mechanics*, Vol. 73, Part 2, pp. 265-304, 1976.

Saripalli, K.R., "Visualization of Multijet Impingement Flow", *AIAA Journal*, Vol. 21, pp. 483-484, 1983

Saripalli, K.R., "Laser Doppler Velocimeter Measurements in 3D Impinging Twin-Jet Fountain Flows", *Turbulent Shear Flows*, Vol. 5, edited by Durst et al., Springer-Verlag, Berlin, 1987, pp. 147-168, 1987.

Cimbala, J.M., Stinebring, D.R., Treaster, A.L. and Billet, M.L., "Experimental Investigation of a Jet Impinging on a Ground Plane in Crossflow", *Journal of Aircraft*, Vol. 25, No. 10:923-931, 1988.

Cimbala, J.M., Billet, M.L., Glaubomme, D.P. and Ofelein, J.C., "Experiments on the Unsteadiness Associated with a Ground Vortex", *Journal of Aircraft*, Vol. 28, No. 4, pp. 261-267, April 1991

Harman, T.B., Cimbala, J.M., Billet, M.L., "Reduction in Size and Unsteadiness of V/STOL Ground Vortices by Ground Fences", *Journal of Aircraft*, Vol. 31, No. 3:579-584, 1994.

Knowles, K., Bray, D., Bailey, P.J. and Curtis, P., "Impinging Jets in Crossflow", *International Powered Lift Conference*, Royal Aeronautical Society, London, 29-31 August, 1990.

Knowles, K. and Bray, D., "The Ground Vortex Formed by Impinging Jets in Crossflow", *AIAA 29th Aerospace Sciences Meeting*, AIAA Paper 91-0768, January 7-10, Reno Nevada, 1991.

Barata, J.M.M., "Estudo Numérico e Experimental de Jactos Incidentes sobre Placas Planas através de um Escoamento Cruzado", PhD Thesis in Mechanical Engineering, UTL, Lisbon, Portugal, 1989.

Barata, J.M.M., Durão, D.F.G. and Heitor, M.V., "Turbulent Energy Budgets in Impinging Zones", *Eight Symposium on Turbulent Shear Flows*, September 9-11, Munich, 1991a.

Barata, J.M.M., Durão, D.F.G., Heitor, M.V. and McGuirk J.J., “On the Analysis of an Impinging Jet on Ground Effects”, *Experiments in Fluids*, Vol. 15, pp. 117 -129, Springer-Verlag, 1993.

Barata, J.M.M., Durão, D.F.G., Heitor, M.V. and McGuirk J.J., “The Turbulence Characteristics of a Single Impinging Jet Through a Crossflow”, *Experiments in Thermal and Fluid Science*, 1991b.

Tennekes, H. and Lumley, J.L., “A First Course in Turbulence”, The MIT Press, 1972

Barata, J.M.M., Durão, D.F.G. and Heitor, “The Turbulence Characteristics of a Single Impinging Jet Through a Crossflow”, *Sixth Symposium on Turbulent Shear* Flows, September 7-9, Toulouse, 1987.

Barata, J.M.M., Durão, D.F.G. and McGuirk, J.J., “Numerical Study of Single Impinging Jets Through a Crossflow”, *Journal of Aircraft*, Vol. 26, No. 11, p. 1002-1008, 1989

Barata, J.M.M., Durão, D.F.G. and Heitor, “Impingement of SIngle and Twin Turbulent Jets through a Crossflow”, *AIAA Journal*, Vol. 29, No. 4, pp. 595-602, 1991c.

Barata, J.M.M., “Fountain Flows Produced by Multiple Jets in a Crossflow”, *AIAA Journal*, Vol. 34, No. 12, pp. 2523-2530, 1996.

Barata, J.M.M. and Durão, D.F.G., “Laser-Doppler Measurements of Impinging Jets Through a Crossflow”, *Experiments in Fluids*, Vol. 36, No. 5:665-674, 2004.

Barata, J.M.M. and Durão, D.F.G., “Laser-Doppler Measurements of a Highly Curved Flow”, *AIAA Journal*, Vol. 43, No. 12, pp. 2652-2655, 2005.

Barata, J.M.M., Ribeiro, S., Santos, P., Silva, A. and Silvestre, M., “Experimental Study of Instabilities and Secondary Effects of a Ground Vortex Flow”, *46th AIAA Aerospace Sciences Meeting & Exhibit*, 7-10 January, Reno, NV, 2008.

Silva, A.R.R., Durão, D.F.G., Barata, J.M.M., Santos, P.J.T. and Ribeiro, S.D.G., “Laser-Doppler Analysis of the Separation Zone of a Ground Vortex Flow”, *14th International Symposium in Applications of Laser Techniques to Fluid Mechanics*, 07-10 July, Lisbon, Portugal, 2008.

Silva, A.R.R., Durão, D.F.G., Barata, J.M.M., Santos, P.J.T. and Ribeiro, S.D.G., “Laser-Doppler Analysis of the Separation Zone of a Ground Vortex Flow”, *Experiments in Fluids*, 2009a (accepted for publication).

Barata, J.M.M., Ribeiro, S., Santos, P. and Silva, A., “Experimental Study of a Ground Vortex”, *Journal of Aircraft*, 2009.

Barata, J.M.M., Durão, D.F.G. and Heitor, M.V., "Experimental and Numerical Study on the Aerodynamics of Jets in Ground Effect", *10th Symposium on Turbulence*, September 22-24, Rolla, Missouri,1986.

Saddington, A.J., Knowles, K. and Cabrita, P.M., "Turbulence Measurements in a STOVL Fountain", *Flow, Turbulence and Combustion*, 2009 (accepted for publication).

Saddington, A.J., Cabrita, P.M. and Knowles, K., "Large-scale Instabilities in a STOVL Upwash Fountain", *Engineering Turbulence Modelling and Experiments 6*, Elsevier Science Ltd., Oxford, UK, pp. 667-676, 2005.

Cabrita, P.M., Saddington, A.J. and Knowle, K., "Unsteady Features of Twin-jet STOVL Ground Effects", *International Powered Lift Conference and Exhibit*, Williamsburg, VA, USA, Paper 2002-6014, 2002.

Vans Dalsem, W.R., Panaras, A.G., Steger, J.L., "Numerical Investigation of a Jet in a Ground Effect with a Crossflow", *International Powered Lift Conferences*, SAE Paper 872344, December 7-10, Santa Clara, California, 1987

Pandaya, S.A., Murman, S.M. and Sankaran, V., "Unsteady Computations of a Jet in Crossflow with Ground Effect", *AIAA Paper* No. 2003-3898, 2003.

Smith, M.H., Chawla, K. and Van Dalsem, W.R., "Numerical Simulation of a Complete STOVL Aircraft in Ground Effect", *AIAA Paper*, No. 91-3293, 1991.

Chanderjian, N.M., Pandaya, S.A., Ahmad, J. and Murman, S.M., "Parametric Time-Dependent Navier-Stokes Computations for a YAV-8B Harrier in Ground Effect", *AIAA Paper* No. 2002-0950, 2002

Page, G.J., Jiang, D., McGuirk, J.J. and Harper, C., "Application of Computational Fluid Dynamics to Hot Gas Ingestion Modelling", *International Power Lift Conference*, London, U.K., pp. 23.1-23.11, 1998.

Jiang, D. and McGuirk, J.J., "A Numerical Study of Intake Ingestion Relevant to Short Take-Off Vertical Landing Aircraft", *Proceedings of International Conference on Applied CFD*, Beijing, PR China, 2000, pp. 1-8.

Worth, N.A. and Yang, Z., "Simulation of an Impinging Jet in a Crossflow Using a Reynolds Stress Transport Model". *Int. J. Numer. Meth. Fluids*, Vol.52, pp.199-211, 2006.

Silva, A., Barata, J., Santos, P. and Nunes, R., “Unsteadiness of a Ground Vortex Flow”, *AIAA Paper* 2009-0407, *47th Aerospace Sciences Meeting and Exhibit*, Orlando, Florida 5-8, January, 2009b.

Gilbert, J.M., “Detailed Turbulence Measurements in a Two-Dimmensional Upwash”, *AIAA 16th Fluid and Plasma Dynamics Conference*, AIAA Paper 83-1678, July 12-14, Danvers, Massachusetts, 1983.

Metha R.D., Bradshaw P., “Design Rules for Small Low-Speed Wind Tunnels”, 1979.

Yanta, Z., Smith, R.A., “Measurements of Turbulent-Transport Properties with Laser-Doppler Velocimeter, *11th Aerospace Sciences Meeting*, AIAA Paper 73-0169, Washington, 1973.